



UNIVERSIDAD REGIONAL AMAZÓNICA IKIAM

Facultad de Ciencias de la Tierra y Agua

Carrera de Hidrología

Pronóstico de inundaciones basado en un sistema acoplado de modelación atmosférica-hidrológica en subcuencas amazónicas del Ecuador con escasez de datos

Juseth Enrique Chancay Sánchez

Tena, enero 2022

Napo, Ecuador

DECLARACIÓN DE DERECHO DE AUTOR, AUTENTICIDAD Y RESPONSABILIDAD

Tena, 24 de enero de 2022

Yo, **Juseth Enrique Chancay Sánchez** con documento de identidad N° **1350580005**, declaro que los resultados obtenidos en la investigación que presento en este documento final, previo a la obtención del título de Ingeniero en Ciencias del Agua son absolutamente inéditos, originales, auténticos y personales.

En virtud de lo cual, el contenido, criterios, opiniones, resultados, análisis, interpretaciones, conclusiones, recomendaciones y todos los demás aspectos vertidos en la presente investigación son de mi autoría y de mi absoluta responsabilidad.

Por la favorable atención a la presente, suscribo de usted,

Atentamente,

Firma:

Juseth Enrique Chancay Sánchez

CERTIFICADO DE DIRECCIÓN DE TRABAJO DE INTEGRACIÓN CURRICULAR

Certifico que el trabajo de integración curricular titulado: **“Pronóstico de inundaciones basado en un sistema acoplado de modelación atmosférica-hidrológica en subcuencas amazónicas del Ecuador con escasez de datos”**, en la modalidad de: Artículo original en español y de manera optativa en inglés, adaptado a los parámetros y normas de una revista indexada, fue realizado por **Juseth Enrique Chancay Sánchez**, bajo mi dirección.

El mismo ha sido revisado en su totalidad y analizado por la herramienta de verificación de similitud de contenido; por lo tanto, cumple con los requisitos teóricos, científicos, técnicos, metodológicos y legales establecidos por la Universidad Regional Amazónica Ikiam, para su entrega y defensa.

Tena, 24 de enero de 2022

Firma:



Edgar Fabian Espitia Sarmiento, PhD.

C.I: 1758828709

AGRADECIMIENTOS

Mis más sinceros agradecimientos a:

Mi tutor y mi amigo, PhD. Edgar Fabian Espitia Sarmiento, por su confianza, apoyo y dirección durante todo mi proceso de titulación, así como por sus valiosas enseñanzas académicas y personales.

A mis instructores, PhD. Luis Maisincho y MSc. Maylee Iza, por su asesoría técnica y valiosa aportación científica.

Al Instituto Nacional de Meteorología e Hidrología (INAMHI) por proveer al proyecto de capacidad técnica y datos hidrometeorológicos.

A mis amigos y compañeros del Servicio Hidrometeorológico Ikiam, entre ellos: Brian Coronel, Carlos Carrasco, Lizeth Sabando, Elizabeth Naranjo, Ángel Intriago, Víctor Segarra y Oscar Lucas, por su apoyo en el mantenimiento de las estaciones hidrometeorológicas, obtención y procesamiento de datos.

A la Universidad Regional Amazónica Ikiam y a todos mis profesores, entre ellos: Jorge Celi, Mariana Capparelli, Gabriel Moulatlet, Jorge Hurtado, Bryan Valencia, José Serrano, Verónica Gallardo, Yanet Villasana, Fabrizio Logiurato, Carles Franquesa, Juan Francisco Tlapanco, y Vanessa Yáñez, por acompañarme en mi carrera estudiantil, transmitirme sus conocimientos y amor por la ciencia, recordando que la ciencia siempre debe de enfocarse en mejorar la calidad de vida de nuestra sociedad.

DEDICATORIA

Dedico este trabajo a mis padres, Miriam Sánchez y Wilmer Chancay, así como a la persona más especial de mi vida, mi hermana Julieth Chancay, por ser mi fortaleza durante toda mi vida, por transmitirme su amor, y por toda la confianza que me han brindado siempre. Sin ellos no sería la persona que soy ahora. ¡Muchas gracias, los amo infinitamente!

Quisiera dedicar también este trabajo a mis mejores amigos y colegas, que me han acompañado durante mi carrera estudiantil y muy seguramente me acompañarán en mi carrera profesional: Brian Coronel, Carlos Carrasco, Elizabeth Naranjo, y Oscar Lucas.

Finalmente, pero no menos importante, dedico este trabajo a Dios, por brindarme toda la sabiduría necesaria para afrontar esta etapa de mi vida.

INDICE GENERAL

DECLARACIÓN DE DERECHO DE AUTOR, AUTENTICIDAD Y RESPONSABILIDAD	II
CERTIFICADO DE DIRECCIÓN DE TRABAJO DE INTEGRACIÓN CURRICULAR	III
AGRADECIMIENTOS	IV
DEDICATORIA	V
INDICE GENERAL	VI
INDICE DE TABLAS.....	VIII
INDICE DE FIGURAS.....	IX
RESUMEN GENERAL.....	XII
OVERALL ABSTRACT	1
Improving Hourly Precipitation Estimates for Flash Flood Modeling in Data-Scarce Andean-Amazon Basins: An Integrative Framework Based on Machine Learning and Multiple Remotely Sensed Data	2
Abstract.....	2
1. Introduction	2
2. Study Area.....	4
3. Datasets and Methods.....	6
3.1. Data.....	6
3.2. Integration of Satellite-Based Products.....	7
3.3. Statistical Criteria for Performance Assessment	10
3.4. Hydrological Application	11
4. Results and Discussion	13
4.1. Preliminary Evaluation of the SPPs.....	13
4.2. Variable Importance Analysis	14
4.3. Integration Framework Performance	15
4.4. Spatial Consistency Analysis	18
4.5. Calibration and Validation of the GR4H Model	19
4.6. Flood Event Analysis	21
5. Future Perspectives and Final Remarks.....	23
6. Appendix	25
7. References	27
A multi-physics ensemble approach for high-resolution heavy-rainfall and flash-flood forecasting in data-scarce Andean-Amazon basins.....	36

Abstract.....	36
1. Introduction	36
2. Study area	39
3. Data and methods.....	41
3.1. Precipitation and streamflow data	41
3.2. Ensemble precipitation modeling.....	41
3.3. Ensemble flash flood modeling.....	45
4. Results and discussion	46
4.1. Sensitivity analysis of WRF physical schemes.....	46
4.2. Model performances and suitable parameterizations of CU and MP	48
4.3. Optimal ensemble parameterization.....	51
4.4. Ensemble precipitation forecasting	52
4.5. Ensemble streamflow forecasting	56
5. Future perspectives and final remarks	60
6. Appendix	61
7. References	62

INDICE DE TABLAS

PAPER I

Table 1. General information of satellite-based precipitation and soil-moisture data used in this study.	7
Table 2. Information of the last five flash flood events produced within the study area.	12
Table 3. Results of the event analysis considering the last five floods that occurred in the Tena River Basin (TRB), Jatunyacu River Basin (JRB), and upper Napo River Basin (NRB).	23
Table A1. Statistical criteria used to evaluate the performance of the integrative framework that combine multiples SPPs and SMPs with observed precipitation data and spatio-temporal covariates.	25
Table A2. Statistical criteria used to evaluate the performance of the GR4H model.	25
Table A3. Optimal parameter of the GR4H model for each hydrological unit.	26
Table A4. Calibrated lag times for each connection among the hydrological units.	27

PAPER II

Table 1. Physical schemes used to parameterize the WRF model.	42
Table 2. Information of the last five flash flood events produced within the study subbasins.	46
Table 3. Performance of analyzed experiments considering the Model Skill Score (MSS).	51
Table A1. Statistical criteria used to evaluate the ensemble precipitation and streamflow simulations derive from the WRF and GR4H models.	61

INDICE DE FIGURAS

PAPER I

Figure 1. Study area. (a) Location of the Napo River Basin within the Amazon River Basin. (b) Location of the study area within the NRB. (c) Topography, drainage network, and gauge stations of the three Andean-Amazon sub-basins analyzed in this study: the upper Napo River Basin (NRB), Tena River Basin (TRB), and Jatunyacu River Basin (JRB). (d) Ecosystems related to climate gradient and specific precipitation regime.5

Figure 2. Schematic diagram of the integration framework proposed in this study. The framework integrates multiples satellite-based precipitation and soil-moisture products by random forest modeling and bias correction to generate a new hourly fitting precipitation product.9

Figure 3. Performance assessment of the SPPs used as covariates within the integrative framework. The whisker-box plot shows the performance variation within the study area, considering each rain gauge as an individual data point. Red dashed line indicates the optimal value for each performance metric: root mean square error (RMSE), correlation coefficient (CORR), Kling-Gupta efficiency (KGE), probability of detection (POD), false alarm ratio (FAR), and critical success index (CSI).13

Figure 4. Variable importance analysis. The %IncMSE represents the percentage increase in mean square error. Covariates with high %IncMSE generate a strong influence on the RFP model.14

Figure 5. Scatter density plot for observed and simulated precipitation intensity at the hourly scale. (a) Training period without bias correction. (b) Training period with bias correction. (c) Testing period without bias correction. (d) Testing period with bias correction.16

Figure 6. Assessments of the ability to detect the precipitation occurrence for BC-RFP using POD, FAR, and CSI metrics at different intensity thresholds. The analysis was carried out considering both training and testing periods. Red dashed lines indicate the optimal value for each performance metric.17

Figure 7. Distribution of annual precipitation obtained with BC-RFP used for the spatial consistency analysis along the study area (NRB).18

Figure 8. Performances of the GR4H model for calibration and validation periods, using the BC-RFP method as forcing precipitation input. (a) Tena River Basin, TRB. (b) Jatunyacu River Basin, JRB. (c) Upper Napo River Basin, NRB20

Figure 9. Observed and simulated hydrographs of the last five flash flood events that occurred in Tena River Basin (TRB), Jatunyacu River Basin (JRB), and upper Napo River Basin at Ahuano (NRB). (a) Event 1, September 2017. (b) Event 2, July 2018. (c) Event 3, May 2019. (d) Event 4, June 2019. (e) Event 5, May 2020.22

Figure A1. Disaggregation of the study sub-basins (TRB, JRB, and NRB) into 18 hydrological units for the semi-distributed setting of the GR4H model.27

PAPER II

Figure 1. Study area. (a) Location of the Napo River Basin within the Amazon River Basin and WRF domains. (b) Topography, drainage network, and gauge stations of the three study subbasins: Upper Napo River Basin, Tena River Basin, and Jatunyacu River Basin. (c) Ecosystems within the study area related to climate gradient and hence specific precipitation regime.....40

Figure 2. Sensitivity analysis of the physical schemes. (a) Effect of each physical scheme on the performance of simulated precipitation (main effect), and effect of one physical scheme on another physical scheme (interaction effect). The larger radius (size) of the circle means larger relative importance, while the thicker line connecting two physical schemes means a larger contribution from interactions. (b) Main effect of physical schemes with and without CU parameterization in the finest domain (d03): cumulus parameterized (CP) and cumulus resolved (CR), respectively.47

Figure 3. Performances of the simulated precipitation considering cumulus parameterized (CP) and cumulus resolved (CR) experiments. Each box plot represents the performance variability over the UNRB at pixel-to-pixel scale. Symbology: (**) and (***) mean significant differences, i.e., $p < 0.05$ and $p < 0.005$, respectively.....48

Figure 4. Performance of the 25 experiments derived from combinations of 5 CU and 5 MP parameterizations. Box plots considers the performance variability over the UNRB using a pixel-to-pixel comparison. The metrics used were Root Mean

Square Error (RMSE), Correlation Coefficient (CORR), Bias Error (BIAS), and Probability of Detection (POD).49

Figure 5. Performance of the simulated precipitation considering the variation on the number of ensemble members. The used metrics were: Root Mean Square Error (RMSE), Correlation Coefficient (CORR), Bias Error (BIAS), Probability of Detection (POD), False Alarm Ratio (FAR), and Model Skill Score (MSS).52

Figure 6. Impact of the lead time on the performance of the bias-corrected ensemble precipitation forecast (EPFs), considering a continuous simulation period of five years: from January 2016 to December 2020. The black line represents the mean performance, whereas the ribbon represents the performance variation over the UNRB. The used metrics were: Root Mean Square Error (RMSE), Correlation Coefficient (CORR), Bias Error (BIAS), Probability of Detection (POD), False Alarm Ratio (FAR), and Critical Success Index (CSI). The letter “C” in the x-axis represents the performance of the simulated precipitation used for the ensemble parameterizations, i.e., simulations forced with the 0.25° GFS analysis data.54

Figure 7. Spatial performance of the bias-corrected ensemble precipitation forecast within the UNRB (lead time 3h), considering a continuous simulation period of five years: January 2016 to December 2020. The used metrics were: Root Mean Square Error (RMSE), Correlation Coefficient (CORR), Bias Error (BIAS), Probability of Detection (POD), False Alarm Ratio (FAR), and Critical Success Index (CSI).55

Figure 8. Performance of the ensemble streamflow forecasting for (a) Tena River Basin, TRB; (b) Jatunyacu River Basin, JRB; and (c) Upper Napo River Basin, UNRB. Scatter density plot for observed and simulated data at the hourly scale (left side). The non-exceedance probability curve for observed data and ensemble streamflow forecast (right side).57

RESUMEN GENERAL

El aumento de la intensidad y recurrencia de las inundaciones repentinas es una creciente preocupación, especialmente en cuencas amazónicas con escasez de datos donde los sistemas de pronóstico y alerta temprana de crecidas suelen ser inexistentes. Es crucial comprender y modelar las condiciones que desencadenan las inundaciones repentinas, para así, planificar estrategias de mitigación. El presente estudio propone un sistema de pronóstico de inundaciones basado en modelación atmosférica e hidrológica en 3 cuencas amazónicas del Ecuador con escasez de datos: Cuencas de los ríos Tena, Jatunyacu, y Napo (salida en Ahuano).

Considerando la limitada información hidrometeorológica disponible en el área de estudio, la primera parte del estudio se enfocó en la generación de un producto espacial de precipitación mediante la integración de múltiples productos satelitales de precipitation y humedad del suelo a través de machine learning. El producto espacial de precipitation propuesto (BC-RFP) demostró capturar adecuadamente la intensidad, distribución y ocurrencia de los eventos de precipitation a escala horaria. De hecho, con la información derivada de BC-RFP se consiguió calibrar y validar el modelo lluvia-escorrentía GR4H para las tres cuencas de estudio, con rendimientos satisfactorios ($KGE > 0.5$).

La segunda parte se enfocó en determinar las parametrizaciones físicas del modelo WRF que maximicen el rendimiento de los pronósticos de precipitation usando un enfoque de modelación por conjuntos. Para esto, se realizó un previo análisis de sensibilidad utilizando 100 parametrizaciones del modelo WRF obtenidas de la variación de los esquemas físicos de convección (CU), microfísica (MP) y capa límite planetaria (PBL). Los resultados del pronóstico de precipitación por conjuntos (EPF) mostraron rendimientos aceptables, ya que los rendimientos de las simulaciones de caudal forzadas con el EFP presentaron valores de KGE entre 0.14 y 0.4. En general, los resultados brindaron suficiente evidencia para proponer al sistema de modelación atmosférica e hidrológica analizado como una herramienta preliminar para el pronóstico de inundaciones para las cuencas de estudio.

Palabras clave: Modelo GR4H, modelo WRF, inundaciones, pronóstico, alerta temprana.

OVERALL ABSTRACT

The increase in intensity and recurrence of flash floods, derived from heavy rainfalls linked to climate change, is a growing concern worldwide, particularly in data-scarce Andean-Amazon basins, where flood forecasting and early warning systems are usually inexistent. Thus, it is imperative to understand and model the hydrometeorological conditions that trigger the flash flood events for the effective planning of mitigation strategies. The present study aimed at proposing a flash-flood forecasting system based on atmospheric and hydrological modelling for three Ecuadorian data-scarce Andean-Amazon basins: Tena River Basin (TRB), Jatunyacu River Basin (JRB), and Upper Napo River Basin (UNRB, outlet at Ahuano).

Given the limited hydrometeorological information available in the study area, the first part of this study focused on implementing a gridded-precipitation product by integrating multiple satellite-based precipitation and soil moisture products through machine learning techniques. The gridded-precipitation product (hereafter BC-RFP) showed a high ability to reproduce the intensity, distribution, and occurrence of the hourly precipitation events. Indeed, with the BC-RFP, it was possible to calibrate and validate the rainfall-runoff GR4H model for the three study basins, with satisfactory performance ($KGE > 0.5$).

The second part of the study focused on determining the physical parameterizations of the WRF model that maximize the performance of the precipitation forecasts using an ensemble modeling approach. For this, a prior sensitivity analysis was conducted using 100 parameterizations of the WRF model obtained from the variation of physical schemes, such as cumulus convection (CU), microphysics (MP) and planetary boundary layer (PBL). The ensemble precipitation forecasts (EPFs) showed acceptable performances, as the streamflow simulations forced with EPFs presented KGE values between 0.14 and 0.4. Altogether, results provided sufficient insights to propose the analyzed ensemble precipitation and streamflow forecasting as a preliminary tool for generating early warning systems in the study area.

Keywords: GR4H model, WRF model, flash-flood, forecasting, early warning

PAPER I

Published on Remote Sensing (MDPI). <https://doi.org/10.3390/rs13214446>

Improving Hourly Precipitation Estimates for Flash Flood Modeling in Data-Scarce Andean-Amazon Basins: An Integrative Framework Based on Machine Learning and Multiple Remotely Sensed Data

Abstract

Accurate estimation of spatiotemporal precipitation dynamics is crucial for flash flood forecasting; however, it is still a challenge in Andean-Amazon sub-basins due to the lack of suitable rain gauge networks. This study proposes a framework to improve hourly precipitation estimates by integrating multiple satellite-based precipitation and soil-moisture products using random forest modeling and bias correction techniques. The proposed framework is also used to force the GR4H model in three Andean-Amazon sub-basins that suffer frequent flash flood events: upper Napo River Basin (NRB), Jatunyacu River Basin (JRB), and Tena River Basin (TRB). Overall, precipitation estimates derived from the framework (BC-RFP) showed a high ability to reproduce the intensity, distribution, and occurrence of hourly events. In fact, the BC-RFP model improved the detection ability between 43% and 88%, reducing the estimation error between 72% and 93%, compared to the original satellite-based precipitation products (i.e., IMERG-E/L, GSMAP, and PERSIANN). Likewise, simulations of flash flood events by coupling the GR4H model with BC-RFP presented satisfactory performances (KGE* between 0.56 and 0.94). The BC-RFP model not only contributes to the implementation of future flood forecast systems but also provides relevant insights to several water-related research fields and hence to integrated water resources management of the Andean-Amazon region.

Keywords: IMERG, PERSIANN, GSMAP, SMAP, GR4H model, UNRB.

1. Introduction

Accurate estimation of spatiotemporal precipitation dynamics is crucial for several hydrological purposes, especially for operational flash flood forecasting [1,2]. Conventional approaches to estimate the precipitation patterns require rain gauge information. However,

the spatial distribution of rain gauges strongly influences the uncertainty of precipitation estimates [3,4]. This implies important limitations over areas with complex topography, as in the case of the Andean-Amazon sub-basins, where implementing a suitable rain gauge density is often difficult and cost-prohibitive. In recent years, satellite-based precipitation products (hereafter SPPs) have been constituted as an alternative to overcome this limitation [5,6]. Nevertheless, SPPs present multiple sources of random and systematic errors associated with retrieval algorithms, sampling time steps, detection ability, among others [7,8].

In this regard, several studies have proposed different methods to improve the accuracy of SPPs and use them for forcing precipitation in hydrological models [9-12]. Most of these studies have focused on bias correction by statistical techniques and regression-based downscaling using land surface characteristics [13-20]. However, these correction methods still present several issues at high spatial (i.e., <10 km) and temporal (i.e., hourly) resolutions [21]. Thus, their applicability for hydrological modeling in fast-response basins is limited [22,23]. To address these issues, recent investigations have proposed various correction methods based on machine learning. For instance, Le et al. [24] developed a framework to correct daily and sub-daily SPPs by convolutional neural networks, obtaining higher performances than classical correction methods. Likewise, Chivers et al. [25] and Wolfensberger et al. [26] suggested a combination of random forest modeling with classical bias correction methods to improve hourly precipitation estimates derived from SPPs. However, the latter method focuses on the individual correction of SPPs without considering the valuable information that could be better captured by other precipitation products.

In contrast, Baez et al. [27] and Kolluru et al. [28] proposed merging multiples SPPs with rain gauge data and geographical features by random forest modeling. This method extracts the most relevant information from each SPP and combines it to maximize the accuracy of precipitation estimates. Results obtained with this method showed significant increases in performances of precipitation estimates (greater than 60%) compared to using isolated SPPs [27,28]. Further studies have indicated the combination of SPPs with satellite-based soil-moisture products (hereafter SMPs) also provides relevant insights to improve the accuracy of

precipitation estimates [29-32]. In fact, soil-moisture information has proven to be an excellent indicator of the precipitation occurrence, especially at high temporal scales [33].

Although the integration of multiple SPPs and SMPs by machine learning provides an unprecedented opportunity to better estimate the precipitation dynamics in data-scarce regions, its applicability has not been evaluated in the Andean-Amazon basins. A representative Andean-Amazon basin is the upper part of the Napo River Basin, as it presents a complex topography and fast hydrological responses. Given its characteristics, the upper Napo River Basin is prone to recurrent flash floods [34,35]. In spite of this, no operational hydrological modeling and hence flood forecasting systems have been implemented in the region due to the scarce rain gauge data and hence suitable spatiotemporal precipitation estimates.

To address this problem, this study aims to propose an integrative framework for improving the estimation of spatiotemporal precipitation dynamics (i.e., intensity, distribution, and occurrence) at an hourly scale in the upper Napo River Basin. The framework combines multiple SPPs and SMPs with ground observed data and geographical features using random forest modeling and bias correction methods. The potential use of the framework as forcing precipitation inputs for hydrological modeling was illustrated in three gauged sub-basins within the upper Napo River Basin that suffer continuous flood risk. This study might not only contribute to the development of flood forecasting systems, but also to several water-related research fields and hence to integrated water resources management in the Andean-Amazon region.

2. Study Area

The Napo River is an important tributary of the Amazon Basin (Figure 1a) providing a mean annual discharge of about 6300 m³/s. It covers a drainage area of 100,500 km², distributing among Ecuador (59.6%), Peru (40.0%), and Colombia (0.4%) (Figure 1b) [36]. This study focuses on the upper part of the Ecuadorian Napo River Basin (hereafter NRB), located between the Eastern Andes and the Amazonia foothills. The NRB covers 6095 km² above the H1156

hydrological station and presents steep slopes that descend from 5900 to 370 m.a.s.l. over only 100 km (Figure 1c) [37]. Due to this complex topography, the NRB presents a strong climate gradient. Along this climate gradient, several ecosystems can be found, from the higher to lower elevations: (i) paramo, (ii) mountain forest, and (iii) piedmont rainforest (Figure 1d).

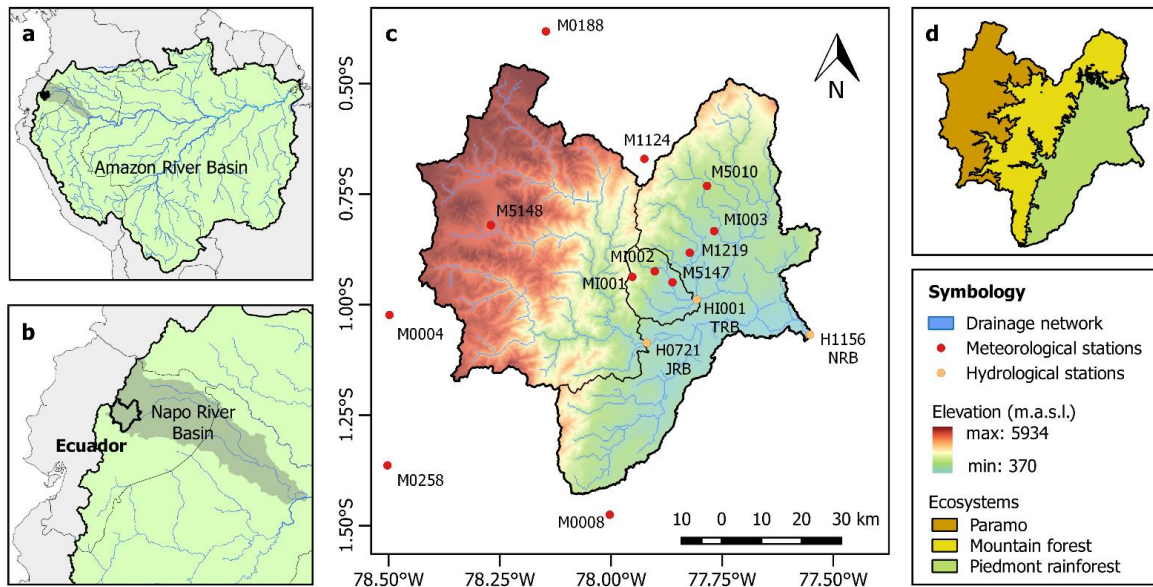


Figure 1. Study area. (a) Location of the Napo River Basin within the Amazon River Basin. (b) Location of the study area within the NRB. (c) Topography, drainage network, and gauge stations of the three Andean-Amazon sub-basins analyzed in this study: the upper Napo River Basin (NRB), Tena River Basin (TRB), and Jatunyacu River Basin (JRB). (d) Ecosystems of the NRB related to climate gradient and specific precipitation regime.

The paramo is located in the western highlands of the NRB (above 3200 m.a.s.l.). It presents mean temperatures that range from 4 to 8 °C. The precipitation is influenced by moisture originated from both the Pacific and Atlantic oceans with annual accumulation that varies from 500 to 2000 mm [38,39]. In the paramo, the precipitation occurs mainly as drizzle (~0.1 mm/h) [40], however, rainfall events with high-relative intensities (60 mm/h) have been reported [38]. The mountain forest, instead, is a transitional region between the paramo and piedmont rainforest. Here, mean annual temperature varies from 12 to 20 °C and the annual precipitation ranges from 2000 to 4000 mm. In general, the precipitation mainly occurs by

orographic and convective events, reaching maximum intensities up to ~85 mm/h [41].

The piedmont rainforest is located in the eastern lowlands of the NRB (i.e., below 900 m.a.s.l.). This region is dominated by a humid tropical climate with annual rainfall between 3500 and 5000 mm, and mean temperatures from 20 to 27 °C [42]. Overall, precipitation presents intensities from 20 to 40 mm/h. However, extreme events above 95 mm/h have been recorded [35]. The piedmont rainforest is the most critical region within the NRB as its soil-saturation conditions and strong precipitation regime generate frequent flooding. Indeed, nine flash floods with peak discharges above 6000 m³/s have been recorded near the NRB outlet during the last 12 years, affecting on average 8000 families per year [42-44].

In the NRB, there are two additional critical points that suffer recurrent flash floods, which are the outlets of the Tena River Basin (TRB) and Jatunyacu River Basin (JRB). The TRB drains 239 km² above the HI001 hydrological station in Tena City. The streamflow and baseflow average 24.4 m³/s and 8 m³/s, respectively [42]. In the last years, four flash floods have been registered in the TRB, reaching peak discharges above 1800 m³/s [35]. On the other hand, the JRB has a drainage area of 3128 km² above the H0721 hydrological station. According to this station, discharge averages 290 m³/s [45]. Since 2010, three flash floods with peak discharges above 2500 m³/s have been recorded near the JRB outlet [45,46].

3. Datasets and Methods

3.1. Data

3.1.1. Ground-Observed Precipitation and Streamflow Data

Hourly precipitation and streamflow data were obtained from 12 meteorological stations and 3 hydrological stations (Figure 1c) belonging to the Ikiam Hydrometeorological Service [42] and the National Institute of Meteorology and Hydrology of Ecuador [45,46]. The analysis period was from January 2016 to December 2020 (5 years). We chose this period due to the availability of hourly data within the study area. Prior to this study, a data quality analysis was performed to find and remove outliers using the graphical method described in Chebana et al.

[47]. It consists in visualizing data by a rainbow plot and then identifying outliers using bagplots and highest-density region boxplots.

3.1.2. Satellite-Based Data

Satellite-based precipitation data were obtained from the Integrated Multi-Satellite Retrievals for GPM Early Run (IMERG-E) and Late Run (IMERG-L) [48,49], the Global Satellite Mapping of Precipitation (GSMAP) [50,51], and the Precipitation Estimation from Remotely Sensed Information using Artificial Neural Networks—Cloud Classification System (PERSIANN-CCS) [52]. We focus on these products as they are widely used for flash flood analysis [53-56] due to their high spatiotemporal resolutions and low latency (Table 1). Likewise, soil moisture data at surface level (SM) and root zone (RM), as well their temporal variation (i.e., Δ SM and Δ RM), were derived from the Soil Moisture Active-Passive Satellite Mission (SMAP L4-SM product).

Table 1. General information of satellite-based precipitation and soil-moisture data used in this study.

Satellite Product	Spatial Resolution	Temporal Resolution	Latency	Download Website
GPM IMERG-E	0.10°	0.5 h	6 h	https://giovanni.gsfc.nasa.gov/giovanni/
GPM IMERG-L	0.10°	0.5 h	12 h	https://giovanni.gsfc.nasa.gov/giovanni/
GSMAP	0.10°	1 h	1 h	https://sharaku.eorc.jaxa.jp/GSMaP/
PERSIANN-CCS	0.04°	1 h	1 h	https://chrsdata.eng.uci.edu/
SMAP L4-SM	0.09°	3 h	7 d	https://nsidc.org/data/SPL4SMGP/versions/5

3.2. Integration of Satellite-Based Products

To achieve a new high-resolution and fitting precipitation product over the NRB, the proposed framework was implemented into three steps (Figure 2): (i) preprocessing, (ii) random forest precipitation modeling, and (iii) postprocessing or bias correction. Further details of the framework are described as follows.

3.2.1. Preprocessing

To ensure spatial consistency, the SPPs and SMPs were resampled to 4 km (the highest

resolution provided by the precipitation products) using the bilinear method, following recommendations presented in Baez et al. [27]. Temporal consistency was obtained by aggregating or disaggregating the satellite-based products to hourly intervals [57]. The SPPs were aggregated by simple sum, whereas SMPs were disaggregated using the proximal interpolation method [58].

Since topographic features and temporal variability play an important role in precipitation patterns [59], variables such as altitude (ALT), monthly variability (MON), and hourly variability (HOUR) were considered as ancillary covariates. Altitude was derived from the Shuttle Radar Topography Mission (SRTM v4.1 90m) which was previously resampled to 4 km. Once the covariates were on the same temporal and spatial scales, we generated a data matrix joining information from the SPPs and SMPs, ancillary covariates, and ground-observed precipitation of each meteorological station. Data extraction was performed by point-to-pixel scale (Figure 2).

3.2.2. Random Forest Precipitation (RFP) Modeling

To integrate the SPPs and SMPs with ground-observed precipitation data and the ancillary covariates, we used a random forest (RF) model as the core of the framework.

A RF model is a machine learning technique that combines a large number of regression trees [60]. Each tree is generated with random data subsets sampled independently. These random data subsets are permuted at each splitting node for each tree, which reduces overfitting and improves the strength of predictions [61]. Thus, the error converges to the minimum possible as the number of trees increases within the forest. Given that the RF model generates a prediction for each tree, the final output is the average of all predictions.

We implemented the RF model using the R package “randomForest” [62]. With this package, the RF model requires two parameters: the number of regression trees (ntree) and the number of predictor variables at each node (ntry). We established ntree = 1000 and ntry = 4, following recommendations presented in Wolfensberger et al. [26]. The k-fold cross-

validation method ($k = 10$) was proposed for model training. For this, the input data was previously divided into training (70%) and testing (30%) subsets.

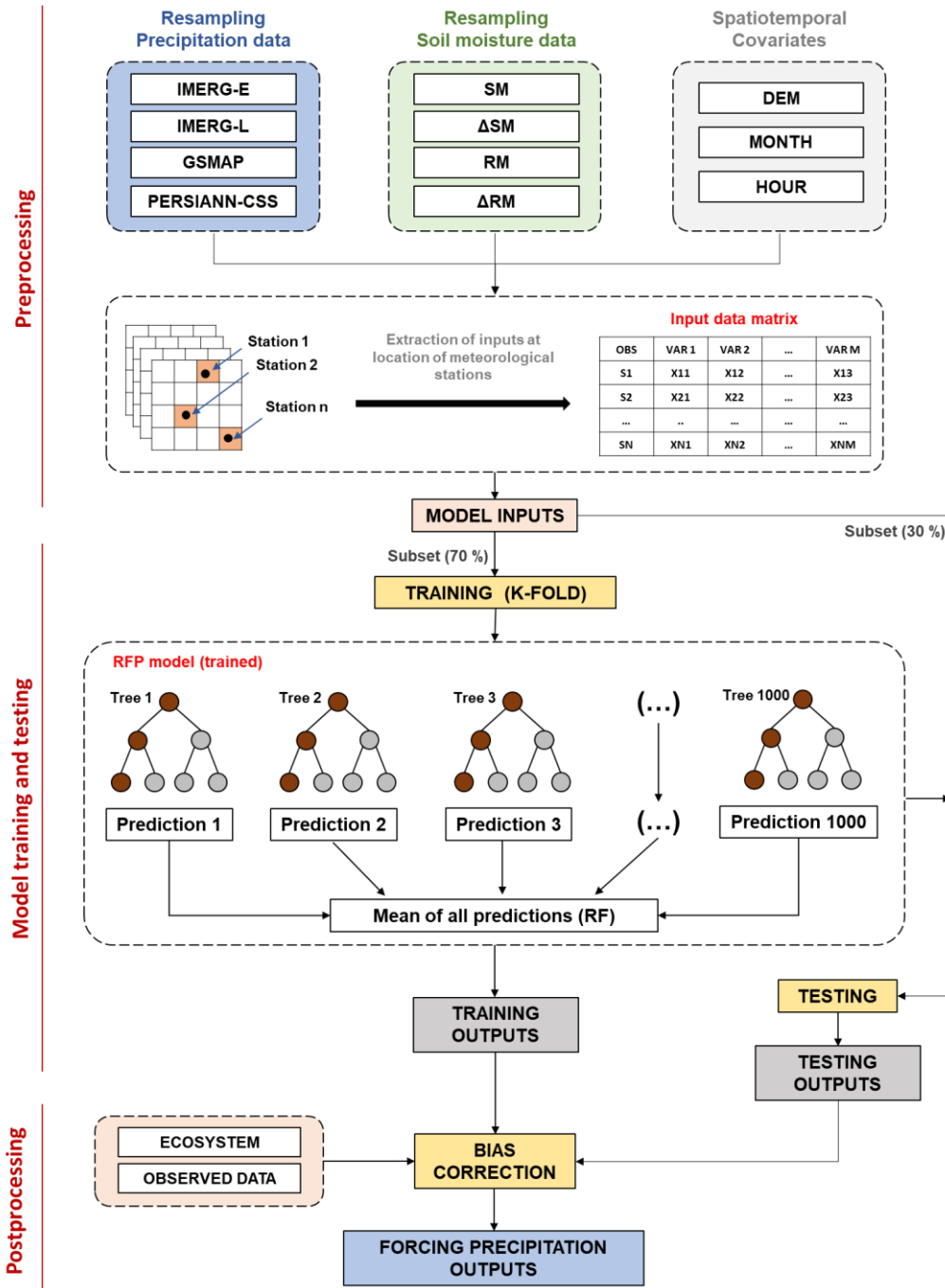


Figure 2. Schematic diagram of the integration framework proposed in this study. The framework integrates multiples satellite-based precipitation and soil-moisture products by random forest modeling and bias correction to generate a new hourly fitting precipitation product.

Additionally, a variable importance analysis was simultaneously performed with the model training, calculating the percentage increase in mean square error (%IncMSE) for out-of-bag samples after permutating each covariate [59]. High %IncMSE values correspond to high importance and hence greatest influence on the precipitation prediction. Since the RF model generates a new gridded precipitation product, we called it random forest precipitation (hereafter RFP).

3.2.3. Postprocessing: The Bias-Corrected Random Forest Precipitation (BC-RFP)

Given the RFP model could present systematic bias due to the error associated with satellite-based covariates and the resampling process [59], we carried out a bias correction by the gamma quantile mapping method (GQM). This parametric method corrects precipitation assuming a gamma distribution. Thus, GQM nonlinearly corrects the mean, variance, intensities, and frequencies of wet hours [63]. A further description of this method is presented in Fang et al. [64]. The bias correction was performed considering the three main ecosystems of the study area. Note that each ecosystem presents a specific precipitation regime (see Section 2).

3.3. Statistical Criteria for Performance Assessment

Performance of precipitation estimates derived from the integration framework (i.e., RFP and BC-RFP) was assessed by comparison with observed precipitation data at a point-to-pixel scale. For this, we used three common continuous-statistic metrics: root mean square error (RMSE), correlation coefficient (R), and Kling–Gupta efficiency (KGE). Furthermore, three categorical statistics were used to assess the precipitation detection ability: probability of detection (POD), false alarm ratio (FAR), and critical success index (CSI).

Likewise, the SPPs used as covariates in the integrative framework were previously assessed to determine a reference for the improvement reached by RFP and BC-RFP. Mathematical definitions and characteristics of the aforementioned statistical metrics are described in Table A1.

3.4. Hydrological Application

The bias-corrected estimates derived from the integrative framework (i.e., BC-RFP) were used as forcing precipitation inputs for the GR4H model. This hydrological model has been widely used for flash floods modeling due to its simple structure, low computing needs, and ability to simulate hourly streamflow [65,66]. Previous studies, such as Llauca et al. [67] and Espitia et al. [68], showed that the GR4H model can satisfactorily simulate the hydrological processes over the Andean-Amazon sub-basins. Details of the hydrological modeling process are described as follows.

3.4.1. Model Parameters and Inputs

The GR4H model has four free parameters that characterize the storage processes and unit hydrograph: X1, maximum capacity of moisture store (mm); X2, groundwater exchange coefficient (mm/h); X3, maximum capacity of the routing store (mm); and X4, base time of the unit hydrograph (h). A complete description of the model structure and equations are shown in Mathevet [65] and Bennett et al. [66]. The GR4H model requires precipitation and potential evapotranspiration (ETP) data as inputs. As previously mentioned, precipitation data were derived from the BC-RFP. ETP was calculated using the modified FAO Penman-Monteith method at hourly steps using the R package “water” [69,70], and interpolated along the study area with the Kriging method. For this, we used the meteorological data (temperature, relative humidity, solar radiation, and wind speed) provided by stations located in the study area.

3.4.2. Hydrological Modeling Setup

The GR4H model was calibrated and validated for the three study sub-basins: TRB, JRB, and NRB (Figure 1). We used the R package “airGR” [65,66] following a semi-distributed setting as shown in Figure A1.

Model calibration considered 40 months for the NRB and JRB (January 2016–March 2019), and 18 months for the TRB (July 2018–December 2019). Before this, we considered a warm-up period of six months to reduce the uncertainty associated with initial moisture conditions of the model. Model parameters were automatically calibrated by the shuffled complex

evolution algorithm [71], using the nonparametric variant of the Kling-Gupta efficiency (KGE*) as the objective function [72]. We chose this metric as it provides better agreement between simulated and observed streamflow at sub-daily and hourly steps compared to the Nash-Sutcliffe efficiency [72,73]. The flow duration curve (FDC) and the percent bias (PBIAS) were also used to assess the model performance in term of streamflow distribution and model bias. The mathematical definition of the evaluation metrics is shown in Table A2.

Model validation consisted of evaluating the GR4H outputs using the optimal parameters obtained in the calibration step. To perform the validation, we used 20 months for the NRB and JRB (April 2019–December 2020), and 12 months for the TRB (January 2020–December 2020).

3.4.3. Flash Flood Event Analysis

The five last flash flood events produced within the study area (Table 2) were used to assess the performance of the coupling of the BC-RFP and GR4H models during high flow conditions. These events were chosen based on:

1. Records of the National Service for Risk Management of Ecuador [44].
2. Streamflow thresholds defined by Hurtado et al. [35] and Lapo et al. [34] for flood events in the TRB, JRB, and NRB (Table 2).

For the event analysis, we focused on the differences between the simulated and observed behavior of four hydrograph aspects widely examined in flash flood modeling [74]: Streamflow dynamic or hydrograph shape, peak discharge, volume discharge, and peak timing.

Table 2. Information of the last five flash flood events produced within the study area.

Event	Start (Datetime)	Duration (h)	Peak Discharge (m ³ /s)		
			TRB	JRB	NRB
1	2017-09-02 19:00	53	1896	1160	3570
2	2018-07-22 01:00	51	657	2579	4574
3	2019-05-25 20:00	28	242	1184	6407
4	2019-06-20 00:00	72	250	2659	6338
5	2020-05-01 00:00	80	593	896	8925
Streamflow threshold for flood events			210	2200	4500

4. Results and Discussion

4.1. Preliminary Evaluation of the SPPs

The SPPs used as covariates in the integration framework showed non-satisfactory performances within the study area (Figure 3). In terms of the RMSE, the SPPs presented errors that ranged between 0.6 and 3.3 mm/h. Compared to previous studies [75-77], these values could be considered acceptable. However, CORR and KGE metrics were below 0.4, indicating a poor agreement between SPPs and observed precipitation data. Similarly, detection performances (POD < 0.6, FAR > 0.5, CSI < 0.4) suggested that SPPs cannot correctly capture the hourly precipitation occurrence. These results agreed with several authors [67-79] who previously found important limitations in precipitation estimates of SPPs at fine temporal scales over complex topography regions, as in the case of the study area.

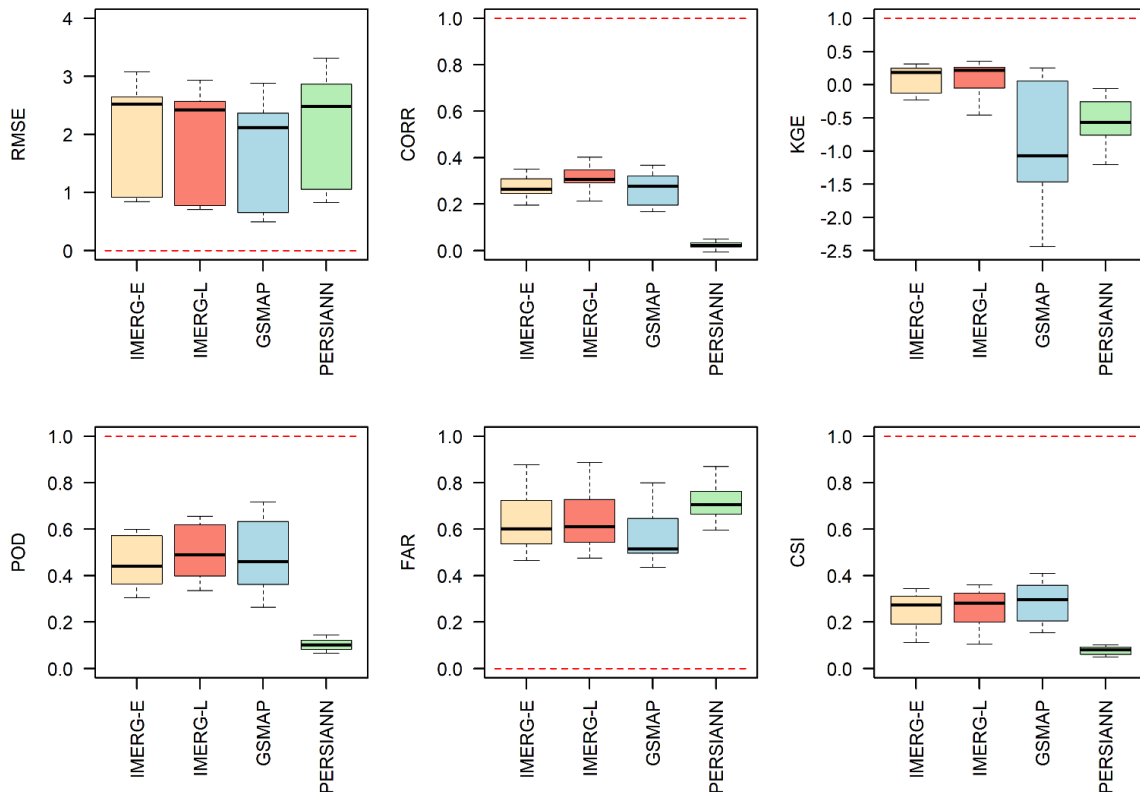


Figure 3. Performance assessment of the SPPs used as covariates within the integrative framework. The whisker-box plot shows the performance variation within the study area, considering each rain gauge as an individual data point. Red dashed line indicates the optimal value for each performance

metric: root mean square error (RMSE), correlation coefficient (CORR), Kling-Gupta efficiency (KGE), probability of detection (POD), false alarm ratio (FAR), and critical success index (CSI).

4.2. Variable Importance Analysis

The variable importance analysis revealed that all covariates, except PERSIANN, strongly influenced the performance of the integration framework as %IncMSE values ranged from 0.25 to 0.88 (Figure 4). The IMERG-E product and the soil-moisture change at root zone (ΔRM) were the most important covariates and hence those that contributed more information to precipitation estimates. Likewise, IMERG-L and soil moisture change at surface level (ΔSM) showed relatively high importance ($\%IncMSE > 50$). These findings complied with those of Bhuiyan et al. [80,81], who discussed that the synergy among IMERG- and SMAP-derived soil-moisture products provides relevant insights to improve the fitting of precipitation patterns.



Figure 4. Variable importance analysis. The %IncMSE represents the percentage increase in mean square error. Covariates with high %IncMSE generate a strong influence on the RFP model.

Monthly variability (MONTH) was the third most important predictor. However, its importance varied along the study area. Note that paramo does not present a strong precipitation seasonality [39,40], whereas the mountain forest and piedmont rainforest have the wettest season from March to July [82]. Altitude (ALT) and hourly variability (HOUR)

showed similar importance. Overall, both covariates are associated with the valley-mountain effect that generates convective precipitation events with high occurrence in the late afternoon and night along the study area [83].

As mentioned, PERSIANN was not a relevant covariate within the integration framework. This finding was consistent with the prior evaluation of SPPs (Figure 3), which indicated that PERSIANN was the worst performing product. In fact, this SPP presented no correlation with the observed data ($CORR < 0.1$) and the lowest detection skill (i.e., $CSI < 0.12$). As discussed Tan et al. [84], the low performance of PERSIANN is related to its low latency and hence lower processing compared to other SPPs. Note the PERSIANN product used in this study was derived from the cloud classification system that runs in real time.

4.3. Integration Framework Performance

The integration framework showed a high ability to capture the hourly precipitation within the study area (Figure 5). Precipitation estimates derived from RFP exhibited good performances for both training and testing periods ($CORR \approx 0.93$, $RMSE \approx 0.77$, and $KGE \approx 0.67$). However, these preliminary results presented a systematic error, underestimating events with intensities greater than 15 mm/h (Figure 5a,c). As discussed by Zhang et al. [85], the RF algorithm uses the average of all prediction trees to generate model outputs. Therefore, it tends to underestimate extreme precipitation events. Nevertheless, this error was minimized in the postprocessing step by applying a bias correction using the GQM method (Figure 5b,d). As result, the corrected precipitation estimates (BC-RFP) showed notable improvements in accuracy and better captured the highest precipitation intensities ($CORR > 0.95$, $RMSE < 0.65$, and $KGE > 0.83$).

While the aforementioned results provide information about precipitation intensity performances, they do not clearly denote the ability of the integration framework to capture the occurrence of precipitation events. Capturing the precipitation occurrence is important because even small amounts of rainfall can affect the initial soil moisture conditions in the study area with subsequent impacts on the flash flood generation [86].

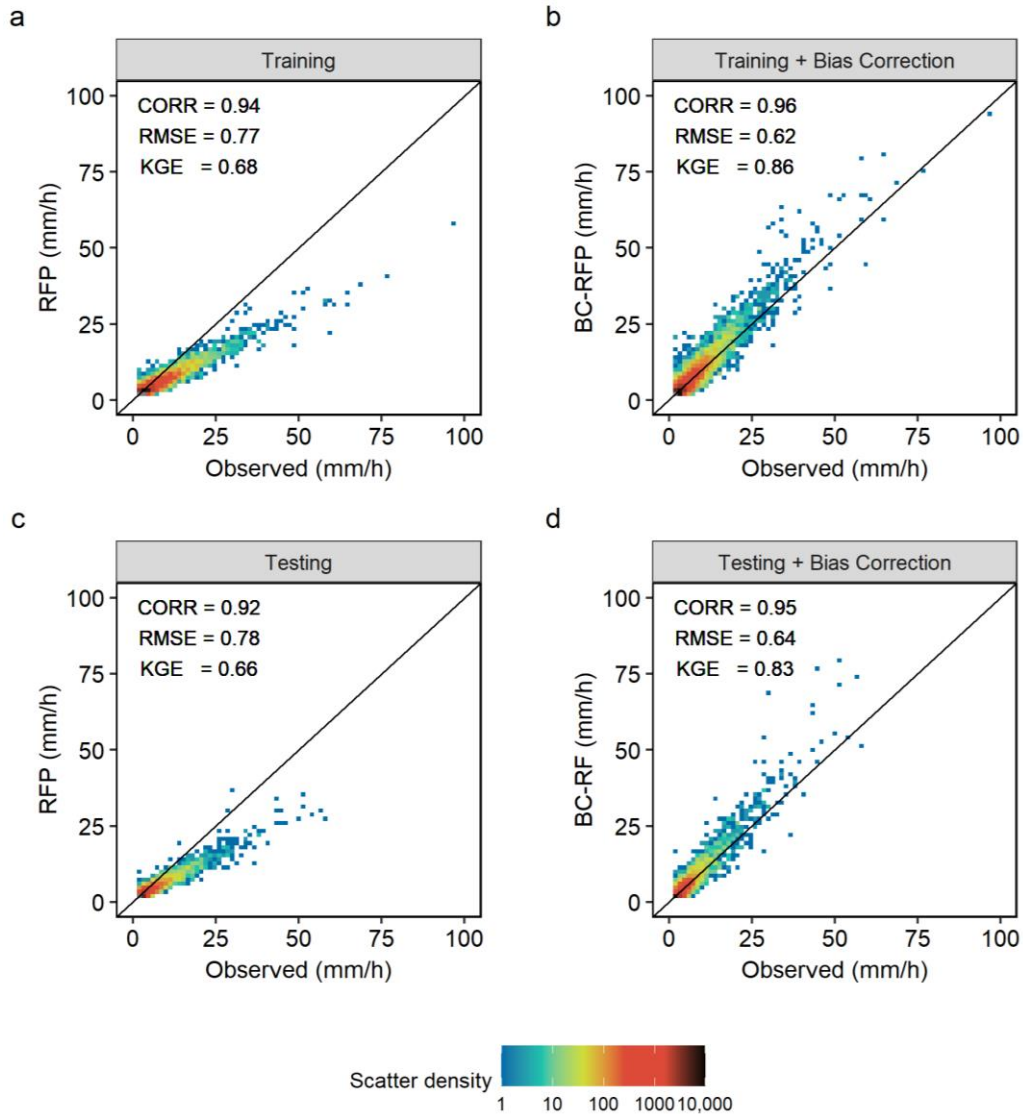


Figure 5. Scatter density plot for observed and simulated precipitation intensity at the hourly scale. **(a)** Training period without bias correction. **(b)** Training period with bias correction. **(c)** Testing period without bias correction. **(d)** Testing period with bias correction.

The precipitation detection ability of the BC-RFP model diminishes as the intensity threshold decreases, meaning that the BC-RFP model is less able to capture the correct magnitude of low-intensity events (Figure 6). Within the study area, low-intensity events (below 0.2 mm/h) mainly occur on the paramo. This denoted the difficulty of estimating precipitation at fine temporal scales over high-elevation regions [87]. For intensities between 2 and 50 mm/h, the precipitation detection ability (based on POD, FAR, and CSI) reaches the

highest performances, suggesting that the BC-RFP model correctly estimates both intensity and occurrence of precipitation events in this precipitation range. Above 50 mm/h, the detection performance decreases slightly compared to precipitation events below 50 mm/h. However, these results suggested that BC-RFP presents a high potential to detect flash flood caused by heavy rainfalls (i.e., 50-100 mm/h).

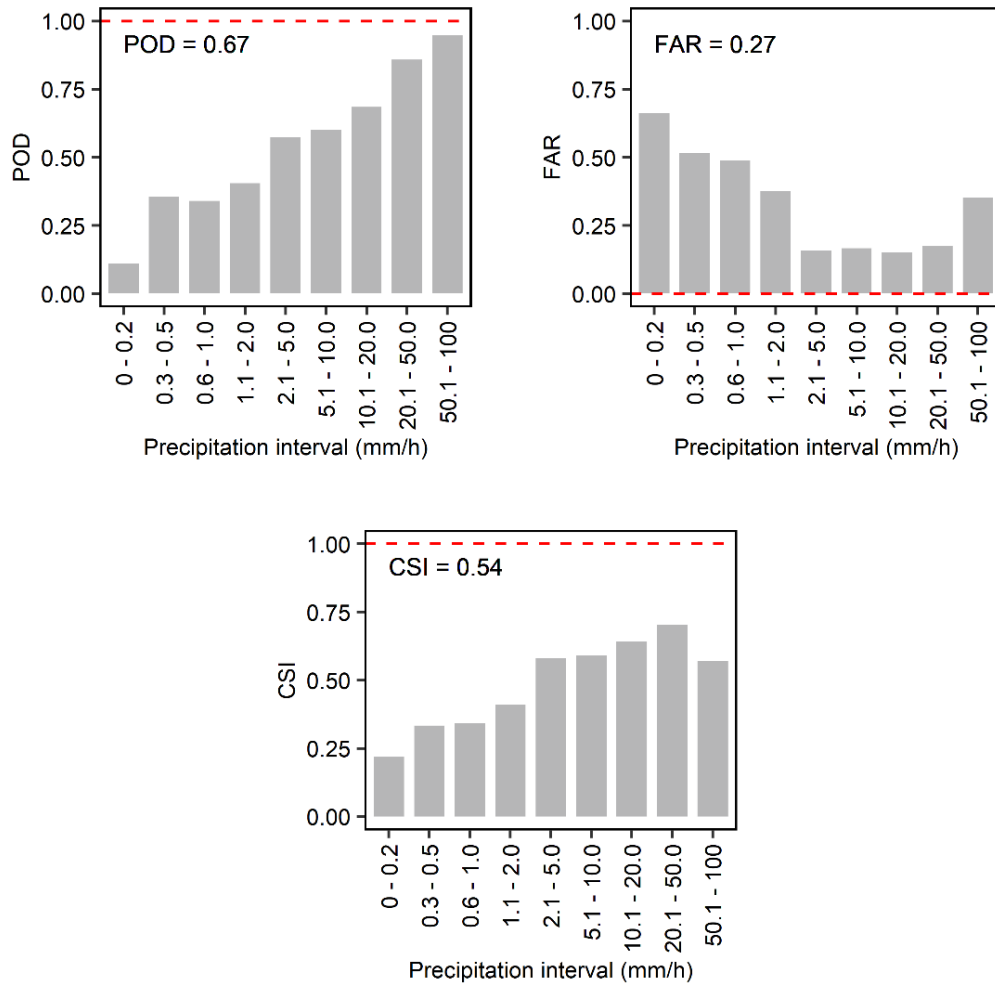


Figure 6. Assessments of the ability to detect the precipitation occurrence for BC-RFP using POD, FAR, and CSI metrics at different intensity thresholds. The analysis was carried out considering both training and testing periods. Red dashed lines indicate the optimal value for each performance metric.

Considering intensity thresholds altogether, the BC-RFP model showed satisfactory performances in detection metrics (POD = 0.67, FAR = 0.27, and CSI = 0.54). This indicates the proposed framework improved the detection ability between 43% and 88% compared to the

original SPPs (i.e., IMERG-E/L, GSMAP, and PERSIANN). In fact, general performances reached by the BC-RFP model were similar to those reported by more complex methods that use RF models to correct and downscale the hourly precipitation estimates [25,26].

4.4. Spatial Consistency Analysis

As shown in Figure 7, the spatial distribution of annual precipitation obtained by the BC-RFP model was consistent with climate precipitation trends that characterize the Andean-Amazon region (see Section 2). No anomalous or out-of-trend pixels were found in the paramo and mountain forest regions. However, few pixels located in the lowest reaches of the NRB (piedmont rainforest) showed an important overestimation.

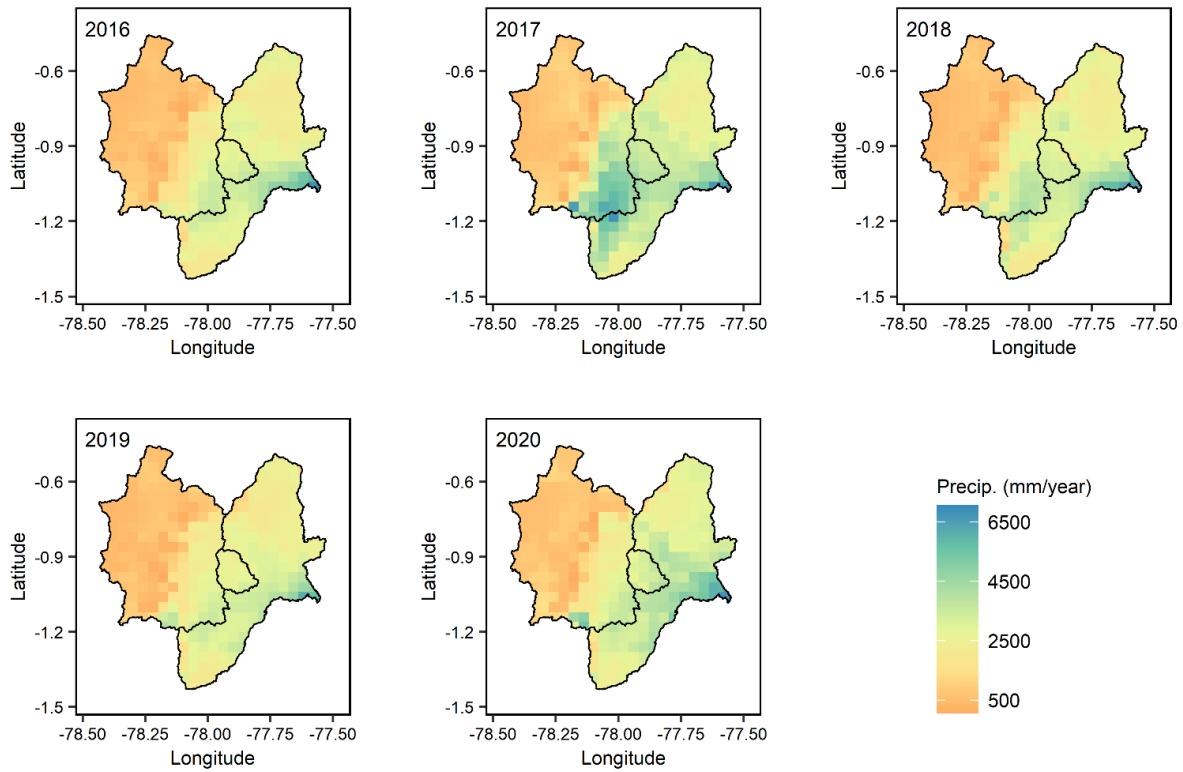


Figure 7. Distribution of annual precipitation obtained with BC-RFP used for the spatial consistency analysis along the study area (NRB).

While the long-term measurements in the aforementioned area indicate that annual precipitation does not exceed 5500 mm [88,89], the BC-RFP model showed values above 6500

mm/year. This can be explained by two reasons: (i) the SMAP-derived data exhibited the highest soil-moisture contents over the lowest reaches of the NRB, and (ii) the training of the integrative framework did not consider a rain gauge in this sector. Therefore, the BC-RFP model incorrectly interpreted these high moisture contents as more amounts of rainfall due to the lack of hourly precipitation data in the training set. Given that few pixels presented this problem, we considered they provided no significant impact in our hydrological modeling.

4.5. Calibration and Validation of the GR4H Model

The assessment of the BC-RFP model's ability to force precipitation input for the GR4H model presented satisfactory performances (Figure 8). Overall, KGE* values between simulated and observed streamflows were above the acceptable threshold ($KGE^* > 0.5$) [72]. Likewise, PBIAS showed scores below $\pm 20\%$, indicating a good fitting [90]. The visual assessment based on the flow duration curve (FDC) revealed that the combination of the BC-RFP and GR4H models correctly captured the cumulative frequency of the streamflow distribution, except above the 95th percentile where the streamflow was underestimated.

In the TRB, the GR4H model showed the highest performances, reaching KGE* of 0.87 and 0.79 for calibration and validation, respectively (Figure 8a). These yields were higher than those reported by Espitia et al. [68], who previously implemented the GR4H model in the TRB. The main limitation faced by previous hydrological studies in the TRB was the lack of spatial precipitation data [35,68]. Our results partially overcame this limitation and corroborated that streamflow simulations of the TRB can be improved by the spatialization of the precipitation.

Regarding the JRB, streamflow simulations showed ~30% lower performance than that shown by the TRB, reaching KGE* values of 0.65 and 0.54 for calibration and validation, respectively (Figure 8b). FDCs revealed a high underestimation of streamflow distribution above 300 m³/s that was corroborated by PBIAS that shows a value of -18.2% for the validation period. This notable reduction in model performance is explained by the larger hydrological heterogeneity of the JRB produced by its complex topography and the transition between the paramo and the mountain forest. In fact, various studies such as Du et al. [91] and Liu et al.

[92] have discussed that uncertainty on the parameter estimation increases considerably under these conditions. The error associated with low-intensity precipitation estimates produced in the paramo was another driver performance reduction in the JRB (see Section 4.3). Given the low ability of the BC-RFP model to detect drizzle events (>0.2 mm/h), the humidity conditions of the JRB may have been underestimated during most of the simulation time which affected the runoff generation [93].

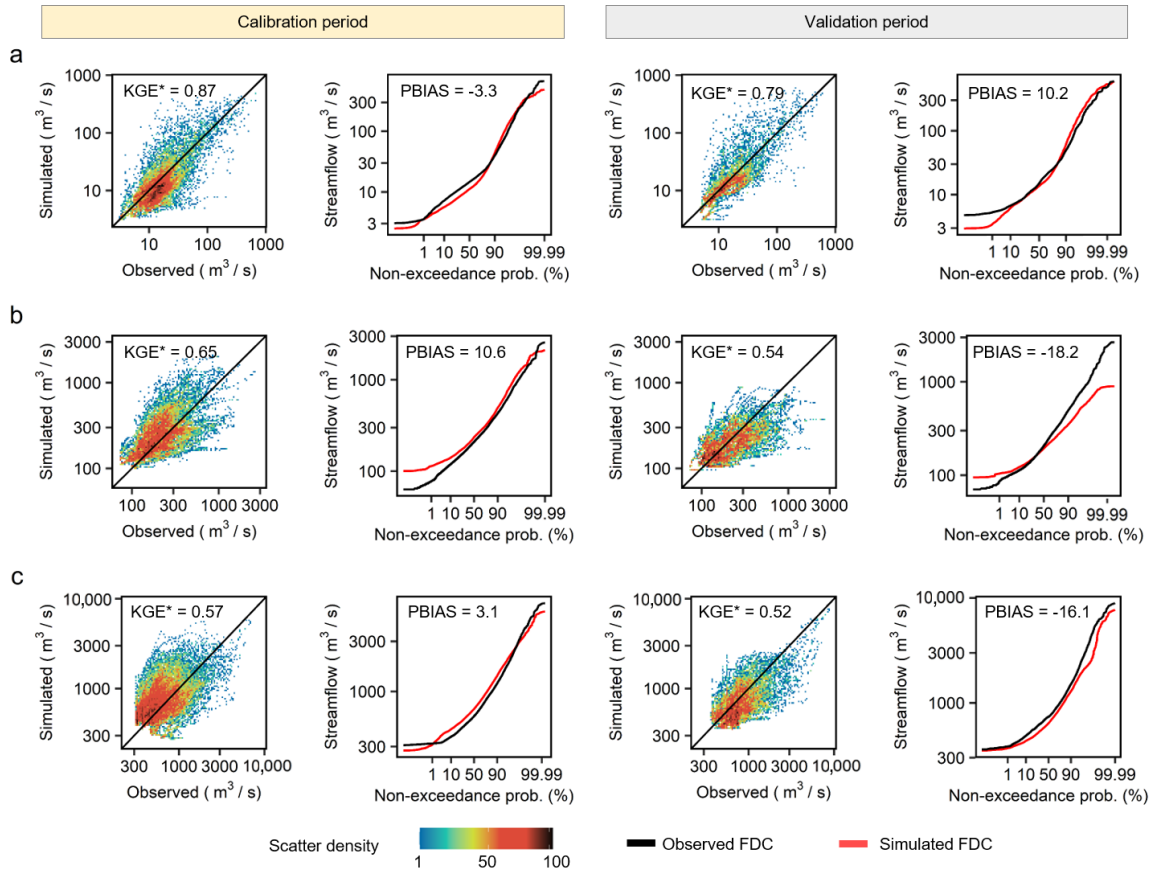


Figure 8. Performances of the GR4H model for calibration and validation periods, using the BC-RFP method as forcing precipitation input. **(a)** Tena River Basin, TRB. **(b)** Jatunyacu River Basin, JRB. **(c)** Upper Napo River Basin, NRB

Considering the whole study basin (NRB), the GR4H model showed KGE^* values of about 0.54 ± 0.03 . The streamflow was overestimated during calibration ($PBIAS = 3.1\%$) and underestimated during the validation ($PBIAS = -16.2\%$). Although this basin presented the lowest performances (Figure 8c), the FDC analysis indicated that high streamflows were better

simulated compared to the JRB. This confirms that regardless of the overestimation problem occurring in lowest reaches of the NRB (see Section 4.4), the BC-RFP model better captured the high precipitation events in the piedmont rainforest compared to other regions within the study area. Note the piedmont rain forest presented the highest precipitation intensities and hence produced more runoff within the NRB [37].

4.6. Flood Event Analysis

As discussed in the previous section, streamflow simulations of the GR4H model underestimated high discharges. For the last five flash flood events that occurred in the TRB, JRB, and NRB (Figure 9), simulated peak flows were 3.8% to 47.8% lower than observed peak flows (Table 3). Similarly, runoff volume was underestimated by 8.1% to 48.9% in most cases, especially during events 2, 3, and 4. Despite this, hydrograph shapes of the analyzed events were suitably simulated. Note that KGE* values ranged from 0.56 to 0.94. Moreover, the visual inspection of hourly precipitation pulses (i.e., hyetograph) revealed high similarities with the observed streamflow, meaning that the BC-RFP model properly captured the temporal distribution of precipitation over the study sub-basins.

Time differences between observed and simulated peak flows were no greater than ± 3 h, except for event 3 in the JRB (Figure 9c) and event 4 in the TRB (Figure 9d) where the peak timing difference was above ± 6 h (Table 3). In both cases, the peak precipitation pulses derived from the BC-RFP model presented better agreements with the observed peak flows contrasted to simulations (Figure 9). Considering the latter, errors in peak timing may be explained by the routing routine used in the semi-distributed GR4H model (i.e., the lag routing method; Table A3 and Table A4). Bentura et al. [94] highlighted that the lag routing method does not consider physical features of the channel, which may produce limitations in the propagation and routing of hydrographs over complex topography areas [95]. In spite of this, altogether, results provided sufficient evidence to propose the coupling of the BC-RFP and the GR4H models as a preliminary tool to recreate streamflow dynamics and flood events.

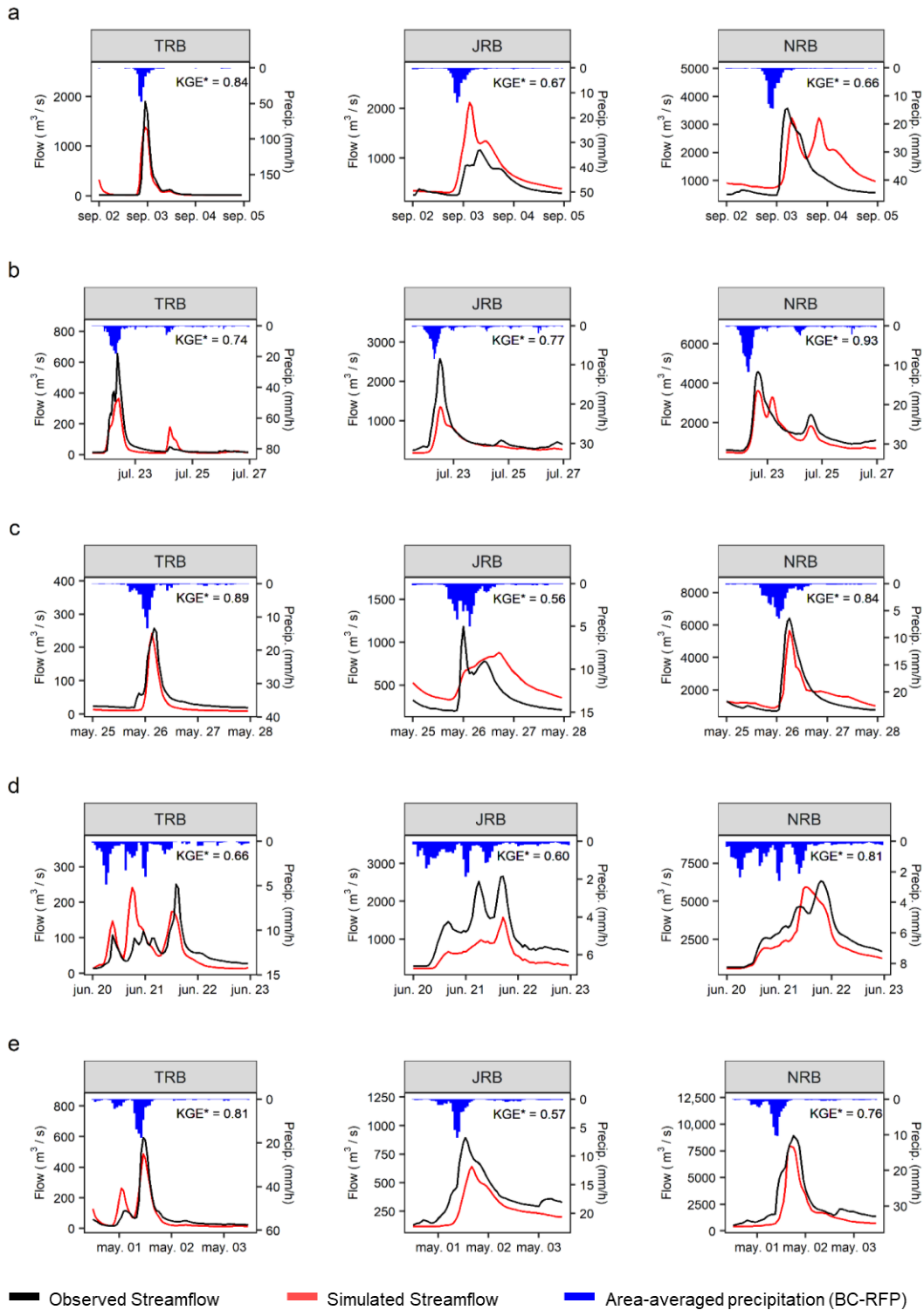


Figure 9. Observed and simulated hydrographs of the last five flash flood events that occurred in Tena River Basin (TRB), Jatunyacu River Basin (JRB), and upper Napo River Basin at Ahuano (NRB). (a) Event 1, September 2017. (b) Event 2, July 2018. (c) Event 3, May 2019. (d) Event 4, June 2019. (e) Event 5, May 2020.

Table 3. Results of the event analysis considering the last five floods that occurred in the Tena River Basin (TRB), Jatunyacu River Basin (JRB), and upper Napo River Basin (NRB).

Event	Basin	Peak Flow (m ³ /s)			Runoff Volume (Hm ³)			Difference in Peak Timing (h)
		Obs.	Sim.	Diff. (%)	Obs.	Sim.	Diff. (%)	
1	TRB	1896	1379	-27.2	33.8	29.9	-11.5	0
	JRB	1160	2117	82.4	109.4	160.8	46.9	-3
	NRB	3570	3231	-9.5	245.5	333.7	35.9	2
2	TRB	657	365	-44.4	30.1	23.0	-23.6	0
	JRB	2579	1344	-47.8	270.3	198.0	-26.2	1
	NRB	4574	3614	-20.9	390.5	359.0	-8.1	1
3	TRB	242	258	6.5	8.7	5.8	-33.3	0
	JRB	1184	877	-25.9	60.2	73.0	21.2	12
	NRB	6407	5661	-11.6	276.2	240.4	-13.0	-1
4	TRB	250	241	-3.8	17.2	16.6	-3.5	-3
	JRB	2659	1573	-40.8	294.3	150.4	-48.9	0
	NRB	6338	5952	-6.1	733.4	605.5	-17.4	-6
5	TRB	593	486	-18.0	19.7	21.3	8.12	0
	JRB	896	640	-28.6	100.1	69.4	-44.2	2
	NRB	8925	7980	-10.6	668.9	453.9	-47.4	-1

5. Future Perspectives and Final Remarks

Precipitation estimates derived from the integration framework (i.e., BC-RFP) showed a high ability to reproduce the intensity, distribution, and occurrence of rainfall events on hourly scales over the study area. Indeed, the BC-RFP model improved the detection ability between 43% and 88%, reducing the estimation error between 72% and 93% compared to the IMERG, GSMAP, and PERSIANN products. This contributes new evidence to corroborate that the combination of soil-moisture products (SMPs) with satellite-based precipitation products (SPPs) significantly improves the spatiotemporal precipitation estimates over complex topography areas, such as the Andean-Amazon region.

Overall, the latency of the BC-RFP model depends on the soil-moisture products used as predictors within the integration framework (~7 days; Table 1). Thus, the use of the BC-RFP model in real-time forecasting systems is limited. However, as we discussed in previous sections, the BC-RFP model provides suitable information to improve the parameterization of hydrological models that are indispensable components of flood-forecasting systems. In fact, our results show that the combination of the BC-RFP and the GR4H models better simulate the fast-hydrological responses of the TRB, JRB, and NRB. However, simulations still present some limitations, such as the underestimation of peak streamflows, that could be addressed by testing other rainfall-runoff models. Physics-based distributed models (e.g., SWAT, TESTIS) are alternatives to reduce the uncertainties produced by the high hydrological heterogeneity of the study sub-basins.

Given that the proposed framework offers a robust way to estimate hourly precipitation dynamics, it opens up new opportunities for the physical parameterization of numerical weather models (e.g., WRF) over the Ecuadorian Andean-Amazon region. These models are essential for flood forecasting and early warning systems, as they provide valuable information on the future atmospheric state that could produce heavy rainfalls. However, there are no studies that determine the optimal physical schemes of the WRF model in the Ecuadorian Andean-Amazon region. Thus, we consider that future studies should focus on this underexplored issue.

The information generated in this study not only contributes to flood forecast or weather prediction but also to new research avenues on environmental modelling, providing relevant insight in different research fields such as ecology, ecohydrology, hydrogeology, water quality, and hence integrated water resources management over the Andean-Amazon region.

6. Appendix

Table A1. Statistical criteria used to evaluate the performance of the integrative framework that combine multiples SPPs and SMPs with observed precipitation data and spatio-temporal covariates.

Metric	Definition	Optimum value	Range	Unit
RMSE	$RMSE = \sqrt{\frac{\sum_{i=1}^n (S_i - O_i)^2}{n}}$	0	(0, Inf)	mm/h
CORR	$CORR = \frac{cov(S, O)}{\sqrt{var(S)} \sqrt{var(O)}}$	1	(-1, 1)	-
KGE	$KGE = 1 - \sqrt{(\alpha - 1)^2 + (\beta - 1)^2 + (r - 1)^2}$	1	(-Inf, 1)	-
POD	$POD = \frac{A}{A + B}$	1	(0, 1)	-
FAR	$FAR = \frac{C}{A + C}$	0	(0, 1)	-
CSI	$CSI = \frac{A}{A + B + C}$	1	(0, 1)	-

Where, **n** is the total number of observations, **Si** is the i-th simulated element, **Oi** is the i-th observed element, **cov()** is the covariance, **var()** is the variance, **α** is the ratio between simulated and observed mean, **β** is the ratio between simulated and observed standard deviation, **r** = CORR, **A** is the number of hits (**Si** > 0 and **Oi** > 0), **B** is the number of misses (**Si** = 0 and **Oi** > 0), **C** is the number of false positive (**Si** > 0 and **Oi** = 0)

Table A2. Statistical criteria used to evaluate the performance of the GR4H model.

Metric	Definition	Optimum value	Range	Unit
KGE*	$KGE^* = 1 - \sqrt{(\alpha - 1)^2 + (\beta_{NP} - 1)^2 + (r_{NP} - 1)^2}$	1	(-Inf, 1)	-
PBIAS	$PBIAS = \frac{\sum_{i=1}^n (S_i - O_i)}{\sum_{i=1}^n (O_i)}$	0	(-1, 1)	-

For KGE*, the variability and dynamic terms (i.e. **β** and **r**, see Table A1) are expressed in non-parametric way using the flow duration curve (**β_{NP}**) and the Spearman rank correlation (**r_{NP}**), respectively. Mathematical definitions are show in equations A1 and A2.

$$\beta_{NP} = 1 - \frac{1}{2} \sum_{k=1}^n \left| \frac{Q_{sim}(I_k) - Q_{obs}(J_k)}{n} \right| \quad (A1)$$

$$r_{NP} = \frac{\sum_{i=1}^n (R_{Obs}(i) - \bar{R}_{Obs}) (R_{Sim}(i) - \bar{R}_{Sim})}{\sqrt{(\sum_{i=1}^n (R_{Obs}(i) - \bar{R}_{Obs})^2) (\sum_{i=1}^n (R_{Sim}(i) - \bar{R}_{Sim})^2)}} \quad (A2)$$

Where, I_k and J_k represent the time steps when the k th largest flow occurs within the simulated (Q_{sim}) and observed (Q_{obs}) time series, respectively. R_{obs} and R_{sim} are the ranks of the observed and simulated streamflow, respectively.

Table A3. Optimal parameter of the GR4H model for each hydrological unit.

Hydrological Unit	Drainage area (km ²)	X1 (mm)	X2 (mm/h)	X3 (mm)	X4 (h)
1	328.39	372.531	3.545	91.785	1.457
2	466.98	798.960	2.912	203.279	5.888
3	369.02	1427.643	-0.616	381.813	6.067
4	423.61	372.098	4.673	208.614	3.718
5	319.81	862.500	-3.369	25.443	4.300
6	377.84	1655.687	-2.707	37.678	5.290
7	397.35	637.224	-2.467	42.853	11.838
8	443.70	1525.332	-1.473	95.359	4.400
9	290.62	7793.437	5.571	11.600	46.452
10	250.62	3343.290	0.395	376.779	20.223
11	342.42	1965.463	2.554	306.836	16.395
12	317.35	7165.090	-3.850	672.142	22.799
13	239.31	1764.858	0.237	9.706	4.586
14	230.22	2624.721	9.469	929.230	6.712
15	423.28	195.575	1.922	657.576	11.714
16	312.19	10.933	-0.507	98.951	1.902
17	319.57	24.993	4.878	45.301	4.939
18	240.08	10.734	6.262	66.297	13.210

To transfer the volume of runoff generated in each hydrological unit (Figure B1), the semi-distributed GR4H model uses the Lag Routing Method. For this method is required to know the travel time (or lag time). This parameter represents the time that the inflow hydrograph will be translated as it moves through the reach. Calibrated lag times are presented as follows.

Table A4. Calibrated lag times for each connection among the hydrological units.

Hydrological Unit		Lag time (h)
Upstream	Downstream	
1	2	0.81
2	3	2.84
4	5	3.09
3	5	3.53
6	7	2.33
7	8	4.01
9	10	5.54
10	11	0.97
12	13	3.15
11	14	6.89
13	14	5.96
15	16	3.94
16	17	10.84
8	17	10.47
17	18	7.10

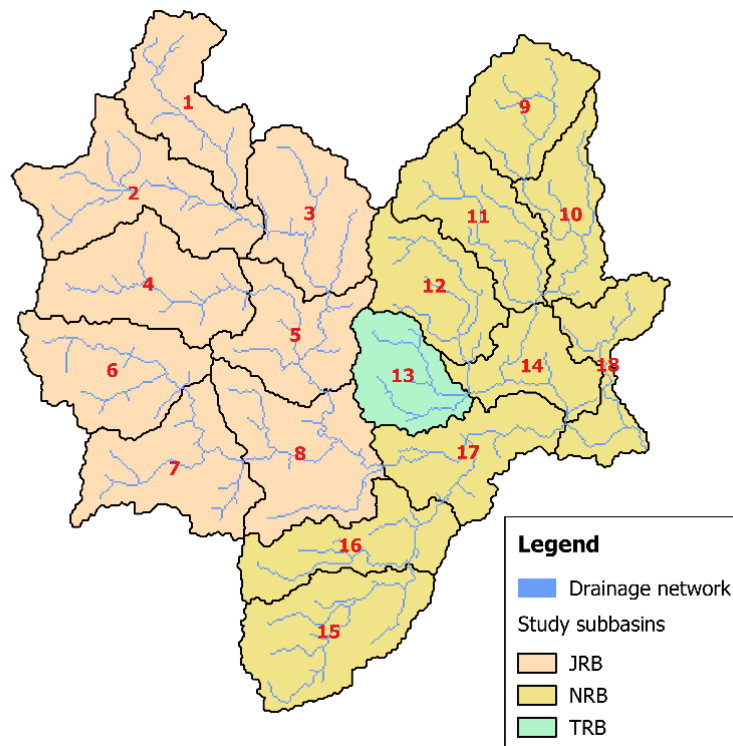


Figure A1. Disaggregation of the study sub-basins (TRB, JRB, and NRB) into 18 hydrological units for the semi-distributed setting of the GR4H model.

7. References

1. Sun, Q.; Miao, C.; Duan, Q.; Ashouri, H.; Sorooshian, S.; Hsu, K. A Review of Global Precipitation Data Sets: Data Sources, Estimation, and Intercomparisons. *Rev. Geophys.* 2018, *56*, 79–107.
2. Zanchetta, A.; Coulibaly, P. Recent Advances in Real-Time Pluvial Flash Flood Forecasting. *Water* 2020, *12*, 570.
3. Alazzy, A.A.; Lü, H.; Chen, R.; Ali, A.B.; Zhu, Y.; Su, J. Evaluation of Satellite Precipitation Products and Their Potential Influence on Hydrological Modeling over the Ganzi River Basin of the Tibetan Plateau. *Adv. Meteorol.* 2017, *2017*, 3695285.
4. Xu, H.; Xu, C.-Y.; Chen, H.; Zhang, Z.; Li, L. Assessing the influence of rain gauge density and distribution on hydrological model performance in a humid region of China. *J. Hydrol.* 2013, *505*, 1–12.
5. Derin, Y.; Anagnostou, E.; Berne, A.; Borga, M.; Boudevillain, B.; Buytaert, W.; Chang, C.-H.; Chen, H.; Delrieu, G.; Hsu, Y.; et al. Evaluation of GPM-Era Global Satellite Precipitation Products over Multiple Complex Terrain Regions. *Remote Sens.* 2019, *11*, 2936.
6. Domeneghetti, A.; Schumann, G.J.-P.; Tarpanelli, A. Preface: Remote Sensing for Flood Mapping and Monitoring of Flood Dynamics. *Remote Sens.* 2019, *11*, 943.
7. Villarini, G.; Krajewski, W.F.; Smith, J.A. New paradigm for statistical validation of satellite precipitation estimates: Application to a large sample of the TMPA 0.25° 3-hourly estimates over Oklahoma. *J. Geophys. Res.* 2009, *114*, D12106.
8. Maggioni, V.; Sapiano, M.R.P.; Adler, R.F. Estimating Uncertainties in High-Resolution Satellite Precipitation Products: Systematic or Random Error? *J. Hydrometeorol.* 2016, *17*, 1119–1129.
9. Serrat-Capdevila, A.; Valdes, J.B.; Stakhiv, E.Z. Water Management Applications for Satellite Precipitation Products: Synthesis and Recommendations. *JAWRA J. Am. Water Resour. Assoc.* 2014, *50*, 509–525.
10. Ciupak, M.; Ozga-Zielinski, B.; Adamowski, J.; Deo, R.C.; Kochanek, K. Correcting Satellite Precipitation Data and Assimilating Satellite-Derived Soil Moisture Data to Generate Ensemble Hydrological Forecasts within the HBV Rainfall-Runoff Model. *Water* 2019, *11*, 2138.
11. Tobin, K.J.; Bennett, M.E. Adjusting Satellite Precipitation Data to Facilitate Hydrologic Modeling. *J. Hydrometeorol.* 2010, *11*, 966–978.
12. He, Z.; Hu, H.; Tian, F.; Ni, G.; Hu, Q. Correcting the TRMM rainfall product for hydrological modelling in sparsely-gauged mountainous basins. *Hydrol. Sci. J.* 2017, *62*, 306–318.

13. Lu; Tang; Wang; Liu; Wei; Zhang The Development of a Two-Step Merging and Downscaling Method for Satellite Precipitation Products. *Remote Sens.* 2020, *12*, 398.
14. Hessami, M.; Gachon, P.; Ouarda, T.B.M.J.; St-Hilaire, A. Automated regression-based statistical downscaling tool. *Environ. Model. Softw.* 2008, *23*, 813–834.
15. Duan, Z.; Bastiaanssen, W.G.M. First results from Version 7 TRMM 3B43 precipitation product in combination with a new downscaling–calibration procedure. *Remote Sens. Environ.* 2013, *131*, 1–13.
16. Chen, C.; Zhao, S.; Duan, Z.; Qin, Z. An Improved Spatial Downscaling Procedure for TRMM 3B43 Precipitation Product Using Geographically Weighted Regression. *IEEE J. Sel. Top. Appl. Earth Obs. Remote Sens.* 2015, *8*, 4592–4604.
17. Bhatti, H.; Rientjes, T.; Haile, A.; Habib, E.; Verhoef, W. Evaluation of Bias Correction Method for Satellite-Based Rainfall Data. *Sensors* 2016, *16*, 884.
18. Vernimmen, R.R.E.; Hooijer, A.; Aldrian, E.; van Dijk, A.I.J.M. Evaluation and bias correction of satellite rainfall data for drought monitoring in Indonesia. *Hydrol. Earth Syst. Sci.* 2012, *16*, 133–146.
19. Hashemi, H.; Nordin, M.; Lakshmi, V.; Huffman, G.J.; Knight, R. Bias Correction of Long-Term Satellite Monthly Precipitation Product (TRMM 3B43) over the Conterminous United States. *J. Hydrometeorol.* 2017, *18*, 2491–2509.
20. Saber, M.; Yilmaz, K. Evaluation and Bias Correction of Satellite-Based Rainfall Estimates for Modelling Flash Floods over the Mediterranean region: Application to Karpuz River Basin, Turkey. *Water* 2018, *10*, 657.
21. Chen, F.; Yuan, H.; Sun, R.; Yang, C. Streamflow simulations using error correction ensembles of satellite rainfall products over the Huaihe river basin. *J. Hydrol.* 2020, *589*, 125179.
22. Maggioni, V.; Massari, C. On the performance of satellite precipitation products in riverine flood modeling: A review. *J. Hydrol.* 2018, *558*, 214–224.
23. Camici, S.; Crow, W.T.; Brocca, L. Recent advances in remote sensing of precipitation and soil moisture products for riverine flood prediction. In *Extreme Hydroclimatic Events and Multivariate Hazards in a Changing Environment*; Elsevier: Amsterdam, The Netherlands, 2019; pp. 247–266.
24. Le, X.-H.; Lee, G.; Jung, K.; An, H.; Lee, S.; Jung, Y. Application of Convolutional Neural Network for Spatiotemporal Bias Correction of Daily Satellite-Based Precipitation. *Remote Sens.* 2020, *12*, 2731.
25. Chivers, B.D.; Wallbank, J.; Cole, S.J.; Sebek, O.; Stanley, S.; Fry, M.; Leontidis, G. Imputation of

- missing sub-hourly precipitation data in a large sensor network: A machine learning approach. *J. Hydrol.* 2020, *588*, 125126.
26. Wolfensberger, D.; Gabella, M.; Boscacci, M.; Germann, U.; Berne, A. RainForest: A random forest algorithm for quantitative precipitation estimation over Switzerland. *Atmos. Meas. Tech.* 2021, *14*, 3169–3193.
 27. Baez-Villanueva, O.M.; Zambrano-Bigiarini, M.; Beck, H.E.; McNamara, I.; Ribbe, L.; Nauditt, A.; Birkel, C.; Verbist, K.; Giraldo-Osorio, J.D.; Xuan Tinh, N. RF-MEP: A novel Random Forest method for merging gridded precipitation products and ground-based measurements. *Remote Sens. Environ.* 2020, *239*, 111606.
 28. Kolluru, V.; Kolluru, S.; Wagle, N.; Acharya, T.D. Secondary Precipitation Estimate Merging Using Machine Learning: Development and Evaluation over Krishna River Basin, India. *Remote Sens.* 2020, *12*, 3013.
 29. Crow, W.T.; van den Berg, M.J.; Huffman, G.J.; Pellarin, T. Correcting rainfall using satellite-based surface soil moisture retrievals: The Soil Moisture Analysis Rainfall Tool (SMART). *Water Resour. Res.* 2011, *47*, W08521.
 30. Pellarin, T.; Louvet, S.; Gruhier, C.; Quantin, G.; Legout, C. A simple and effective method for correcting soil moisture and precipitation estimates using AMSR-E measurements. *Remote Sens. Environ.* 2013, *136*, 28–36.
 31. Brocca, L.; Moramarco, T.; Melone, F.; Wagner, W.; Hasenauer, S.; Hahn, S. Assimilation of Surface- and Root-Zone ASCAT Soil Moisture Products Into Rainfall Runoff Modeling. *IEEE Trans. Geosci. Remote Sens.* 2012, *50*, 2542–2555.
 32. Bhuiyan, M.A.E.; Nikolopoulos, E.I.; Anagnostou, E.N.; Quintana-Seguí, P.; Barella-Ortiz, A. A nonparametric statistical technique for combining global precipitation datasets: Development and hydrological evaluation over the Iberian Peninsula. *Hydrol. Earth Syst. Sci.* 2018, *22*, 1371–1389.
 33. Chan, S.K.; Bindlish, R.; O'Neill, P.; Jackson, T.; Njoku, E.; Dunbar, S.; Chaubell, J.; Piepmeier, J.; Yueh, S.; Entekhabi, D.; et al. Development and assessment of the SMAP enhanced passive soil moisture product. *Remote Sens. Environ.* 2018, *204*, 931–941.
 34. Lapo, C. Análisis Espacio-Temporal del Riesgo de Inundacion Mediante Simulación Espacial en la Parroquia Puerto Napo, Universidad Nacional de Chimborazo. 2017. Available online: <http://dspace.unach.edu.ec/handle/51000/5842> (accessed on 20 March 2021).
 35. Hurtado, J.; Acero Triana, J.S.; Espitia-Sarmiento, E.; Jarrín-Pérez, F. Flood Hazard Assessment in Data-Scarce Watersheds Using Model Coupling, Event Sampling, and Survey Data. *Water* 2020, *12*, 2768.

36. Laraque, A.; Bernal, C.; Bourrel, L.; Darrozes, J.; Christophoul, F.; Armijos, E.; Fraizy, P.; Pombosa, R.; Guyot, J.L. Sediment budget of the Napo River, Amazon basin, Ecuador and Peru. *Hydrol. Process.* 2009, *23*, 3509–3524.
37. Wittmann, H.; von Blanckenburg, F.; Guyot, J.L.; Laraque, A.; Bernal, C.; Kubik, P.W. Sediment production and transport from in situ-produced cosmogenic ¹⁰Be and river loads in the Napo River basin, an upper Amazon tributary of Ecuador and Peru. *J. S. Am. Earth Sci.* 2011, *31*, 45–53.
38. Muñoz, P.; Orellana-Alvear, J.; Willems, P.; Célleri, R. Flash-Flood Forecasting in an Andean Mountain Catchment—Development of a Step-Wise Methodology Based on the Random Forest Algorithm. *Water* 2018, *10*, 1519.
39. Padrón, R.S.; Wilcox, B.P.; Crespo, P.; Célleri, R. Rainfall in the Andean Páramo: New Insights from High-Resolution Monitoring in Southern Ecuador. *J. Hydrometeorol.* 2015, *16*, 985–996.
40. Ochoa-Sánchez, A.; Crespo, P.; Célleri, R. Quantification of rainfall interception in the high Andean tussock grasslands. *Ecohydrology* 2018, *11*, e1946.
41. Laraque, A.; Ronchail, J.; Cochonneau, G.; Pombosa, R.; Guyot, J.L. Heterogeneous Distribution of Rainfall and Discharge Regimes in the Ecuadorian Amazon Basin. *J. Hydrometeorol.* 2007, *8*, 1364–1381.
42. IHS Meteorological and Hydrological Stations Network. Available online: <http://hidrometeorologia.ikiam.edu.ec/meteoviewer> (accessed on 24 March 2021).
43. Cruz Cueva, G.E. *Elaboración de un Plan de Contingencia por Inundación del río Tena en Los Barrios: Bellavista, Las Hierbitas, El Tereré y Barrio Central de la Ciudad de Tena*; PUCE: Quito, Ecuador, 2016.
44. Servicio Nacional de Gestión de Riesgos y Emergencias. *Base de Datos de Eventos de Inundación Registrados en Napo y Orellana, Periodo 2010–2019*; SNGRE: Tena, Ecuador, 2020.
45. INAMHI. *Anuario Hidrológico del Ecuador: 2014–2016*; INAMHI: Quito, Ecuador, 2019.
46. INAMHI Red de Estaciones Automáticas Hidrometeorológicas. Available online: <http://186.42.174.236/InamhiEmas/> (accessed on 12 June 2020).
47. Chebana, F.; Dabo-Niang, S.; Ouarda, T.B.M.J. Exploratory functional flood frequency analysis and outlier detection. *Water Resour. Res.* 2012, *48*.
48. Skofronick-Jackson, G.; Kirschbaum, D.; Petersen, W.; Huffman, G.; Kidd, C.; Stocker, E.; Kakar, R. The Global Precipitation Measurement (GPM) mission’s scientific achievements and societal contributions: Reviewing four years of advanced rain and snow observations. *Q. J. R. Meteorol. Soc.* 2018, *144*, 27–48.

49. Skofronick-Jackson, G.; Petersen, W.A.; Berg, W.; Kidd, C.; Stocker, E.F.; Kirschbaum, D.B.; Kakar, R.; Braun, S.A.; Huffman, G.J.; Iguchi, T.; et al. The Global Precipitation Measurement (GPM) Mission for Science and Society. *Bull. Am. Meteorol. Soc.* 2017, *98*, 1679–1695.
50. Kubota, T.; Shige, S.; Hashizume, H.; Aonashi, K.; Takahashi, N.; Seto, S.; Hirose, M.; Takayabu, Y.N.; Ushio, T.; Nakagawa, K.; et al. Global Precipitation Map Using Satellite-Borne Microwave Radiometers by the GSMaP Project: Production and Validation. *IEEE Trans. Geosci. Remote Sens.* 2007, *45*, 2259–2275.
51. Aohashi, K.; Awaka, J.; Hirose, M.; Kozu, T.; Kubota, T.; Liu, G.; Shige, S.; Kida, S.; Seto, S.; Takahashi, N.; et al. GSMaP Passive Microwave Precipitation Retrieval Algorithm: Algorithm Description and Validation. *J. Meteorol. Soc. Jpn.* 2009, *87*, 119–136.
52. Mahrooghy, M.; Anantharaj, V.G.; Younan, N.H.; Aanstoos, J.; Hsu, K.-L. On an Enhanced PERSIANN-CCS Algorithm for Precipitation Estimation. *J. Atmos. Ocean. Technol.* 2012, *29*, 922–932.
53. Khodadoust, S.; Saghafian, B.; Moazami, S. Comprehensive evaluation of 3-hourly TRMM and half-hourly GPM-IMERG satellite precipitation products. *Int. J. Remote Sens.* 2017, *38*, 558–571.
54. Ma, M.; Wang, H.; Jia, P.; Tang, G.; Wang, D.; Ma, Z.; Yan, H. Application of the GPM-IMERG Products in Flash Flood Warning: A Case Study in Yunnan, China. *Remote Sens.* 2020, *12*, 1954.
55. Bakheet, A.; Sefelnasr, A. Application of Remote Sensing data (GSMaP) to Flash Flood Modeling in an Arid Environment, Egypt. *Int. Conf. Chem. Environ. Eng.* 2018, *9*, 252–272.
56. Tang, S.; Li, R.; He, J.; Wang, H.; Fan, X.; Yao, S. Comparative Evaluation of the GPM IMERG Early, Late, and Final Hourly Precipitation Products Using the CMPA Data over Sichuan Basin of China. *Water* 2020, *12*, 554.
57. Senanayake, I.P.; Yeo, I.-Y.; Willgoose, G.R.; Hancock, G.R. Disaggregating satellite soil moisture products based on soil thermal inertia: A comparison of a downscaling model built at two spatial scales. *J. Hydrol.* 2021, *594*, 125894.
58. Lepot, M.; Aubin, J.-B.; Clemens, F. Interpolation in Time Series: An Introductory Overview of Existing Methods, Their Performance Criteria and Uncertainty Assessment. *Water* 2017, *9*, 796.
59. Zhang, J.; Fan, H.; He, D.; Chen, J. Integrating precipitation zoning with random forest regression for the spatial downscaling of satellite-based precipitation: A case study of the Lancang–Mekong River basin. *Int. J. Climatol.* 2019, *39*, 3947–3961.
60. Nashwan, M.S.; Shahid, S. Symmetrical uncertainty and random forest for the evaluation of gridded precipitation and temperature data. *Atmos. Res.* 2019, *230*, 104632.

61. Das, S.; Chakraborty, R.; Maitra, A. A random forest algorithm for nowcasting of intense precipitation events. *Adv. Sp. Res.* 2017, *60*, 1271–1282.
62. Liaw, A.; Wiener, M. Classification and Regression by randomForest. *News. R Proj.* 2002, *2*, 18–22.
63. Mendez, M.; Maathuis, B.; Hein-Griggs, D.; Alvarado-Gamboa, L.-F. Performance Evaluation of Bias Correction Methods for Climate Change Monthly Precipitation Projections over Costa Rica. *Water* 2020, *12*, 482.
64. Fang, G.H.; Yang, J.; Chen, Y.N.; Zammit, C. Comparing bias correction methods in downscaling meteorological variables for a hydrologic impact study in an arid area in China. *Hydrol. Earth Syst. Sci.* 2015, *19*, 2547–2559.
65. Mathevet, T. Quels Modeles Pluie-Debit Globaux au Pas de Temps Horaire? Développements Empiriques et Intercomparaison de Modeles Sur un Large Echantillon de Bassins Versants, Ecole Nationale Du Genie Rural, Des eaux et des Forêts. 2005. Available online: <https://hal.inrae.fr/tel-02587642> (accessed on 14 September 2020).
66. Bennett, J.C.; Robertson, D.E.; Shrestha, D.L.; Wang, Q.J.; Enever, D.; Hapuarachchi, P.; Tuteja, N.K. A System for Continuous Hydrological Ensemble Forecasting (SCHEF) to lead times of 9 days. *J. Hydrol.* 2014, *519*, 2832–2846.
67. Llauca, H.; Lavado-Casimiro, W.; León, K.; Jimenez, J.; Traverso, K.; Rau, P. Assessing Near Real-Time Satellite Precipitation Products for Flood Simulations at Sub-Daily Scales in a Sparsely Gauged Watershed in Peruvian Andes. *Remote Sens.* 2021, *13*, 826.
68. Espitia, E.F.; Chancay, J.E.; Acero-Triana, J. A Preliminary Approach for Flood Forecasting in Data-Scarce Ecuadorian Amazon Subbasin Using the GR4H model. Submitted IEI. 2021. Available online: <http://hidrometeorologia.ikiam.edu.ec/research/articles/espitia2021.pdf> (accessed on 14 September 2020).
69. Olmedo, G.F.; Ortega-Farías, S.; de La Fuente-Sáiz, D.; Fonseca, D.; Fuentes-Peñailillo, F. water: Tools and Functions to Estimate Actual Evapotranspiration Using Land Surface Energy Balance Models in R. *R J.* 2016, *8*, 352.
70. Snyder, R.; Eching, S. Penman-Monteith (hourly) Reference Evapotranspiration Equations for Estimating ETos and ETrs with Hourly Weather Data. *Regents Univ. Calif.* 2001, *8*. Available online: https://www.researchgate.net/publication/237412886_Penman-Monteith_hourly_Reference_Evapotranspiration_Equations_for_Estimating_ETos_and_ETrs_with_Hourly_Weather_Data (accessed on 16 September 2020).
71. Vrugt, J.A.; Gupta, H.V.; Bouten, W.; Sorooshian, S. A Shuffled Complex Evolution Metropolis algorithm for optimization and uncertainty assessment of hydrologic model parameters. *Water*

- Resour. Res.* 2003, 39, 1201.
72. Pool, S.; Vis, M.; Seibert, J. Evaluating model performance: Towards a non-parametric variant of the Kling-Gupta efficiency. *Hydrol. Sci. J.* 2018, 63, 1941–1953.
 73. Liu, D. A rational performance criterion for hydrological model. *J. Hydrol.* 2020, 590, 125488.
 74. Katwal, R.; Li, J.; Zhang, T.; Hu, C.; Rafique, M.A.; Zheng, Y. Event-based and continuous flood modeling in Zijinguan watershed, Northern China. *Nat. Hazards* 2021, 108, 733–753.
 75. Bulovic, N.; McIntyre, N.; Johnson, F. Evaluation of IMERG V05B 30-Min Rainfall Estimates over the High-Elevation Tropical Andes Mountains. *J. Hydrometeorol.* 2020, 21, 2875–2892.
 76. Contreras, J.; Ballari, D.; de Bruin, S.; Samaniego, E. Rainfall monitoring network design using conditioned Latin hypercube sampling and satellite precipitation estimates: An application in the ungauged Ecuadorian Amazon. *Int. J. Climatol.* 2019, 39, 2209–2226.
 77. Chua, Z.-W.; Kuleshov, Y.; Watkins, A. Evaluation of Satellite Precipitation Estimates over Australia. *Remote Sens.* 2020, 12, 678.
 78. Manz, B.; Páez-Bimos, S.; Horna, N.; Buytaert, W.; Ochoa-Tocachi, B.; Lavado-Casimiro, W.; Willems, B. Comparative Ground Validation of IMERG and TMPA at Variable Spatiotemporal Scales in the Tropical Andes. *J. Hydrometeorol.* 2017, 18, 2469–2489.
 79. Hobouchian, M.P.; Salio, P.; García Skabar, Y.; Vila, D.; Garreaud, R. Assessment of satellite precipitation estimates over the slopes of the subtropical Andes. *Atmos. Res.* 2017, 190, 43–54.
 80. Bhuiyan, M.A.E.; Nikolopoulos, E.I.; Anagnostou, E.N. Machine Learning–Based Blending of Satellite and Reanalysis Precipitation Datasets: A Multiregional Tropical Complex Terrain Evaluation. *J. Hydrometeorol.* 2019, 20, 2147–2161.
 81. Bhuiyan, M.A.E.; Yang, F.; Biswas, N.K.; Rahat, S.H.; Neelam, T.J. Machine Learning-Based Error Modeling to Improve GPM IMERG Precipitation Product over the Brahmaputra River Basin. *Forecasting* 2020, 2, 248–266.
 82. Ballari, D.; Giraldo, R.; Campozano, L.; Samaniego, E. Spatial functional data analysis for regionalizing precipitation seasonality and intensity in a sparsely monitored region: Unveiling the spatio-temporal dependencies of precipitation in Ecuador. *Int. J. Climatol.* 2018, 38, 3337–3354.
 83. Nunes, A.M.P.; Silva Dias, M.A.F.; Anselmo, E.M.; Morales, C.A. Severe Convection Features in the Amazon Basin: A TRMM-Based 15-Year Evaluation. *Front. Earth Sci.* 2016, 4, 37.
 84. Tan, M.L.; Santo, H. Comparison of GPM IMERG, TMPA 3B42 and PERSIANN-CDR satellite precipitation products over Malaysia. *Atmos. Res.* 2018, 202, 63–76.

85. Zhang, G.; Lu, Y. Bias-corrected random forests in regression. *J. Appl. Stat.* 2012, *39*, 151–160.
86. Behrangi, A.; Khakbaz, B.; Jaw, T.C.; AghaKouchak, A.; Hsu, K.; Sorooshian, S. Hydrologic evaluation of satellite precipitation products over a mid-size basin. *J. Hydrol.* 2011, *397*, 225–237.
87. Arvor, D.; Funatsu, B.; Michot, V.; Dubreuil, V. Monitoring Rainfall Patterns in the Southern Amazon with PERSIANN-CDR Data: Long-Term Characteristics and Trends. *Remote Sens.* 2017, *9*, 889.
88. UNESCO. *Atlas Pluviométrico del Ecuador*; ESPOL: Quito, Ecuador, 2010.
89. Espinoza Villar, J.C.; Ronchail, J.; Guyot, J.L.; Cochonneau, G.; Naziano, F.; Lavado, W.; De Oliveira, E.; Pombosa, R.; Vauchelh, P. Spatio-temporal rainfall variability in the Amazon basin countries (Brazil, Peru, Bolivia, Colombia, and Ecuador). *J. Climatol.* 2009, *29*, 1574–1594.
90. Moriasi, D.; Arnold, J.; Van Liew, M.; Bingner, R.; Harmel, R.; Veith, T. Model evaluation guidelines for systematic quantification of accuracy in watershed simulations. *Am. Soc. Agric. Biol. Eng.* 2007, *50*, 885–900.
91. Du, E.; Tian, Y.; Cai, X.; Zheng, Y.; Li, X.; Zheng, C. Exploring spatial heterogeneity and temporal dynamics of human-hydrological interactions in large river basins with intensive agriculture: A tightly coupled, fully integrated modeling approach. *J. Hydrol.* 2020, *591*, 125313.
92. Liu, Y.; Gupta, H.V. Uncertainty in hydrologic modeling: Toward an integrated data assimilation framework. *Water Resour. Res.* 2007, *43*, W07401.
93. Shahrban, M.; Walker, J.P.; Wang, Q.J.; Robertson, D.E. On the importance of soil moisture in calibration of rainfall–runoff models: Two case studies. *Hydrol. Sci. J.* 2018, *63*, 1292–1312.
94. Bentura, P.L.F.; Michel, C. Flood routing in a wide channel with a quadratic lag-and-route method. *Hydrol. Sci. J.* 1997, *42*, 169–189.
95. Wilson, J.P.; Lam, C.S.; Deng, Y. Comparison of the performance of flow-routing algorithms used in GIS-based hydrologic analysis. *Hydrol. Process.* 2007, *21*, 1026–1044.

PAPER II

Submitted to Environmental Modelling and Software (Elsevier)

A multi-physics ensemble approach for high-resolution heavy-rainfall and flash-flood forecasting in data-scarce Andean-Amazon basins

Abstract

The increase in intensity and recurrence of flash floods, derived from heavy rainfalls linked to climate change, is a growing concern over data-scarce Andean-Amazon basins, where flood forecasting and early warning systems are usually inexistent. In this regard, the present study aimed at testing a multi-physics ensemble modeling approach to forecast heavy rainfall and flash flood events on hourly scales in a representative data-scarce Andean-Amazon basin: the Upper Napo River Basin (UNRB). A sensitive analysis by using 100 WRF parameterizations was prior conducted to determine suitable combinations of the CU, MP, and PBL schemes for ensemble precipitation forecasts (EPFs). The potential use of EPFs as forcing inputs for flash flood forecasting was then illustrated by using the rainfall-runoff GR4H model. The ensemble flash-flood forecasting showed acceptable performances (KGE: 0.24 – 0.40), considering the limitations that imply the high-resolution hydrometeorological simulations. Altogether, results provided sufficient insights to propose the analyzed ensemble modeling approach as a preliminary tool for generating early warning systems in the study area.

Keywords: WRF model, GR4H model, flash-flood, Napo River Basin, early warning.

1. Introduction

Flash floods are among the most common and costliest natural disasters worldwide (Sun et al., 2020; Tanaka et al., 2020; Unduche et al., 2018). On average, 72 million people are annually affected by flash flood events, representing economic losses above 40 billion USD (CRED, 2019). In tropical regions, particularly in headwaters of the Amazon River Basin, the effects of flash floods are expected to worsen during the next decades due to the increased intensity of extreme precipitations linked to climate change (Barichivich et al., 2018; Espinoza Villar et al., 2009a; Gloor et al., 2013; Hoch et al., 2017; Sena et al., 2012; Winsemius et al., 2016). In this

regard, it is imperative to understand and model the hydrometeorological conditions that trigger flash floods for the effective planning of mitigation strategies (Dubey et al., 2021; Kim et al., 2019), especially over data-scarce regions where flood forecasting and early warning systems are usually inexistent (Hurtado et al., 2020).

Flash floods are characterized by heavy rainfall events that present sudden occurrences and uneven spatiotemporal distributions (Liu et al., 2020). Thus, the quantitative forecast of heavy rainfalls is crucial for early warning systems as it extends the lead time of flash flood forecasting (Tsuboki and Luo, 2021). However, despite the continuous improvement of numerical weather prediction (NWP) models, the quantitative precipitation forecast (QPF) is still a challenge due to the nonlinear and chaotic properties of the atmosphere (Morrison et al., 2020; Tian et al., 2019). Likewise, the high computational costs -required by NWP models- often make it difficult that QPFs present suitable resolutions to capture the whole spatiotemporal variability of the precipitation (Li et al., 2016; Sikder and Hossain, 2016). For instance, the Global Forecasting System (GFS) provides gridded 0.25° precipitation forecasts with a 3-hourly resolution (NCEP, 2015). In complex topography areas, such as the Andean-Amazon region, QPFs with coarse spatiotemporal resolutions (e.g., GFS) are not adequately to force flood forecasting systems as most river basins present fast hydrological responses and a strong precipitation variability (Rogelis and Werner, 2018).

In recent years, dynamical downscaling has been widely used to increase the spatiotemporal resolutions of QPFs and thus improve flood forecasting in complex topography regions (Dubey et al., 2021; Kim et al., 2021; Wang et al., 2021). Nowadays, the Weather Research and Forecasting (WRF) model is the most used tool for the dynamical downscaling, as it provides a computationally-efficient platform with robust physical schemes (Duzenli et al., 2021; Khansalari et al., 2021; Kim et al., 2021; Mori et al., 2021; Tu et al., 2021). These physical schemes represent detailed processes of the land-atmosphere continuum, such as cloud microphysics (MP), longwave (LW) and shortwave (SW) radiation, cumulus convection (CU), surface layer (SL), land surface model (LSM), and planetary boundary layer (PBL).

Although all physical schemes are relevant to simulate the precipitation, most authors have

recommended focusing on the parameterization of CU, MP, and PBL since they strongly influence the uncertainty of the simulated precipitation (Chawla et al., 2018; Gsella et al., 2014; Patel et al., 2019). The CU scheme captures the subgrid-scale effects of the vertical transport of heat, moisture, and momentum by turbulent eddies, updrafts, and downdrafts (Arakawa, 2004). The MP scheme, instead, describes the physical processes occurring within clouds, such as the nucleation of cloud particles, diffusional growth from water vapor, collision and coalescence, freezing, melting, evaporation, among others (Morrison et al., 2020). The PBL scheme represents the structure of the lower troposphere, where the surface processes affect the behavior of hydrometeors. Indeed, the PBL directly influence the vertical profiles of temperature and moisture, as well the turbulent mixing of air, which interact with the remained physical schemes and usually trigger convection (Comin et al., 2021; Qian et al., 2016).

Selecting the suitable set of physical scheme parameterizations is a challenge as the atmospheric processes involved in heavy rainfalls are subject to chaotic variations (Ruiz et al., 2010; Sikder and Hossain, 2016). Conclusions on the optimal set of physical parameterizations are diverse and mismatched over different regions worldwide, even for different rainfall events in the same region (Meynadier et al., 2015; Tian et al., 2019). For most cases, there is no unique set of physical parameterizations that is consistently better than any other (Pervin and Gan, 2021; Ruiz et al., 2010). For instance, Jeworrek et al. (2021) found that winter precipitations of British Columbia are better simulated when Kain-Fritsch is used as the CU scheme; whereas, summer precipitations are better simulated using the Grell-Freitas CU scheme. In Mu et al. (2019), four type of precipitation events over northwestern China were simulated using different set of physical parameterizations. They found that even for the same type of precipitation, two or more sets of physical parameterizations were suitable.

To overcome discrepancies derived from the selection of a single set of physical parameterizations, multi-physics ensemble modeling approaches have been widely used in heavy rainfall and flash flood forecasting (Gharamti et al., 2021; Kirthiga et al., 2021). For instance, Yang et al. (2021) simulated five heavy rainfall events in Eastern China using a multi-

physics ensemble of 18 members. Their results showed that the mean ensemble better simulate the analyzed events compared to single physical parameterizations. Likewise, Calvetti et al. (2014) evaluated a multi-physics ensemble of 11 members for 32 heavy rainfall events in south Brazil. Their results indicated the ensemble yielded up to 20% better skill than single physical parameterizations.

Although the multi-physics ensemble approach provides new avenues to better predict heavy rainfall and flash flood events, its applicability has not been explored in the Ecuadorian Andean-Amazon region. In fact, there is no operational hydrometeorological forecasting system over this region, despite it being prone to frequent flash floods (Chancay and Espitia, 2021). To address this issue, the present study aimed at testing a multi-physics ensemble modeling approach in order to forecast heavy rainfall and flash flood events in a representative data-scarce Andean-Amazon basin: The Upper Napo River Basin (UNRB). For this, we assessed 100 physical parameterizations of the WRF model to determine suitable combinations of CU, MP, and PBL schemes, which providing relevant insights to maximize the performance of ensemble precipitation forecasting. The potential use of ensemble precipitation forecasts as forcing inputs for flash flood forecasting was then illustrated by hydrological modelling, using three gauged subbasins within the UNRB that suffer continuous flood risk.

2. Study area

The UNRB is an important headwater tributary basin of the Amazon River (Fig. 1a). It is located at the transition between the Eastern Andes and Amazonia foothills in Ecuador, covering a drainage area of about 6095 km² above the H1156 hydrological station (Fig. 1b). It presents a mean discharge of about 632 m³/s (Chancay and Espitia, 2021). The UNRB is characterized by a complex topography with steep slopes that descend from 5900 to 370 masl over 100 km (Laraque et al., 2009). As consequence, the UNRB presents a strong climate gradient described by three ecoregions, from the higher to lower elevations: (i) paramo, (ii) mountain forest, and (iii) piedmont rainforest (Fig. 1c). In the paramo, temperature ranges from 4 to 8 °C and precipitation varies from 500 to 2000 mm per year (Muñoz et al., 2018; Padrón et al., 2015). In the mountain forest, instead, temperature ranges from 12 to 20 °C and

annual precipitation varies between 2000 to 4000 mm (Laraque et al., 2007). The piedmont rainforest presents a humid tropical climate with annual precipitation between 3500 and 5000 mm, and mean temperatures from 20 to 27°C (Espinoza Villar et al., 2009b; UNESCO, 2010).

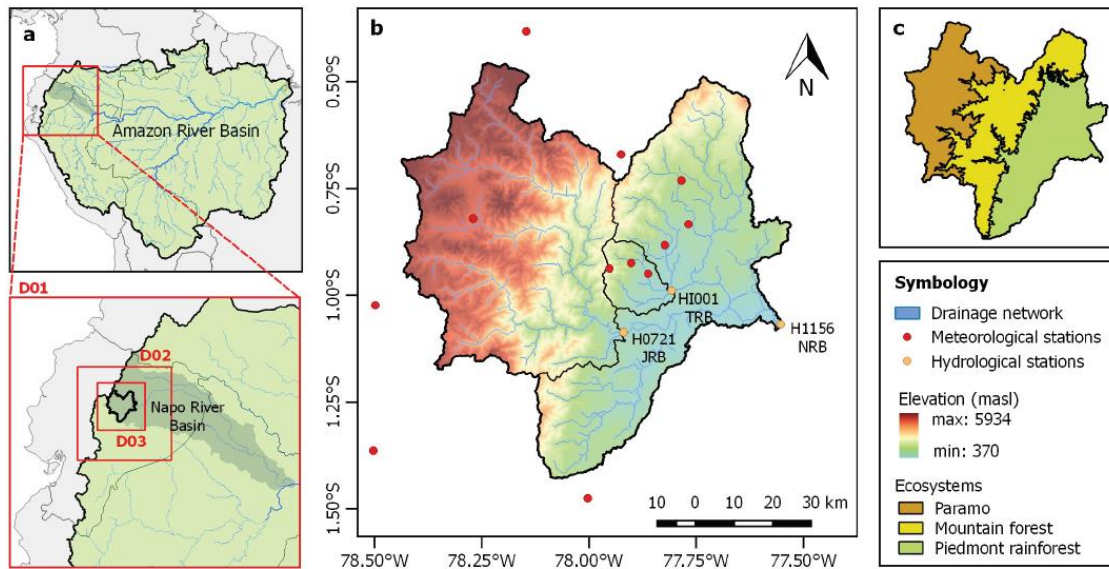


Figure 1. Study area. (a) Location of the Napo River Basin within the Amazon River Basin and WRF domains. (b) Topography, drainage network, and gauge stations of the three study subbasins: Upper Napo River Basin, Tena River Basin, and Jatunyacu River Basin. (c) Ecosystems within the study area related to climate gradient and hence specific precipitation regime.

Given its continuous soil-saturation conditions, strong precipitation regimen, and steep slopes, the UNRB is prone to frequent flash-flood events, especially in the lowest reaches (i.e., piedmont rainforest) where most of the urban settlements are located (Chancay and Espitia, 2021). In fact, there are three critical points along the lowest reaches of the UNRB where more than 16 flash-flood events have been recorded during the last 12 years (Fig. 1b), affecting on average 8000 families per year over locations such as Tena, Misahuallí, and Ahuano (Cruz Cueva, 2016; SNGRE, 2020), which will be beneficiaries of this study. In addition to outlet of the UNRB, these critical points include outlets of the Tena River Basin (TRB) and Jatunyacu River Basin (JRB). The TRB drains 239 km² and presents a mean discharge of about 25 m³/s; however, its peak discharges reach 1800 m³/s during flash-flood events (Hurtado et al., 2020).

The JRB covers 3128 km² and generates a mean discharge of 290 m³/s. Flash-flood events in the JRB have shown peak discharges above 2100 m³/s, whereas, peak discharges in the outlet of the UNRB exceed 5000 m³/s (Lapo, 2017).

3. Data and methods

3.1. Precipitation and streamflow data

Hourly precipitation and streamflow data were obtained from 12 meteorological and 3 hydrological stations (Fig. 1b; Table A1) belonging to the Ikiam Hydrometeorological Service (IHS, 2020) and the National Institute of Meteorology and Hydrology of Ecuador (INAMHI, 2020, 2019). Since the distribution of meteorological stations is not sufficient to capture all spatiotemporal precipitation dynamics, we used the BC-RFP gridded-precipitation product as reference rainfall data. It covers the whole UNRB with high spatiotemporal resolutions (4 km, 1 hour), presenting correlation coefficients above 0.9 and root mean square errors below 0.7 mm/h regarding to observed precipitation data (Chancay and Espitia, 2021). Currently, the BC-RFP is supported by the Ikiam Hydrometeorological Service (IHS, 2020).

3.2. Ensemble precipitation modeling

3.2.1. Model setup and parameterization

The Weather Research and Forecasting (WRF) model version 4.0 (Skamarock et al., 2019) was used to simulate the precipitation, which is crucial to force hydrological models. The WRF model was set up with three nested domains, using two-way communication without smoothing (Fig. 1a). The coarsest domain (D01) covered the whole Ecuadorian territory and the Napo River Basin with a spatial resolution of 27 km. The intermediate domain (D02) was located at the transition Andean-Amazon region with a resolution of 9 km. The finest domain (D03) covered the UNRB with a 3-km resolution. Initial and lateral conditions were forced with 0.25° GFS analysis data (NCEP, 2015), using a vertical discretization of 32 levels up to 50 hPa.

Physical parameterizations of the WRF model (Table 1) were derived from the operational weather forecast system of INAMHI (Iza, 2020), except for cumulus (CU), microphysics (MP),

and planetary boundary layer (PBL) schemes, with which, a sensitivity analysis was prior conducted.

Table 1. Physical schemes used to parameterize the WRF model.

Schemes	Parameterization	Acronym	References
Land surface	Unified Noah land-surface model	Noah	(Chen and Dudhia, 2001)
Surface layer	Monin-Obukhov similarity	MOS	(Monin and Obukhov, 1954)
Shortwave radiation	New Goddard shortwave	Goddard	(Zhong et al., 2016)
Longwave radiation	Rapid radiative transfer model	RRTMG	(Thompson et al., 2016)
Planetary boundary layer	Yonsei University PBL	YSU	(Hong et al., 2006)
	Mellor-Yamada-Janjić	MYJ	(Janjić, 2001, 1990)
Cumulus convection	Grell-Devenyi	GD	(Grell and Dévényi, 2002)
	Grell-Freitas	GF	(Grell and Freitas, 2014)
	Grell 3D	G3D	(Grell and Dévényi, 2002)
	Kain-Fritsch	KF	(Kain, 2004)
	Betts-Miller-Janjić	BMJ	(Janjić, 2000, 1994)
Microphysics	Two-moment six-class Morrison	Morrison	(Morrison et al., 2005)
	Lin et al	Lin	(Lin et al., 1983)
	WRF single-moment 6-class graupel	WSM6	(Hong et al., 2006)
	WRF double-moment 5-class	WDM5	(Lim and Hong, 2010)
	Eta Ferrier	Ferrier	(Ferrier et al., 2002)

We assessed 50 model parameterizations (hereafter experiments) derived from combinations of 5 MP, 5 CU, and 2 PBL schemes (Table 1). Each combination was evaluated with and without CU parameterization at the finest domain, i.e., 100 experiments in total. The MP, CU, and PBL parameterizations were selected based on previous studies carried out in the Andean-Amazon region (Beck et al., 2013; Langenbrunner et al., 2019; Martínez et al., 2019; Moya-Álvarez et al., 2018b; Moya et al., 2020; Rogelis and Werner, 2018; Wang et al., 2020). Overall, 32 heavy-rainfall events were simulated. The events were selected based on the 99.9th percentile of maximum precipitation intensities recorded over the TRB, JRB, and UNRB between 2016 and 2021; i.e., 48.9 mm/h (Chancay and Espitia, 2021).

3.2.2. Evaluation metrics

The performance of the WRF experiments was evaluated by comparison of the simulated

precipitation with the BC-RFP precipitation product. For this, we used three recommended statistical metrics: root mean square error (RMSE), correlation coefficient (CORR), and percent bias (BIAS). Likewise, three categorical statistics were used to assess the detection ability of the simulations: probability of detection (POD), false alarm ratio (FAR), and critical success index (CSI). Mathematical definitions and details of the used metrics are shown in Appendix A.

To summarize and compare the model performance of the experiments, we modified and computed the comparative model skill score (MSS) developed by Gbode et al. (2019). For this, the sum of the normalized statistical metrics (X_n) was calculated as shown in equations 1-2.

$$X_n = \frac{X_i - X_{min}}{X_{max} - X_{min}} \quad (\text{Eq. 1})$$

$$MSS = \frac{1}{\sqrt{M}} (CORR_n + (1 - RMSE_n) + (1 - |PBIAS|_n) + POD_n + (1 - FAR_n) + CSI_n) \quad (\text{Eq. 2})$$

Where, X could be either averaged statistical metric; M is the number of metrics (in this study N=6). Model experiments with higher MSS values perform better while those with lower values have poorer performance.

3.2.3. Selection of ensemble members

The optimal set of WRF parameterizations for ensemble precipitation forecasting was selected by using the analysis framework proposed by Wang et al. (2021b). Note that parameterizations with the best individual performances are not necessarily those that maximize the performance of ensemble precipitation forecast (Carlberg et al., 2018). First, we computed the main effect of each physical scheme (i.e., CU, MP, and PBL) and the interaction effect among them on the performance of precipitation forecast (i.e., on MSS) to reduce the physical schemes on which we should focus. For this, we used the modified multi-way ANOVA method (Wang et al., 2021b), as follows:

For each experiment, the deviation of its performance was calculated using the equation 3.

$$\text{deviation} = \text{individual performance} - \text{overall mean} \quad / \quad (\text{Eq. 3})$$

The “total sum of squares” (TSS) was then calculated by squaring each deviation and summing them.

The effect of a physical scheme on the performance (main effect) and the effect of one physical scheme on another physical scheme (interaction effect) were calculated using equations 4-6.

$$\text{Main effect (A)} = \frac{TSS(A)}{df_A-1} \quad (\text{Eq. 4})$$

$$\text{Main effect (B)} = \frac{TSS(B)}{df_B-1} \quad (\text{Eq. 5})$$

$$\text{Interaction effect (A, B)} = \frac{TSS(A,B)}{(df_A-1)(df_B-1)} \quad (\text{Eq. 6})$$

Where, A and B can be any of the analyzed physical schemes (i.e., CU, MP, PBL) and df is their respective degree of freedom.

Once the most sensitive physical schemes were determined, we used their respective parameterization options to generate different sets of parameterizations (or members) for the ensemble precipitation forecast. The set of members that maximize the performance of the mean ensemble precipitation forecast (hereafter “optimal ensemble parameterization”) was selected for next steps. To determine the optimal ensemble parameterization, we used a Monte Carlo approach by varying the members and the number of members in the ensemble.

3.2.4. Bias correction and ensemble precipitation forecasts

The optimal ensemble parameterization was used to generate continuous simulations of precipitation from January 2016 to December 2020 (5 years). For these simulations, initial and lateral conditions were forced with the 0.25° GFS forecast data initialized on 00Z, 06Z, 12Z, and 18Z (NCEP, 2015). The simulations were subsequently bias-corrected using three methods recommended for the Andean-Amazon region: (i) potential transformation, (ii) gamma quantile mapping, and (iii) empirical quantile mapping (Campozano et al., 2016; Heredia et al., 2018; Velasquez et al., 2020). A further description of these bias-correction methods is presented in Fang et al. (2015).

3.3. Ensemble flash flood modeling

The bias-corrected ensemble precipitation forecast was used to force the semi-distributed GR4H model for generating continuous streamflow simulations and subsequently predict flash flood events over the three study subbasins (TRB, JRB, and UNRB). Further details are shown in the following sections.

3.3.1. Model description and parameterization

GR4H is a conceptual rainfall-runoff model that has been widely used for flash flood modeling due to its simple structure, low computing needs, and ability to simulate hourly streamflows (Bennett et al., 2014; Mathevet, 2005). Previous studies showed that the GR4H model can satisfactorily simulate the hydrological processes over the Andean-Amazon basins (Chancay and Espitia, 2021; Espitia et al., 2020; Llauca et al., 2021). In general, the GR4H model has four free parameters that characterize the storage processes and unit hydrograph: **X1**, maximum capacity of moisture store (mm); **X2**, groundwater exchange coefficient (mm/h); **X3**, maximum capacity of the routing store (mm); and **X4**, base time of the unit hydrograph (h). A complete description of the model structure and equations are shown in Mathevet (2005). For this study, we adopted the semi-distributed model configuration and parameterization previously described in Chancay and Espitia (2021).

3.3.2. General assessment of streamflow simulations

Streamflow simulations forced by bias-corrected ensemble precipitation forecasting were assessed using the Kling-Gupta Efficiency (KGE), Peak Flow Criterion (PFC), and Probability of Flood Detection (PFD). In general, KGE captures the streamflow dynamics over the time, whereas, PFC and PFD quantify the error in magnitude and occurrence of peak flows (Pool et al., 2018; Wijayarathne et al, 2020). Mathematical definitions and further details of the used metrics are shown in Appendix A.

3.3.3. Flash flood event analysis

The five last flash floods occurred in the three study subbasins (Table 2) were used to assess

the performance of streamflow simulations at an event-scale. These flash flood events were chosen based on records of the National Service for Risk Management of Ecuador (SNGRE, 2020) and streamflow thresholds defined by Hurtado et al. (2020) and Lapo (2017) for flood events in the TRB, JRB, and UNRB.

Table 2. Information of the last five flash flood events produced within the study subbasins.

Event	Start (Datetime)	Duration (h)	Peak Discharge (m ³ /s)		
			TRB	JRB	UNRB
1	2017-09-02 19:00	53	1896	1160	3570
2	2018-07-22 01:00	51	657	2579	4574
3	2019-05-25 20:00	28	242	1184	6407
4	2019-06-20 00:00	72	250	2659	6338
5	2020-05-01 00:00	80	593	896	8925
Streamflow threshold for flood events			210	2200	4500

4. Results and discussion

4.1. Sensitivity analysis of WRF physical schemes

The sensitivity analysis showed that cumulus convection (CU) is the most relevant physical scheme for precipitation simulations over the UNRB (Fig 2). The effect on the simulated precipitation performance by shifting CU parameterizations was higher than effects reached by varying microphysics (MP) and planetary boundary layer (PBL) parameterizations (Fig. 2a). This result is related to the complex topography of the Andean-Amazon region and its circulation patterns, which induce the orographic lifting of humid air originated from the lower Amazon, favoring the convection processes on storm-scales over headwaters of the Amazon River Basin, where the UNRB is located (Espinoza et al., 2020; Insel et al., 2010; Laraque et al., 2007).

Despite previous studies indicated that PBL strongly influences the performance of the simulated precipitation (e.g., Comin et al., 2021; Ulate et al., 2014; Argüeso et al., 2011), our results suggested that PBL is practically insensitive. In fact, the interaction effect of PBL on CU and MP was no significant compared to the interaction effect between CU and MP (Fig. 2a). These results agree with those reported by Wang et al. (2021b) for the whole Amazon River Basin and Moya-Álvarez et al. (2018) for the Peruvian Andean-Amazon region. Qian et al.

(2016), instead, argued that the behavior of the PBL scheme has a close relationship with the parameterization of the surface layer (SL) scheme. Note that SL describes the effects of the surface sensible and latent heat, the basis to estimate moisture fluxes between land-surface model (LSM) and PBL (Bright and Mullen, 2002; Qian et al., 2016). In this study, however, the variation of SL and LSM parameterizations were not analyzed, which could partially explain the low sensitivity of PBL. Further studies that include the sensitive analysis of SL and LSM are required to contrast the aforementioned idea.

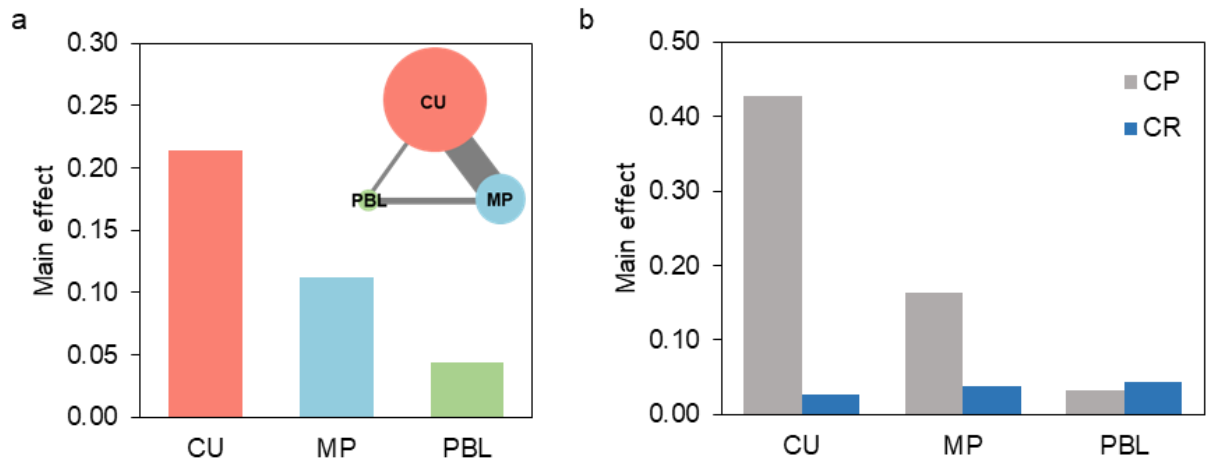


Figure 2. Sensitivity analysis of the physical schemes. (a) Effect of each physical scheme on the performance of simulated precipitation (main effect), and effect of one physical scheme on another physical scheme (interaction effect). The larger radius (size) of the circle means larger relative importance, while the thicker line connecting two physical schemes means a larger contribution from interactions. (b) Main effect of physical schemes with and without CU parameterization in the finest domain (d03): cumulus parameterized (CP) and cumulus resolved (CR), respectively.

The sensibility analysis also revealed that cumulus resolved (CR) experiments presented no significant variation on the precipitation performance by shifting parameterizations compared to cumulus parameterized (CP) experiments (Fig. 2b). Likewise, the CP experiments showed significantly better performance than CR experiments ($p < 0.05$) in terms of the RMSE, CORR, BIAS, and POD (Fig. 3). According to several studies, the explicit resolution of CU at spatial resolutions below 5 km (convective-permitting scales) better capture the complex processes of the rainfall formation (Hsiao et al., 2013; Pennelly et al., 2014; Zheng et al., 2016). In this

study, the finest domain was configured with a spatial resolution of 3 km, however, precipitation was better simulated by parameterization and not by explicit CU resolution. Studies such as Moya-Álvarez et al. (2018) and Martínez et al. (2019) discussed similar results and suggested that convective-permitting scales for the Andean-Amazon region could be on spatial resolutions below 1 km. The results showed in this study provide new insights that support the latter hypothesis.

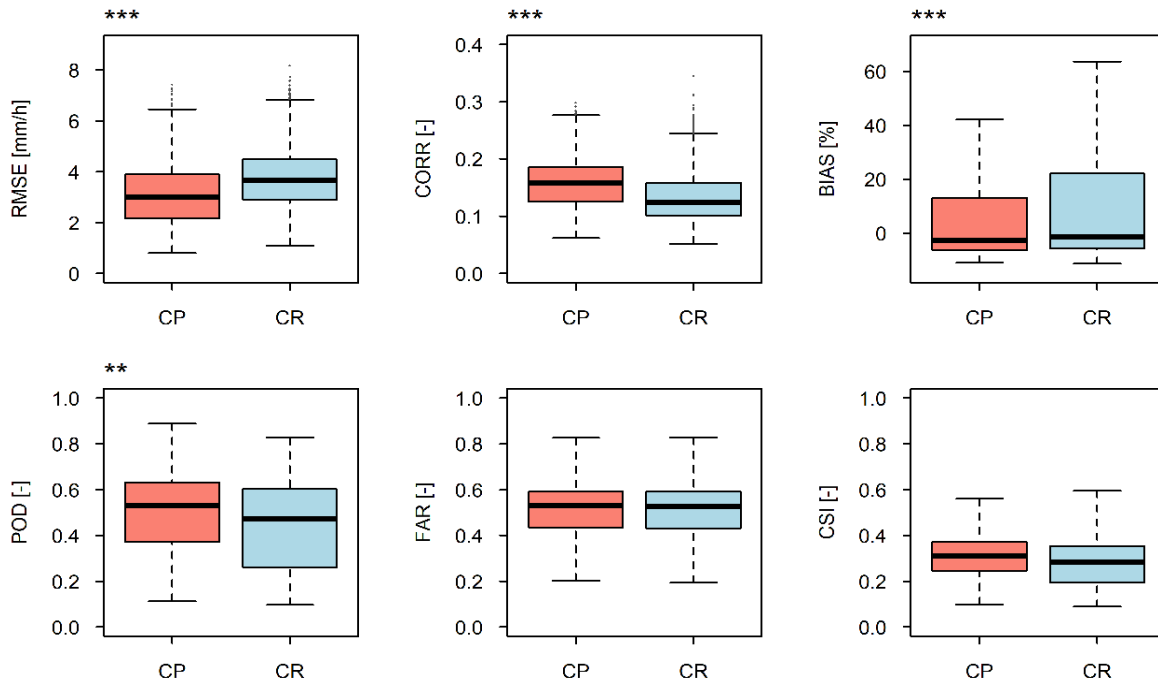


Figure 3. Performances of the simulated precipitation considering cumulus parameterized (CP) and cumulus resolved (CR) experiments. Each box plot represents the performance variability over the UNRB at pixel-to-pixel scale. Symbology: (**) and (***) mean significant differences, i.e., $p < 0.05$ and $p < 0.005$, respectively.

4.2. Model performances and suitable parameterizations of CU and MP

As discussed in section 4.1, the PBL scheme was practically insensitive. Ergo, the selection of Yonsei University (YSU) or Mellor-Yamada-Janjić (MYJ) schemes as the PBL parameterization does not influence the performance of the simulated precipitation over the UNRB. However, we decided to use the YSU configuration as previous studies have recommended it for humid regions (Moya-Álvarez et al., 2018b; Sikder and Hossain, 2016; Ulate et al., 2014). Also, we

decided to use the CP experiments as they presented better performances than CR experiments (Fig. 3). In this regard, from the initial 100 experiments, the analysis was reduced to 25 experiments derived from 5 MP and 5 CU (Fig. 4).

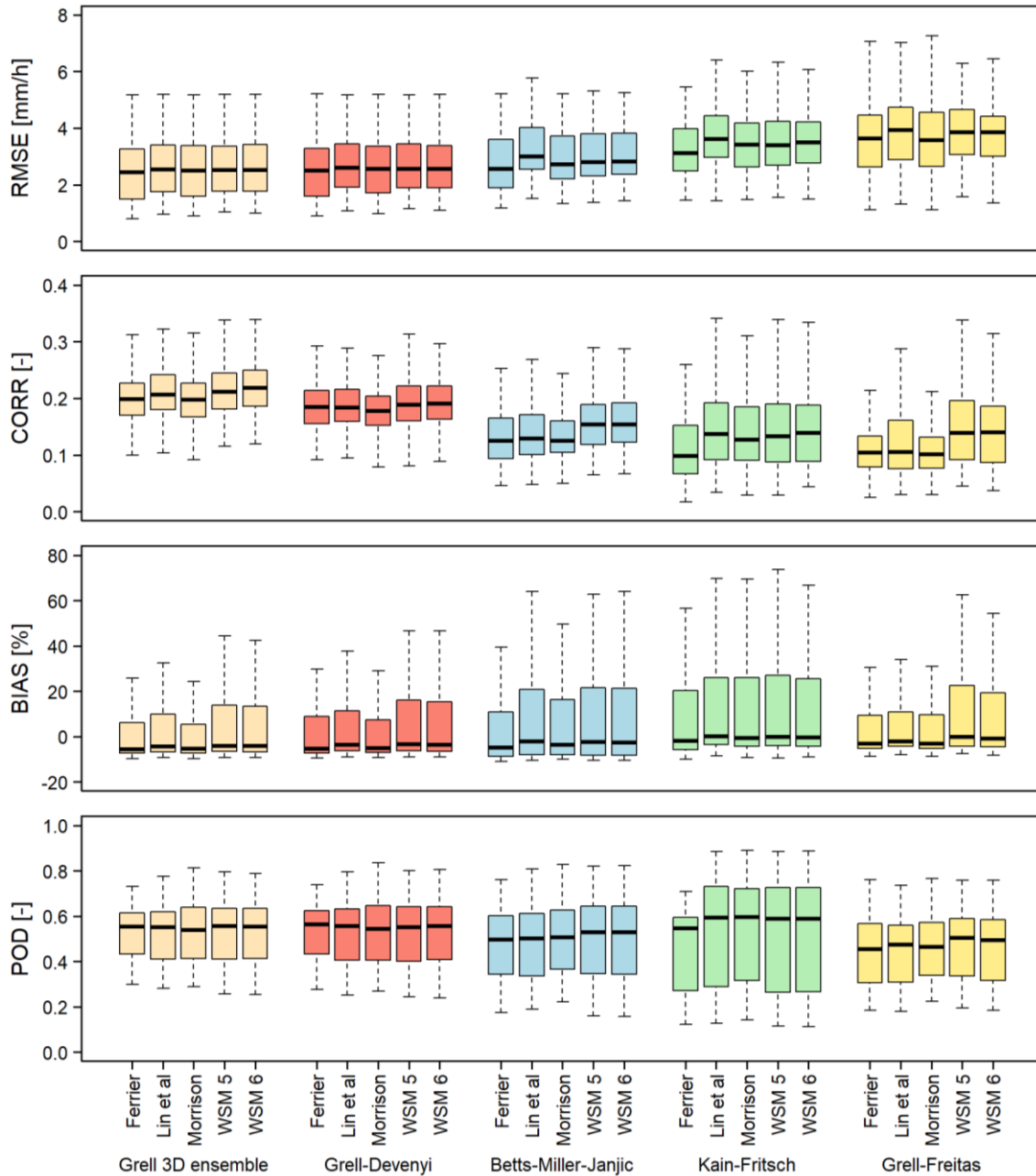


Figure 4. Performance of the 25 experiments derived from combinations of 5 CU and 5 MP parameterizations. Box plots considers the performance variability over the UNRB using a pixel-to-pixel comparison. The metrics used were Root Mean Square Error (RMSE), Correlation Coefficient (CORR), Bias Error (BIAS), and Probability of Detection (POD).

Overall, experiments that were configured with the Grell 3D scheme as the CU parameterization showed the best precipitation performances in averaged terms of RMSE (2.3 mm/h), CORR (0.20), and BIAS (-4.3 %). Previous studies such as Li et al. (2018) and Grell and Dévényi (2002) highlighted that Grell 3D usually has high performances at high spatial resolutions, as in the case of this study. Other works such as Jeworrek et al. (2019) and Gao et al. (2017), instead, indicated that Grell-Freitas scheme better captures the distribution and occurrence of precipitation at gray-zone resolutions (i.e., 3 km). However, in this study, the Grell-Freitas scheme was the worst performed CU parameterization (Fig. 4), showing the highest mean RMSE (3.8 mm/h), the lowest mean CORR (0.12), and the lowest mean POD (0.42). Based on the POD, the Kain-Fritsch scheme was the best performed CU parameterization, reaching a mean performance of 0.60. Pennelly et al. (2014) and Yang et al. (2021) pointed out the conservation mass algorithm for convective updrafts and downdrafts of the Kain-Fritsch scheme allows for better capture of the occurrence of convective precipitation events. Nevertheless, the precipitation intensity is often overestimated with this scheme (Wang et al., 2021b), which could explain the largest BIAS presented by the Kain-Fritsch scheme.

The performance assessment, considering both MP and CU (Fig. 4), revealed that MP parameterizations such Ferrier and Morrison works better in combination with Grell 3D and Grell-Devényi CU parameterizations. Based on the MSS, the aforementioned CU and MP parameterizations maximized the performance of the simulated precipitation over the UNRB (Table 2). These results are in line with previous works conducted in the Andean-Amazon region (Martínez et al., 2019; Moya et al., 2020; Sierra et al., 2020). According to Wang et al. (2021b), the simulation of land-atmosphere interactions over the whole Amazon region can be improved using the Morrison (MP) scheme in combination with Grell 3D or Grell-Devényi (CU) schemes. Although the results presented in Wang et al. (2021b) are applicable on a regional scale, our results suggest that their conclusions are even applicable to Andean-Amazon headwaters on convective permitting scales.

Table 3. Performance of analyzed experiments considering the Model Skill Score (MSS). The experiments were order from the best-performed to the worst-performed.

Order	Microphysics (MP)	Cumulus (CU)	MSS
1	Morrison	Grell 3D ensemble	1.294
2	Ferrier	Grell 3D ensemble	1.287
3	Ferrier	Grell-Devenyi	1.244
4	Morrison	Grell-Devenyi	1.242
5	Lin et al	Grell 3D ensemble	1.214
6	WSM 6	Grell 3D ensemble	1.188
7	WSM 5	Grell 3D ensemble	1.181
8	Ferrier	Betts-Miller-Janjić	1.176
9	Lin et al	Grell-Devenyi	1.166
10	WSM 6	Grell-Devenyi	1.133
11	WSM 5	Grell-Devenyi	1.127
12	Morrison	Betts-Miller-Janjić	1.105
13	WSM 6	Betts-Miller-Janjić	1.033
14	WSM 5	Betts-Miller-Janjić	1.021
15	Morrison	Grell-Freitas	0.999
16	Lin et al	Betts-Miller-Janjić	0.998
17	Ferrier	Grell-Freitas	0.993
18	Lin et al	Grell-Freitas	0.935
19	Ferrier	Kain-Fritsch	0.929
20	Morrison	Kain-Fritsch	0.863
21	WSM 6	Grell-Freitas	0.851
22	WSM 6	Kain-Fritsch	0.837
23	WSM 5	Kain-Fritsch	0.827
24	Lin et al	Kain-Fritsch	0.821
25	WSM 5	Grell-Freitas	0.801

4.3. Optimal ensemble parameterization

The Monte Carlo analysis indicated the combination of five WRF parameterizations (hereafter members) minimize the RMSE, whereas combination of eight members maximize the CORR (Fig. 5). Considering BIAS, however, no combination improved the ensemble precipitation performance. In fact, as the number of the ensemble members increases, the BIAS increases. The POD and FAR showed a high increase up to combinations of four members. As the higher the POD and the lower the FAR, the better the performance of the simulated precipitation. However, given the POD increase is higher than the FAR increase, the combination of five or more members are suitable to maximize the detection ability of the

ensemble precipitation forecasts.

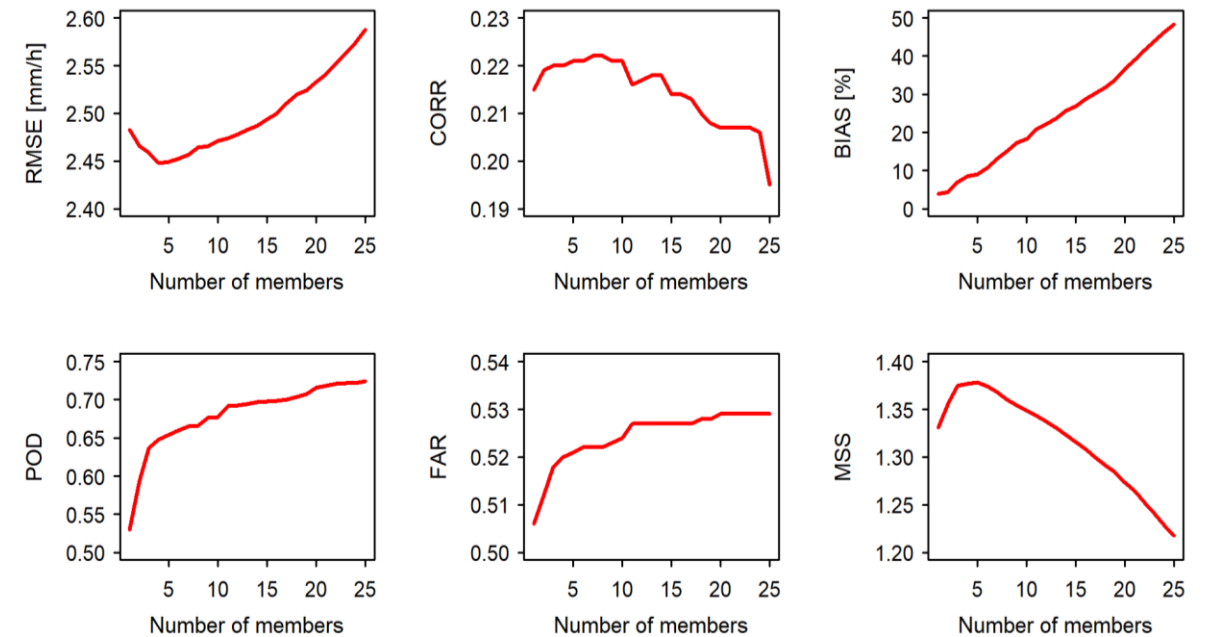


Figure 5. Performance of the simulated precipitation considering the variation on the number of ensemble members. The used metrics were: Root Mean Square Error (RMSE), Correlation Coefficient (CORR), Bias Error (BIAS), Probability of Detection (POD), False Alarm Ratio (FAR), and Model Skill Score (MSS).

Summarizing the statistical metrics by MSS, results suggested the set of five members is the most suitable for the ensemble precipitation simulation in the UNRB (Fig. 5). The optimal set of ensemble members was composed by the following CU-MP combinations: (i) Grell 3D + Ferrier, (ii) Grell 3D + Morrison, (iii) Betts-Miller-Janjić + Ferrier, (iv) Grell-Devenyi + Ferrier, and (v) Grell-Devenyi + Morrison. Note the third member of the ensemble (i.e., Betts-Miller-Janjić + Ferrier) was individually ranked as the eighth best-performed experiment (Table 2). As concluded in previous studies, combinations of members that individually present the best performances are not necessarily those that maximize the performance of the ensemble precipitation forecasts (Athukorala et al., 2021; Lee, 2012).

4.4. Ensemble precipitation forecasting

Results showed in previous sections (sensitivity analysis and ensemble parameterization)

were generated using precipitation simulations forced with the 0.25° GFS analysis data. In the following sections, instead, the bias-corrected ensemble precipitation forecasts forced with the 0.25° GFS forecast data (hereafter EPFs) are evaluated considering a simulation period of 5 years (January 2016 to December 2020) on different lead times (3 to 72 hours).

4.4.1. Impact of the lead time on the performance

In general, the EPFs with lead times beyond 36 hours showed a notable performance improvement in mean terms of RMSE and BIAS compared to simulations used for the ensemble parameterization (Fig. 6). Note that a bias correction process was prior applied to the EPFs. Given the bias correction only reduce the systematic errors and cannot significantly improve the precipitation dynamics, the performance reduction observed in CORR was expected. Considering the analyzed categorical metrics (i.e., POD, FAR, and CSI), the EPFs presented worsened performances than simulations used for ensemble parameterization. These results were also expected due to uncertainties derived from the 0.25° GFS forecast data, which are higher than uncertainties provided by the 0.25° GFS analysis data (Sikder and Hossain, 2016).

As shown in Fig. 6, the performance of the EPFs decreases as the lead time increases, reaching the highest reduction rates in lead times greater than 36 hours. Previous studies such as Li et al. (2017) and Rogelis and Werner (2018) discussed similar results. Due to the chaotic properties of the atmosphere, small errors in the current simulated-state of the atmospheric system could be exponentially magnified toward future previsions (Saedi et al., 2020). Although the precipitation forecasts derived from small ensembles -as in the case of this study- have potential for various limitations on large lead times, previous studies (e.g., Carlberg et al., 2018; Evans et al., 2013) indicated that even a small number of ensemble members (4-10 member) are sufficient to improve short-term precipitation forecasting (lead times < 48h). Our results complied with the latter idea and suggested that parameterization used for EPFs are suitable for lead times up to 36 hours (Fig. 6).

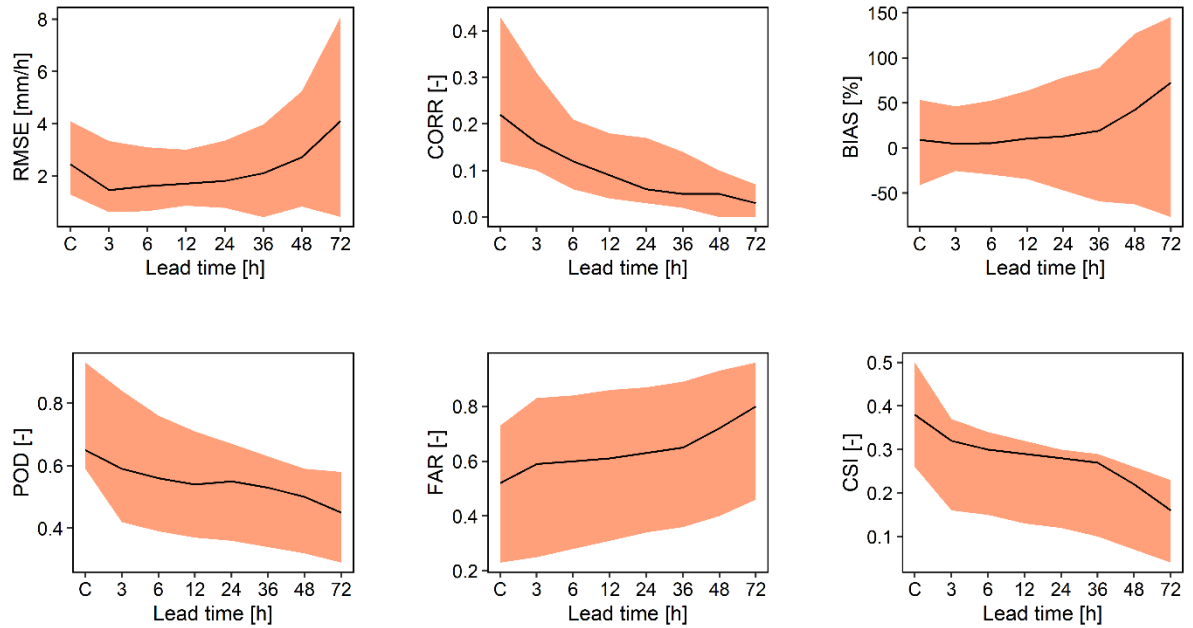


Figure 6. Impact of the lead time on the performance of the bias-corrected ensemble precipitation forecast (EPFs), considering a continuous simulation period of five years: from January 2016 to December 2020. The black line represents the mean performance, whereas the ribbon represents the performance variation over the UNRB. The used metrics were: Root Mean Square Error (RMSE), Correlation Coefficient (CORR), Bias Error (BIAS), Probability of Detection (POD), False Alarm Ratio (FAR), and Critical Success Index (CSI). The letter “C” in the x-axis represents the performance of the simulated precipitation used for the ensemble parameterizations, i.e., simulations forced with the 0.25° GFS analysis data.

4.4.2. Spatial performance analysis

According to the spatial analysis (Fig. 7), the paramo and mountain forest regions (i.e., western UNRB; Fig. 2) presented the worst performed forecasts. Despite the paramo showed low RMSE values (> 1.5 mm/h), it also presented a large precipitation overestimation (BIAS > 40 %). Note the paramo has the lowest rainfall intensities in the study area (Ochoa-Sánchez et al., 2018), which might explain the relative low RMSE values. Likewise, note the WRF model presents limitations for simulating the low intensity precipitation and usually tend to overestimate it (Velasquez et al., 2020; Yang et al., 2019), explaining the largest BIAS in the paramo.

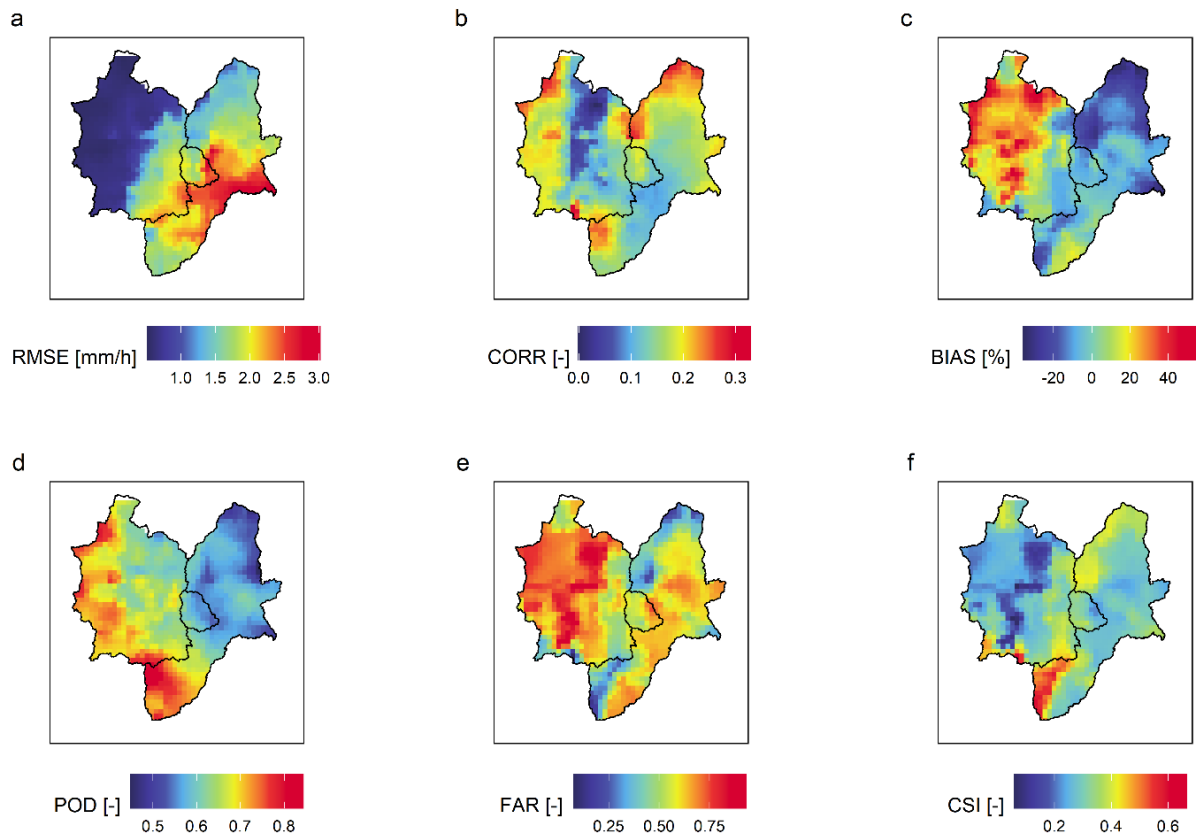


Figure 7. Spatial performance of the bias-corrected ensemble precipitation forecast within the UNRB (lead time 3h), considering a continuous simulation period of five years: January 2016 to December 2020. The used metrics were: Root Mean Square Error (RMSE), Correlation Coefficient (CORR), Bias Error (BIAS), Probability of Detection (POD), False Alarm Ratio (FAR), and Critical Success Index (CSI).

Otherwise, the lowest CORR over the UNRB were obtained in the transition between the paramo and mountain forests (Fig. 7b). This result may be related to the high heterogeneity and steep slopes of this region, which difficult capture and simulate the spatiotemporal precipitation dynamics (Chancay and Espitia, 2021). Although high POD values were reached in the highest zones of the paramo, this region also presented the highest FAR values, indicating that EFPs could overestimate the frequency of wet hours over the paramo. However, other precipitation types such as horizontal rainfall and drizzle that occur in the paramo (Ochoa-Sánchez et al., 2018) were excluded for the analysis, as the reference precipitation data (i.e., BC-RFP) cannot capture them. This could explain the high FAR values and even the low CORR values.

In the lower reaches of the UNRB (i.e., the piedmont rainforest; Fig. 2), high RMSE values were obtained (Fig. 7a). Conversely to the paramo, the piedmont rainforest presented the strongest precipitation regimen (Chancay and Espitia, 2021), and hence the high magnitude errors were expected. Correlation coefficients reached in the piedmont rainforest improved respect to those obtained in the paramo and the mountain forest, however, they were still unsatisfactory ($CORR < 0.2$). In general, results suggested the EFPs poorly capture the precipitation occurrence, demonstrating the difficulty of simulating precipitation on high spatiotemporal scales over complex topography regions such as headwaters of the Amazon Basin (Bulovic et al., 2020; Hobouchian et al., 2017; Manz et al., 2017).

4.5. Ensemble streamflow forecasting

The general assessment of bias-corrected ensemble precipitation forecasts (EPFs) as forcing input for the GR4H model (Fig. 8) yielded acceptable KGE performances (0.24 - 0.40), considering the hourly resolution of precipitation and streamflow simulations (Camera et al., 2020; Knoben et al., 2019). Considering the Probability of Flow Detection (PFD), the ensemble streamflow forecasts (ESFs) captured between 60% and 78% of the flood events. However, the Peak Flow Criterion (PFC) indicated that simulated peak discharges presented intensity errors between 28% and 32%. Although the PFC cannot reveal overestimation or underestimation, the non-exceedance curve (Fig. 8) confirmed that streamflow simulations above the 90th percentile were underestimated, showing BIAS values between -69.4 and -34.8 %. As Chancay and Espitia (2021) discussed, the underestimation of peak flows is mainly related to the underestimation of the simulated precipitation, particularly over the lower reaches of the UNRB (i.e., in the piedmont rainforest; Fig. 2).

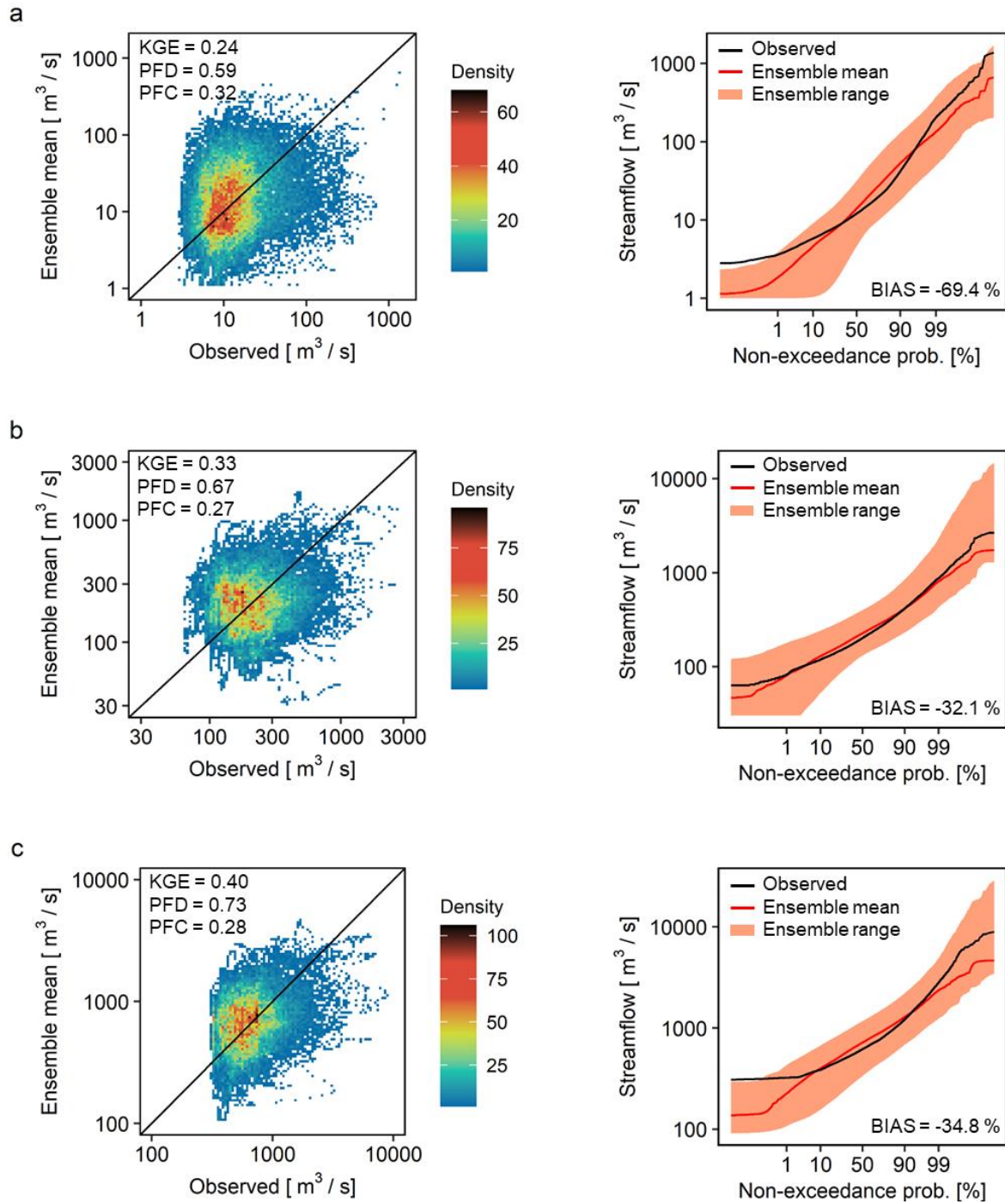


Figure 8. Performance of the ensemble streamflow forecasting for (a) Tena River Basin, TRB; (b) Jatunyacu River Basin, JRB; and (c) Upper Napo River Basin, UNRB. Scatter density plot for observed and simulated data at the hourly scale (left side). The non-exceedance probability curve for observed data and ensemble streamflow forecast (right side).

On balance, streamflow simulations of the TRB presented the lowest performances, whereas streamflow simulations of the UNRB yielded the highest performance. These trends are in accordance with previous studies, which indicated the smaller basins, the more difficult it is to adequately predict the precipitation and hence the streamflow dynamics over them (Camera et al., 2020; Tsegaw et al., 2019). In fact, other studies such as Rogelis and Werner (2018), Rogelis et al. (2016), and Galanaki et al. (2021) highlighted that, with larger river basins, it is possible to minimize errors derived from the spatiotemporal lag of simulated precipitation. Note the TRB is the basin with the smallest drainage area, while UNBR has the largest drainage area.

The event-based analysis, considering the last five flash floods occurred in the study area, suggested that the ensemble streamflow forecast has a limited skill to reproduce the streamflow dynamic during flood processes. As shown in Fig. 9, the KGE on the event scale ranged from -0.47 to 0.49. For the events occurred in September 2017 (Fig. 9a), May 2019 (Fig. 9c), and June 2019 (Fig. 9d), the peak discharge was captured with underestimation, but also with a temporal lag of about ± 3 h. Although the uncertainty derived from EPFs is the main source of errors for the ensemble flash flood forecasting (Rogelis et al., 2016), numerous works discussed that initial moisture conditions have significant impact on the simulated streamflow dynamics (Hurtado et al., 2020; Lee et al., 2011; Wood et al., 2016). Thus, it is not enough to adequately simulate extreme rainfall events, but also the previous precipitation conditions. To reduce the effect of initial conditions, data assimilation techniques (e.g., Kalman Filter, Particle Filter) have been widely used in recent years (Piazzi et al., 2021). However, no data assimilation techniques were included in this study.

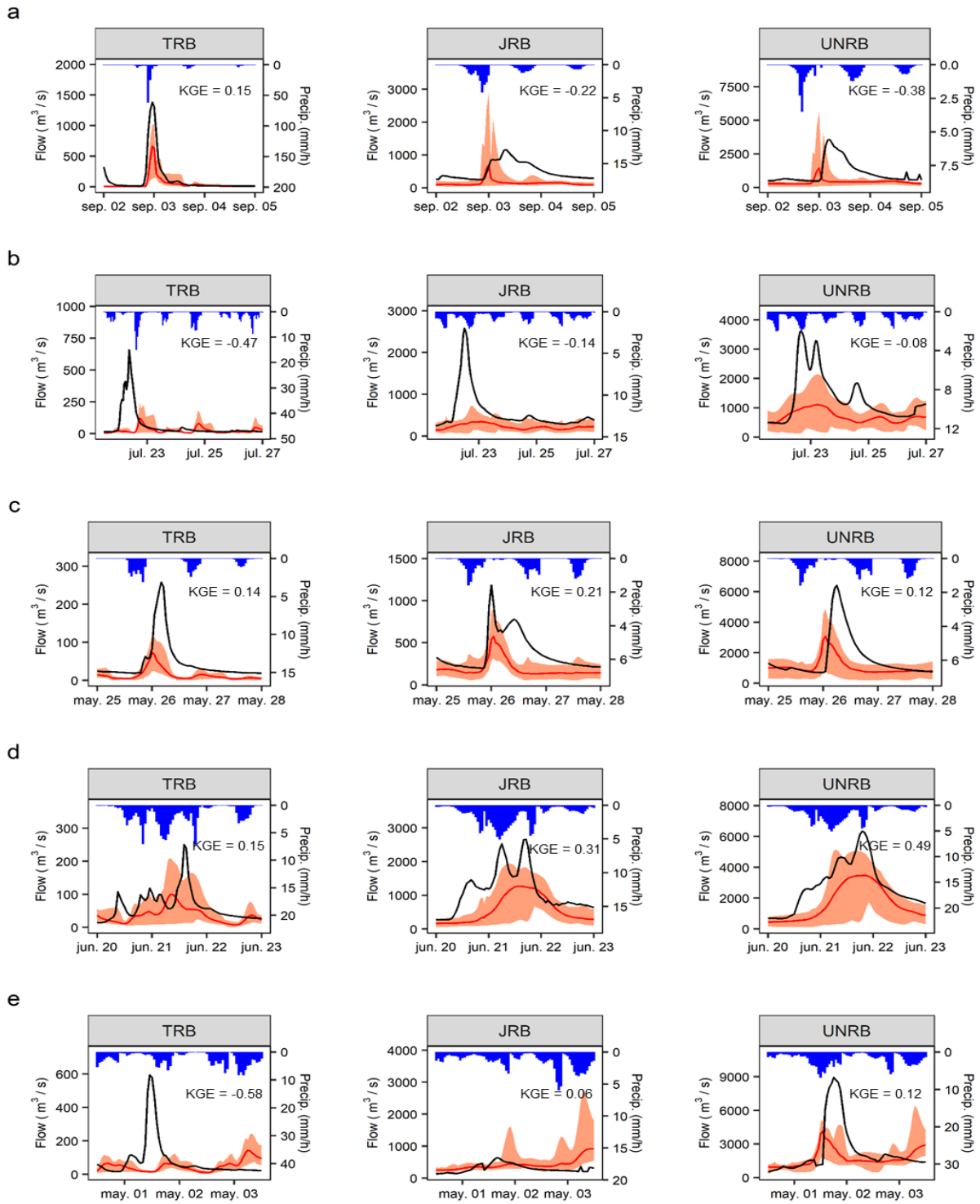


Figure 9. Observed and simulated (ensemble forecast) hydrographs of the last five flash flood events that occurred in the Tena River Basin (TRB), Jatunyacu River Basin (JRB), and Upper Napo River Basin (UNRB). (a) Event 1, September 2017. (b) Event 2, July 2018. (c) Event 3, May 2019. (d) Event 4, June 2019. (e) Event 5, May 2020.

5. Future perspectives and final remarks

The multi-physics ensemble modeling approach used in the present study to forecast heavy rainfall and flash flood events over the Upper Napo River Basin (UNRB) showed acceptable performances, considering the limitations that imply the high-resolution hydrometeorological simulations. Altogether, results provided sufficient insights to propose the analyzed ensemble precipitation and streamflow forecasting as a preliminary tool for generating early warning systems in the study area. However, to improve the operability of the proposed tool it is necessary to explore further modeling aspects. For instance, data used to force the WRF model was obtained only from the Global Forecasting System (GFS), limiting the weather simulations to a single initial boundary condition. In fact, most WRF studies conducted in the Andean-Amazon region have only used GFS data. Other alternatives that could be considered in future studies are the ensemble products derived from the European Centre for Medium-Range Weather Forecasts (ECMWF).

Although the small ensemble (5 member) used to forecast precipitation and streamflow provided acceptable short-term predictions with lead times below 36 hours, deeper sensitivity analysis considering all physical WRF schemes might reveal new parameterizations suitable for increasing lead times and improving prediction performances. Likewise, future sensitivity analyses should consider the effect of the topography data resolution on the simulation performances. Note that for the Andean-Amazon region, the topography has a close relationship with the convective processes on subgrid scale, the most relevant physical scheme for precipitation prediction over the UNRB.

Since the streamflow simulations were only generated by forcing the semi-distributed GR4H model with precipitation forecasts derived from the proposed WRF ensemble parameterization, the uncertainties linked to the structure and parameterization of the hydrological model were not quantified. To address this, future studies should evaluate the proposed WRF ensemble parameterization with other hydrological models, such as TETIS or SWAT. The trends observed between the streamflow simulation performance and the drainage area confirmed that, for small basins (e.g., the TRB), errors derived from the spatiotemporal

lag of simulated precipitation produce a strong impact on the initial moisture conditions, affecting the streamflow dynamics and their respective peak discharges. In this regard, the improvement and expansion of the hydrometeorological monitoring network is essential to make high-quality real-time data available for data assimilation processes, and thus obtain more reliable forecasts.

This study not only contributes to the flash flood predictions, but also improves our general understanding of hydrometeorological processes of the Andean-Amazon region, that despite its importance and direct impact on the whole Amazon, and hence the world, it is still a poorly documented region. In fact, the information generated in this study could be applied to other water-related research fields, such as fluvial hydraulics, hydrogeology, and even integrated water resources management over the UNRB.

6. Appendix

Table A1. Description of the meteorological and hydrological stations used in this study.

Code	Name	Type	Latitude	Longitude
M004	Rumipamba	Meteorological	-1.0200	-78.5946
M0008	Puyo	Meteorological	-1.5057	-77.9560
M0118	Papallacta	Meteorological	-0.3806	-78.1413
M0258	Querochaca	Meteorological	-1.3671	-78.6050
M1124	Sierra Azul	Meteorological	-0.6708	-77.9241
M1219	Chaupishungo	Meteorological	-0.9169	-77.8191
M5010	Narupa	Meteorological	-0.7319	-77.7830
M5147	Universidad	Meteorological	-0.9522	-77.8612
M5148	Chalupas	Meteorological	-0.8205	-78.2693
MI001	Colonso	Meteorological	-0.9378	-77.9405
MI002	Alto Tena	Meteorological	-0.9369	-77.8809
MI003	Cavernas Jumandy	Meteorological	-0.8751	-77.7906
HI001	Puente Tena	Hydrological	-0.9922	-77.8150
H0721	Jatunyacu Iloculin	Hydrological	-1.0872	-77.9188
H1156	Napo-Ahuano	Hydrological	-1.0509	-77.5452

Table A2. Statistical criteria used to evaluate the ensemble precipitation and streamflow simulations derive from the WRF and GR4H models.

Metric	Definition	Optimum	Range	Unit
RMSE	$RMSE = \sqrt{\frac{\sum_{i=1}^n (S_i - O_i)^2}{n}}$	0	(0, Inf)	mm/h
CORR	$CORR = \frac{cov(S, O)}{\sqrt{var(S)} \sqrt{var(O)}}$	1	(-1, 1)	-
BIAS	$BIAS = 100 * \frac{\sum_{i=1}^n (S_i - O_i)^2}{\sum_{i=1}^n (O_i)^2}$	0	(-Inf, Inf)	%
KGE	$KGE = 1 - \sqrt{(\alpha - 1)^2 + (\beta - 1)^2 + (r - 1)^2}$	1	(-Inf, 1)	-
POD	$POD = \frac{A}{A + B}$	1	(0, 1)	-
FAR	$FAR = \frac{C}{A + C}$	0	(0, 1)	-
CSI	$CSI = \frac{A}{A + B + C}$	1	(0, 1)	-
PFC	$PFC = \frac{\sum_{i=1}^n (QS_i - QO_i)^2}{\sum_{i=1}^n (QO_i)^2}$	0	(-Inf, Inf)	%
PFD	$PFD = \frac{DPK}{DPK + nDPK}$	1	(0, 1)	-

Where, **n** is the total number of observations, **Si** is the i-th simulated element, **Oi** is the i-th observed element, **cov()** is the covariance, **var()** is the variance, **α** is the ratio between simulated and observed mean, **β** is the ratio between simulated and observed standard deviation, **r** = CORR, **A** is the number of hits (**Si** > 0 and **Oi** > 0), **B** is the number of misses (**Si** = 0 and **Oi** > 0), **C** is the number of false positive (**Si** > 0 and **Oi** = 0), **Qs** is the peak flow simulated, **Qo** is the peak flow observed, **DPK** is detected peak flow, and **nDPK** is the no detected peak flow.

7. References

- Arakawa, A., 2004. The Cumulus Parameterization Problem: Past, Present, and Future. *J. Clim.* 17, 2493–2525. [https://doi.org/10.1175/1520-0442\(2004\)017<2493:RATCPP>2.0.CO;2](https://doi.org/10.1175/1520-0442(2004)017<2493:RATCPP>2.0.CO;2)
- Argüeso, D., Hidalgo-Muñoz, J.M., Gámiz-Fortis, S.R., Esteban-Parra, M.J., Dudhia, J., Castro-Díez, Y., 2011. Evaluation of WRF Parameterizations for Climate Studies over Southern Spain Using a Multistep Regionalization. *J. Clim.* 24, 5633–5651. <https://doi.org/10.1175/JCLI-D-11-00073.1>
- Athukorala, R., Thol, T., Neluwala, P., Petri, M., Sengxeu, S., Lattada, L., Keomanivong, S., Sithivong, V., 2021. Evaluating the Performance of a WRF Physics Ensemble in Simulating Rainfall over Lao PDR during Wet and Dry Seasons. *Adv. Meteorol.* 2021, 1–16. <https://doi.org/10.1155/2021/6630302>
- Barichivich, J., Gloor, E., Peylin, P., Brienen, R.J.W., Schöngart, J., Espinoza, J.C., Pattnayak, K.C., 2018.

- Recent intensification of Amazon flooding extremes driven by strengthened Walker circulation. *Sci. Adv.* 4, eaat8785. <https://doi.org/10.1126/sciadv.aat8785>
- Beck, V., Gerbig, C., Koch, T., Bela, M.M., Longo, K.M., Freitas, S.R., Kaplan, J.O., Prigent, C., Bergamaschi, P., Heimann, M., 2013. WRF-Chem simulations in the Amazon region during wet and dry season transitions: evaluation of methane models and wetland inundation maps. *Atmos. Chem. Phys.* 13, 7961–7982. <https://doi.org/10.5194/acp-13-7961-2013>
- Bennett, J.C., Robertson, D.E., Shrestha, D.L., Wang, Q.J., Enever, D., Hapuarachchi, P., Tuteja, N.K., 2014. A System for Continuous Hydrological Ensemble Forecasting (SCHEF) to lead times of 9days. *J. Hydrol.* 519, 2832–2846. <https://doi.org/10.1016/j.jhydrol.2014.08.010>
- Bright, D.R., Mullen, S.L., 2002. The Sensitivity of the Numerical Simulation of the Southwest Monsoon Boundary Layer to the Choice of PBL Turbulence Parameterization in MM5. *Weather Forecast.* 17, 99–114. [https://doi.org/10.1175/1520-0434\(2002\)017<0099:TSOTNS>2.0.CO;2](https://doi.org/10.1175/1520-0434(2002)017<0099:TSOTNS>2.0.CO;2)
- Bulovic, N., McIntyre, N., Johnson, F., 2020. Evaluation of IMERG V05B 30-Min Rainfall Estimates over the High-Elevation Tropical Andes Mountains. *J. Hydrometeorol.* 21, 2875–2892. <https://doi.org/10.1175/JHM-D-20-0114.1>
- Calvetti, L., Pereira Filho, A.J., 2014. Ensemble Hydrometeorological Forecasts Using WRF Hourly QPF and TopModel for a Middle Watershed. *Adv. Meteorol.* 2014, 1–12. <https://doi.org/10.1155/2014/484120>
- Camera, C., Bruggeman, A., Zittis, G., Sofokleous, I., Arnault, J., 2020. Simulation of extreme rainfall and streamflow events in small Mediterranean watersheds with a one-way-coupled atmospheric–hydrologic modelling system. *Nat. Hazards Earth Syst. Sci.* 20, 2791–2810. <https://doi.org/10.5194/nhess-20-2791-2020>
- Campozano, L., Tenelanda, D., Sanchez, E., Samaniego, E., Feyen, J., 2016. Comparison of Statistical Downscaling Methods for Monthly Total Precipitation: Case Study for the Paute River Basin in Southern Ecuador. *Adv. Meteorol.* 2016, 1–13. <https://doi.org/10.1155/2016/6526341>
- Carlberg, B.R., Gallus, W.A., Franz, K.J., 2018. A Preliminary Examination of WRF Ensemble Prediction of Convective Mode Evolution. *Weather Forecast.* 33, 783–798. <https://doi.org/10.1175/WAF-D-17-0149.1>
- Centre for Research on the Epidemiology of Disasters, 2020. *Natural Disasters 2019*.
- Chancay, J.E., Espitia, E.F., 2021. Improving Hourly Precipitation Estimates for Flash Flood Modeling in Data-Scarce Andean-Amazon Basins: An Integrative Framework Based on Machine Learning and Multiple Remotely Sensed Data. *Remote Sens.* 13, 4446. <https://doi.org/10.3390/rs13214446>
- Chawla, I., Osuri, K.K., Mujumdar, P.P., Niyogi, D., 2018. Assessment of the Weather Research and Forecasting (WRF) model for simulation of extreme rainfall events in the upper Ganga Basin. *Hydrol. Earth Syst. Sci.* 22, 1095–1117. <https://doi.org/10.5194/hess-22-1095-2018>
- Chen, F., Dudhia, J., 2001. Coupling an Advanced Land Surface–Hydrology Model with the Penn State–NCAR MM5 Modeling System. Part I: Model Implementation and Sensitivity. *Mon. Weather Rev.*

- 129, 569–585. [https://doi.org/10.1175/1520-0493\(2001\)129<0569:CAALSH>2.0.CO;2](https://doi.org/10.1175/1520-0493(2001)129<0569:CAALSH>2.0.CO;2)
- Comin, A.N., Justino, F., Pezzi, L., de Sousa Gurjão, C.D., Shumacher, V., Fernández, A., Sutil, U.A., 2021. Extreme rainfall event in the Northeast coast of Brazil: a numerical sensitivity study. *Meteorol. Atmos. Phys.* 133, 141–162. <https://doi.org/10.1007/s00703-020-00747-0>
- Cruz Cueva, G.E., 2016. Elaboración de un plan de contingencia por inundación del río Tena en los barrios: Bellavista, Las Hierbitas, El Tereré y barrio central de la ciudad de Tena. PUCE.
- Dubey, A.K., Kumar, P., Chembolu, V., Dutta, S., Singh, R.P., Rajawat, A.S., 2021. Flood modeling of a large transboundary river using WRF-Hydro and microwave remote sensing. *J. Hydrol.* 598, 126391. <https://doi.org/10.1016/j.jhydrol.2021.126391>
- Duzenli, E., Yucel, I., Pilatin, H., Yilmaz, M.T., 2021. Evaluating the performance of a WRF initial and physics ensemble over Eastern Black Sea and Mediterranean regions in Turkey. *Atmos. Res.* 248, 105184. <https://doi.org/10.1016/j.atmosres.2020.105184>
- Espinoza, J.C., Garreaud, R., Poveda, G., Arias, P.A., Molina-Carpio, J., Masiokas, M., Viale, M., Scaff, L., 2020. Hydroclimate of the Andes Part I: Main Climatic Features. *Front. Earth Sci.* 8. <https://doi.org/10.3389/feart.2020.00064>
- Espinoza Villar, J.C., Guyot, J.L., Ronchail, J., Cochonneau, G., Filizola, N., Fraizy, P., Labat, D., de Oliveira, E., Ordoñez, J.J., Vauchel, P., 2009a. Contrasting regional discharge evolutions in the Amazon basin (1974–2004). *J. Hydrol.* 375, 297–311. <https://doi.org/10.1016/j.jhydrol.2009.03.004>
- Espinoza Villar, J.C., Ronchail, J., Guyot, J.L., Cochonneau, G., Naziano, F., Lavado, W., De Oliveira, E., Pombosa, R., Vauchelh, P., 2009b. Spatio-temporal rainfall variability in the Amazon basin countries (Brazil, Peru, Bolivia, Colombia, and Ecuador). *J. Climatol.* 29, 1574–1594. <https://doi.org/10.1002/joc.1791>
- Espitia, E.F., Chancay, J.E., Acero-Triana, J., 2020. A preliminary approach for flood forecasting in data-scare Ecuadorian Amazon Subbasin using the GR4H model. Artículo en Prep.
- Evans, J.P., Ji, F., Abramowitz, G., Ekström, M., 2013. Optimally choosing small ensemble members to produce robust climate simulations. *Environ. Res. Lett.* 8, 044050. <https://doi.org/10.1088/1748-9326/8/4/044050>
- Fang, G.H., Yang, J., Chen, Y.N., Zammit, C., 2015. Comparing bias correction methods in downscaling meteorological variables for a hydrologic impact study in an arid area in China. *Hydrol. Earth Syst. Sci.* 19, 2547–2559. <https://doi.org/10.5194/hess-19-2547-2015>
- Ferrier, B.S., Jin, Y., Lin, Y., Black, T., Rogers, E., DiMego, G., 2002. Implementation of a new grid-scale cloud and precipitation scheme in the NCEP Eta model, in: Proceedings of the in the 19th Conf. on Weather Analysis and Forecasting/15th Conf. on Numerical Weather. American Meteorological Society, pp. 280–283.
- Galanaki, E., Lagouvardos, K., Kotroni, V., Giannaros, T., Giannaros, C., 2021. Implementation of WRF-Hydro at two drainage basins in the region of Attica, Greece, for operational flood forecasting. *Nat. Hazards Earth Syst. Sci.* 21, 1983–2000. <https://doi.org/10.5194/nhess-21-1983-2021>

- Gao, Y., Leung, L.R., Zhao, C., Hagos, S., 2017. Sensitivity of U.S. summer precipitation to model resolution and convective parameterizations across gray zone resolutions. *J. Geophys. Res. Atmos.* 122, 2714–2733. <https://doi.org/10.1002/2016JD025896>
- Gbode, I.E., Dudhia, J., Ogunjobi, K.O., Ajayi, V.O., 2019. Sensitivity of different physics schemes in the WRF model during a West African monsoon regime. *Theor. Appl. Climatol.* 136, 733–751. <https://doi.org/10.1007/s00704-018-2538-x>
- Gharamti, M., McCreight, J.L., Noh, S.J., Hoar, T.J., RafieeiNasab, A., Johnson, B.K., 2021. Ensemble streamflow data assimilation using WRF-Hydro and DART: novel localization and inflation techniques applied to Hurricane Florence flooding. *Hydrol. Earth Syst. Sci.* 25, 5315–5336. <https://doi.org/10.5194/hess-25-5315-2021>
- Gloor, M., Brienen, R.J.W., Galbraith, D., Feldpausch, T.R., Schöngart, J., Guyot, J.-L., Espinoza, J.C., Lloyd, J., Phillips, O.L., 2013. Intensification of the Amazon hydrological cycle over the last two decades. *Geophys. Res. Lett.* 40, 1729–1733. <https://doi.org/10.1002/grl.50377>
- Grell, G.A., Dévényi, D., 2002. A generalized approach to parameterizing convection combining ensemble and data assimilation techniques. *Geophys. Res. Lett.* 29, 38-1-38-4. <https://doi.org/10.1029/2002GL015311>
- Grell, G.A., Freitas, S.R., 2014. A scale and aerosol aware stochastic convective parameterization for weather and air quality modeling. *Atmos. Chem. Phys.* 14, 5233–5250. <https://doi.org/10.5194/acp-14-5233-2014>
- Gsella, A., de Meij, A., Kerschbaumer, A., Reimer, E., Thunis, P., Cuvelier, C., 2014. Evaluation of MM5, WRF and TRAMPER meteorology over the complex terrain of the Po Valley, Italy. *Atmos. Environ.* 89, 797–806. <https://doi.org/10.1016/j.atmosenv.2014.03.019>
- Heredia, M.B., Junquas, C., Prieur, C., Condom, T., 2018. New Statistical Methods for Precipitation Bias Correction Applied to WRF Model Simulations in the Antisana Region, Ecuador. *J. Hydrometeorol.* 19, 2021–2040. <https://doi.org/10.1175/JHM-D-18-0032.1>
- Hobouchian, M.P., Salio, P., García Skabar, Y., Vila, D., Garreaud, R., 2017. Assessment of satellite precipitation estimates over the slopes of the subtropical Andes. *Atmos. Res.* 190, 43–54. <https://doi.org/10.1016/j.atmosres.2017.02.006>
- Hoch, J.M., Haag, A. V., van Dam, A., Winsemius, H.C., van Beek, L.P.H., Bierkens, M.F.P., 2017. Assessing the impact of hydrodynamics on large-scale flood wave propagation – a case study for the Amazon Basin. *Hydrol. Earth Syst. Sci.* 21, 117–132. <https://doi.org/10.5194/hess-21-117-2017>
- Hong, S.-Y., Noh, Y., Dudhia, J., 2006. A New Vertical Diffusion Package with an Explicit Treatment of Entrainment Processes. *Mon. Weather Rev.* 134, 2318–2341. <https://doi.org/10.1175/MWR3199.1>
- Hsiao, L.-F., Yang, M.-J., Lee, C.-S., Kuo, H.-C., Shih, D.-S., Tsai, C.-C., Wang, C.-J., Chang, L.-Y., Chen, D.Y.-C., Feng, L., Hong, J.-S., Fong, C.-T., Chen, D.-S., Yeh, T.-C., Huang, C.-Y., Guo, W.-D., Lin, G.-F.,

2013. Ensemble forecasting of typhoon rainfall and floods over a mountainous watershed in Taiwan. *J. Hydrol.* 506, 55–68. <https://doi.org/10.1016/j.jhydrol.2013.08.046>
- Hurtado, J., Acero Triana, J.S., Espitia-Sarmiento, E., Jarrín-Pérez, F., 2020. Flood Hazard Assessment in Data-Scarce Watersheds Using Model Coupling, Event Sampling, and Survey Data. *Water* 12, 2768. <https://doi.org/10.3390/w12102768>
- IHS, 2020. Meteorological and Hydrological stations network [WWW Document]. URL <http://hidrometeorologia.ikiam.edu.ec/meteoviewer> (accessed 3.24.21).
- INAMHI, 2020. Red de estaciones automáticas hidrometeorológicas [WWW Document]. URL <http://186.42.174.236/InamhiEmas/> (accessed 6.12.20).
- INAMHI, 2019. Anuario hidrológico del Ecuador: 2014 - 2016. Quito, Ecuador.
- Insel, N., Poulsen, C.J., Ehlers, T.A., 2010. Influence of the Andes Mountains on South American moisture transport, convection, and precipitation. *Clim. Dyn.* 35, 1477–1492. <https://doi.org/10.1007/s00382-009-0637-1>
- Iza, A., 2020. Evaluación del pronóstico de precipitación usando el modelo WRF en el Ecuador. Quito, Ecuador.
- Janjić, Z.I., 2001. Nonsingular implementation of the Mellor-Yamada level 2.5 scheme in the NCEP Meso model. Office note (National Centers for Environmental Prediction (U.S.)) ; 437.
- Janjić, Z.I., 2000. Comments on “Development and Evaluation of a Convection Scheme for Use in Climate Models.” *J. Atmos. Sci.* 57, 3686–3686. [https://doi.org/10.1175/1520-0469\(2000\)057<3686:CODAEO>2.0.CO;2](https://doi.org/10.1175/1520-0469(2000)057<3686:CODAEO>2.0.CO;2)
- Janjić, Z.I., 1994. The Step-Mountain Eta Coordinate Model: Further Developments of the Convection, Viscous Sublayer, and Turbulence Closure Schemes. *Mon. Weather Rev.* 122, 927–945. [https://doi.org/10.1175/1520-0493\(1994\)122<0927:TSMECM>2.0.CO;2](https://doi.org/10.1175/1520-0493(1994)122<0927:TSMECM>2.0.CO;2)
- Janjić, Z.I., 1990. The Step-Mountain Coordinate: Physical Package. *Mon. Weather Rev.* 118, 1429–1443. [https://doi.org/10.1175/1520-0493\(1990\)118<1429:TSMCPP>2.0.CO;2](https://doi.org/10.1175/1520-0493(1990)118<1429:TSMCPP>2.0.CO;2)
- Jeworrek, J., West, G., Stull, R., 2021. WRF Precipitation Performance and Predictability for Systematically Varied Parameterizations over Complex Terrain. *Weather Forecast.* <https://doi.org/10.1175/WAF-D-20-0195.1>
- Jeworrek, J., West, G., Stull, R., 2019. Evaluation of Cumulus and Microphysics Parameterizations in WRF across the Convective Gray Zone. *Weather Forecast.* 34, 1097–1115. <https://doi.org/10.1175/WAF-D-18-0178.1>
- Kain, J.S., 2004. The Kain–Fritsch Convective Parameterization: An Update. *J. Appl. Meteorol.* 43, 170–181. [https://doi.org/10.1175/1520-0450\(2004\)043<0170:TKCPAU>2.0.CO;2](https://doi.org/10.1175/1520-0450(2004)043<0170:TKCPAU>2.0.CO;2)
- Khansalari, S., Ranjbar-Saadatabadi, A., Fazel-Rastgar, F., Raziei, T., 2021. Synoptic and dynamic analysis of a flash flood-inducing heavy rainfall event in arid and semi-arid central-northern Iran and its simulation using the WRF model. *Dyn. Atmos. Ocean.* 93, 101198.

<https://doi.org/10.1016/j.dynatmoce.2020.101198>

- Kim, D.-E., Gourbesville, P., Liong, S.-Y., 2019. Overcoming data scarcity in flood hazard assessment using remote sensing and artificial neural network. *Smart Water* 4, 2. <https://doi.org/10.1186/s40713-018-0014-5>
- Kim, S., Shen, H., Noh, S., Seo, D.-J., Welles, E., Pelgrim, E., Weerts, A., Lyons, E., Philips, B., 2021. High-resolution modeling and prediction of urban floods using WRF-Hydro and data assimilation. *J. Hydrol.* 598, 126236. <https://doi.org/10.1016/j.jhydrol.2021.126236>
- Kirthiga, S.M., Narasimhan, B., Balaji, C., 2021. A multi-physics ensemble approach for short-term precipitation forecasts at convective permitting scales based on sensitivity experiments over southern parts of peninsular India. *J. Earth Syst. Sci.* 130, 68. <https://doi.org/10.1007/s12040-021-01556-8>
- Knoben, W.J.M., Freer, J.E., Woods, R.A., 2019. Technical note: Inherent benchmark or not? Comparing Nash–Sutcliffe and Kling–Gupta efficiency scores. *Hydrol. Earth Syst. Sci.* 23, 4323–4331. <https://doi.org/10.5194/hess-23-4323-2019>
- Langenbrunner, B., Pritchard, M.S., Kooperman, G.J., Randerson, J.T., 2019. Why Does Amazon Precipitation Decrease When Tropical Forests Respond to Increasing CO₂? *Earth's Futur.* 7, 450–468. <https://doi.org/10.1029/2018EF001026>
- Lapo, C., 2017. Análisis espacio-temporal del riesgo de inundación mediante simulación espacial en la parroquia Puerto Napo. Universidad Nacional de Chimborazo.
- Laraque, A., Bernal, C., Bourrel, L., Darrozes, J., Christophoul, F., Armijos, E., Fraizy, P., Pombosa, R., Guyot, J.L., 2009. Sediment budget of the Napo River, Amazon basin, Ecuador and Peru. *Hydrol. Process.* 23, 3509–3524. <https://doi.org/10.1002/hyp.7463>
- Laraque, A., Ronchail, J., Cochonneau, G., Pombosa, R., Guyot, J.L., 2007. Heterogeneous Distribution of Rainfall and Discharge Regimes in the Ecuadorian Amazon Basin. *J. Hydrometeorol.* 8, 1364–1381. <https://doi.org/10.1175/2007JHM784.1>
- Lee, H., Seo, D.-J., Koren, V., 2011. Assimilation of streamflow and in situ soil moisture data into operational distributed hydrologic models: Effects of uncertainties in the data and initial model soil moisture states. *Adv. Water Resour.* 34, 1597–1615. <https://doi.org/10.1016/j.advwatres.2011.08.012>
- Lee, J., 2012. Techniques for Down-selecting Numerical Weather Prediction Ensembles. The Pennsylvania State University. <https://doi.org/10.13140/RG.2.2.29268.81280>
- Li, Ji, Chen, Y., Wang, H., Qin, J., Li, Jie, Chiao, S., 2017. Extending flood forecasting lead time in a large watershed by coupling WRF QPF with a distributed hydrological model. *Hydrol. Earth Syst. Sci.* 21, 1279–1294. <https://doi.org/10.5194/hess-21-1279-2017>
- Li, Y., Lu, G., Wu, Z., He, H., Shi, J., Ma, Y., Weng, S., 2016. Evaluation of Optimized WRF Precipitation Forecast over a Complex Topography Region during Flood Season. *Atmosphere (Basel).* 7, 145. <https://doi.org/10.3390/atmos7110145>

- Li, Y., Pickering, K.E., Barth, M.C., Bela, M.M., Cummings, K.A., Allen, D.J., 2018. Evaluation of Parameterized Convective Transport of Trace Gases in Simulation of Storms Observed During the DC3 Field Campaign. *J. Geophys. Res. Atmos.* 123. <https://doi.org/10.1029/2018JD028779>
- Lim, K.-S.S., Hong, S.-Y., 2010. Development of an Effective Double-Moment Cloud Microphysics Scheme with Prognostic Cloud Condensation Nuclei (CCN) for Weather and Climate Models. *Mon. Weather Rev.* 138, 1587–1612. <https://doi.org/10.1175/2009MWR2968.1>
- Lin, Y.-L., Farley, R.D., Orville, H.D., 1983. Bulk Parameterization of the Snow Field in a Cloud Model. *J. Clim. Appl. Meteorol.* 22, 1065–1092. [https://doi.org/10.1175/1520-0450\(1983\)022<1065:BPOTSF>2.0.CO;2](https://doi.org/10.1175/1520-0450(1983)022<1065:BPOTSF>2.0.CO;2)
- Liu, Y., Chen, X., Li, Q., Yang, J., Li, L., Wang, T., 2020. Impact of different microphysics and cumulus parameterizations in WRF for heavy rainfall simulations in the central segment of the Tianshan Mountains, China. *Atmos. Res.* 244, 105052. <https://doi.org/10.1016/j.atmosres.2020.105052>
- Llauca, H., Lavado-Casimiro, W., León, K., Jimenez, J., Traverso, K., Rau, P., 2021. Assessing Near Real-Time Satellite Precipitation Products for Flood Simulations at Sub-Daily Scales in a Sparsely Gauged Watershed in Peruvian Andes. *Remote Sens.* 13, 826. <https://doi.org/10.3390/rs13040826>
- Manz, B., Páez-Bimos, S., Horna, N., Buytaert, W., Ochoa-Tocachi, B., Lavado-Casimiro, W., Willems, B., 2017. Comparative Ground Validation of IMERG and TMPA at Variable Spatiotemporal Scales in the Tropical Andes. *J. Hydrometeorol.* 18, 2469–2489. <https://doi.org/10.1175/JHM-D-16-0277.1>
- Martínez-Castro, D., Kumar, S., Flores Rojas, J.L., Moya-Álvarez, A., Valdivia-Prado, J.M., Villalobos-Puma, E., Castillo-Velarde, C. Del, Silva-Vidal, Y., 2019. The Impact of Microphysics Parameterization in the Simulation of Two Convective Rainfall Events over the Central Andes of Peru Using WRF-ARW. *Atmosphere (Basel)*. 10, 442. <https://doi.org/10.3390/atmos10080442>
- Martínez, D., Kumar, S., Flores Rojas, J.L., Moya-Álvarez, A., Valdivia-Prado, J.M., Villalobos-Puma, E., Castillo-Velarde, C. Del, Silva-Vidal, Y., 2019. The Impact of Microphysics Parameterization in the Simulation of Two Convective Rainfall Events over the Central Andes of Peru Using WRF-ARW. *Atmosphere (Basel)*. 10, 442. <https://doi.org/10.3390/atmos10080442>
- Mathevet, T., 2005. Quels modeles pluie-debit globaux au pas de temps horaire? Développements empiriques et intercomparaison de modeles sur un large échantillon de bassins versants. Ecole Nationale Du Genie Rural, des eaux et des forêts.
- Meynadier, R., de Coëtlogon, G., Bastin, S., Eymard, L., Janicot, S., 2015. Sensitivity testing of WRF parameterizations on air–sea interaction and its impact on water cycle in the Gulf of Guinea. *Q. J. R. Meteorol. Soc.* 141, 1804–1820. <https://doi.org/10.1002/qj.2483>
- Monin, A.S., Obukhov, M., 1954. Basic laws of turbulent mixing in the surface layer of the atmosphere. *Contrib. Geophys. Inst. Acad. Sci. USSR* 151, 187.
- Mori, P., Schwitalla, T., Ware, M.B., Warrach-Sagi, K., Wulfmeyer, V., 2021. Downscaling of seasonal ensemble forecasts to the convection-permitting scale over the Horn of Africa using the

- <sc>WRF</sc> model. *Int. J. Climatol.* 41. <https://doi.org/10.1002/joc.6809>
- Morrison, H., Curry, J.A., Khvorostyanov, V.I., 2005. A New Double-Moment Microphysics Parameterization for Application in Cloud and Climate Models. Part I: Description. *J. Atmos. Sci.* 62, 1665–1677. <https://doi.org/10.1175/JAS3446.1>
- Morrison, H., Lier-Walqui, M., Fridlind, A.M., Grabowski, W.W., Harrington, J.Y., Hoose, C., Korolev, A., Kumjian, M.R., Milbrandt, J.A., Pawlowska, H., Posselt, D.J., Prat, O.P., Reimel, K.J., Shima, S., Didenhoven, B., Xue, L., 2020. Confronting the Challenge of Modeling Cloud and Precipitation Microphysics. *J. Adv. Model. Earth Syst.* 12. <https://doi.org/10.1029/2019MS001689>
- Moya-Álvarez, A., Gálvez, J., Holguín, A., Estevan, R., Kumar, S., Villalobos, E., Martínez-Castro, D., Silva, Y., 2018a. Extreme Rainfall Forecast with the WRF-ARW Model in the Central Andes of Peru. *Atmosphere (Basel)*. 9, 362. <https://doi.org/10.3390/atmos9090362>
- Moya-Álvarez, A., Martínez-Castro, D., Flores, J.L., Silva, Y., 2018b. Sensitivity Study on the Influence of Parameterization Schemes in WRF_ARW Model on Short- and Medium-Range Precipitation Forecasts in the Central Andes of Peru. *Adv. Meteorol.* 2018, 1–16. <https://doi.org/10.1155/2018/1381092>
- Moya, A.S., Martínez-Castro, D., Kumar, S., Flores Rojas, J.L., Estevan, R., Saavedra-Huanca, M., Silva, Y., 2020. Statistical characterization of vertical meteorological profiles obtained with the WRF-ARW model on the central Andes of Peru and its relationship with the occurrence of precipitation on the region. *Atmos. Res.* 239, 104915. <https://doi.org/10.1016/j.atmosres.2020.104915>
- Mu, Z., Zhou, Y., Peng, L., He, Y., 2019. Numerical Rainfall Simulation of Different WRF Parameterization Schemes with Different Spatiotemporal Rainfall Evenness Levels in the Ili Region. *Water* 11, 2569. <https://doi.org/10.3390/w11122569>
- Muñoz, P., Orellana-Alvear, J., Willems, P., Céleri, R., 2018. Flash-Flood Forecasting in an Andean Mountain Catchment—Development of a Step-Wise Methodology Based on the Random Forest Algorithm. *Water* 10, 1519. <https://doi.org/10.3390/w10111519>
- NCEP, 2015. NCEP GFS 0.25 Degree Global Forecast Grids Historical Archive. *Res. Data Arch. Natl. Cent. Atmos. Res. Comput. Inf. Syst. Lab.* <https://doi.org/https://doi.org/10.5065/D65D8PWK>
- Ochoa-Sánchez, A., Crespo, P., Céleri, R., 2018. Quantification of rainfall interception in the high Andean tussock grasslands. *Ecohydrology* 11, e1946. <https://doi.org/10.1002/eco.1946>
- Padrón, R.S., Wilcox, B.P., Crespo, P., Céleri, R., 2015. Rainfall in the Andean Páramo: New Insights from High-Resolution Monitoring in Southern Ecuador. *J. Hydrometeorol.* 16, 985–996. <https://doi.org/10.1175/JHM-D-14-0135.1>
- Patel, P., Ghosh, S., Kagainalkar, A., Islam, S., Karmakar, S., 2019. Performance evaluation of WRF for extreme flood forecasts in a coastal urban environment. *Atmos. Res.* 223, 39–48. <https://doi.org/10.1016/j.atmosres.2019.03.005>
- Pennelly, C., Reuter, G., Flesch, T., 2014. Verification of the WRF model for simulating heavy precipitation in Alberta. *Atmos. Res.* 135–136, 172–192.

<https://doi.org/10.1016/j.atmosres.2013.09.004>

- Pervin, L., Gan, T.Y., 2021. Sensitivity of physical parameterization schemes in WRF model for dynamic downscaling of climatic variables over the MRB. *J. Water Clim. Chang.* 12, 1043–1058. <https://doi.org/10.2166/wcc.2020.036>
- Piazzzi, G., Thirel, G., Perrin, C., Delaigue, O., 2021. Sequential Data Assimilation for Streamflow Forecasting: Assessing the Sensitivity to Uncertainties and Updated Variables of a Conceptual Hydrological Model at Basin Scale. *Water Resour. Res.* 57. <https://doi.org/10.1029/2020WR028390>
- Pool, S., Vis, M., Seibert, J., 2018. Evaluating model performance: towards a non-parametric variant of the Kling-Gupta efficiency. *Hydrol. Sci. J.* 63, 1941–1953. <https://doi.org/10.1080/02626667.2018.1552002>
- Qian, Y., Yan, H., Berg, L.K., Hagos, S., Feng, Z., Yang, B., Huang, M., 2016. Assessing Impacts of PBL and Surface Layer Schemes in Simulating the Surface–Atmosphere Interactions and Precipitation over the Tropical Ocean Using Observations from AMIE/DYNAMO. *J. Clim.* 29, 8191–8210. <https://doi.org/10.1175/JCLI-D-16-0040.1>
- Rogelis, M.C., Werner, M., 2018. Streamflow forecasts from WRF precipitation for flood early warning in mountain tropical areas. *Hydrol. Earth Syst. Sci.* 22, 853–870. <https://doi.org/10.5194/hess-22-853-2018>
- Rogelis, M.C., Werner, M., Obregón, N., Wright, N., 2016. Hydrological model assessment for flood early warning in a tropical high mountain basin. *Hydrol. Earth Syst. Sci. Discuss.* <https://doi.org/10.5194/hess-2016-30>
- Ruiz, J.J., Saulo, C., Nogués-Paegle, J., 2010. WRF Model Sensitivity to Choice of Parameterization over South America: Validation against Surface Variables. *Mon. Weather Rev.* 138, 3342–3355. <https://doi.org/10.1175/2010MWR3358.1>
- Saedi, A., Saghafian, B., Moazami, S., Aminyavari, S., 2020. Performance evaluation of sub-daily ensemble precipitation forecasts. *Meteorol. Appl.* 27. <https://doi.org/10.1002/met.1872>
- Sena, J.A., de Deus, L.A.B., Freitas, M.A. V., Costa, L., 2012. Extreme Events of Droughts and Floods in Amazonia: 2005 and 2009. *Water Resour. Manag.* 26, 1665–1676. <https://doi.org/10.1007/s11269-012-9978-3>
- Servicio Nacional de Gestión de Riesgos y Emergencias, 2020. Base de datos de eventos de inundación registrados en Napo y Orellana, periodo 2010-2019.
- Sierra, J.P., Junquas, C., Epinoza, J.C., Lebel, T., Segura, H., 2020. High Resolution WRF Regional Climate Modeling for the Andes-Amazon Transition Region: Model Validation Early Results, in: *EGU General Assembly 2020*. pp. EGU2020-11687. <https://doi.org/https://doi.org/10.5194/egusphere-egu2020-11687>
- Sikder, S., Hossain, F., 2016. Assessment of the weather research and forecasting model generalized parameterization schemes for advancement of precipitation forecasting in monsoon-driven river

- basins. *J. Adv. Model. Earth Syst.* 8, 1210–1228. <https://doi.org/10.1002/2016MS000678>
- Skamarock, W.C., Klemp, J.B., Dudhia, J., Gill, D.O., Liu, Z., Berner, J., Wang, W., Powers, J.G., Duda, M.G., Barker, D.M., Huang, X.Y., 2019. A description of the advanced research WRF model version 4. Tech. report. Natl. Cent. Atmos. Res. <https://doi.org/http://dx.doi.org/10.5065/1dfh-6p97>
- Sun, M., Li, Z., Yao, C., Liu, Z., Wang, J., Hou, A., Zhang, K., Huo, W., Liu, M., 2020. Evaluation of Flood Prediction Capability of the WRF-Hydro Model Based on Multiple Forcing Scenarios. *Water* 12, 874. <https://doi.org/10.3390/w12030874>
- Tanaka, T., Kiyohara, K., Tachikawa, Y., 2020. Comparison of fluvial and pluvial flood risk curves in urban cities derived from a large ensemble climate simulation dataset: A case study in Nagoya, Japan. *J. Hydrol.* 584, 124706. <https://doi.org/10.1016/j.jhydrol.2020.124706>
- Thompson, G., Tewari, M., Ikeda, K., Tessorndorf, S., Weeks, C., Otkin, J., Kong, F., 2016. Explicitly-coupled cloud physics and radiation parameterizations and subsequent evaluation in WRF high-resolution convective forecasts. *Atmos. Res.* 168, 92–104. <https://doi.org/10.1016/j.atmosres.2015.09.005>
- Tian, J., Liu, J., Yan, D., Ding, L., Li, C., 2019. Ensemble flood forecasting based on a coupled atmospheric-hydrological modeling system with data assimilation. *Atmos. Res.* 224, 127–137. <https://doi.org/10.1016/j.atmosres.2019.03.029>
- Tsegaw, A.T., Alfredsen, K., Skaugen, T., Muthanna, T.M., 2019. Predicting hourly flows at ungauged small rural catchments using a parsimonious hydrological model. *J. Hydrol.* 573, 855–871. <https://doi.org/10.1016/j.jhydrol.2019.03.090>
- Tsuboki, K., Luo, Y., 2021. High-resolution Simulations of Heavy Rainfalls in Association with Monsoon Systems and Typhoons Using Cloud-Resolving Models. pp. 113–131. https://doi.org/10.1142/9789811216602_0010
- Tu, T., Ishida, K., Ercan, A., Kiyama, M., Amagasaki, M., Zhao, T., 2021. Hybrid precipitation downscaling over coastal watersheds in Japan using WRF and CNN. *J. Hydrol. Reg. Stud.* 37, 100921. <https://doi.org/10.1016/j.ejrh.2021.100921>
- Ulate, M., Dudhia, J., Zhang, C., 2014. Sensitivity of the water cycle over the Indian Ocean and Maritime Continent to parameterized physics in a regional model. *J. Adv. Model. Earth Syst.* 6, 1095–1120. <https://doi.org/10.1002/2014MS000313>
- Unduche, F., Tolossa, H., Senbeta, D., Zhu, E., 2018. Evaluation of four hydrological models for operational flood forecasting in a Canadian Prairie watershed. *Hydrol. Sci. J.* 63, 1133–1149. <https://doi.org/10.1080/02626667.2018.1474219>
- UNESCO, 2010. Atlas pluviométrico del Ecuador. Quito, Ecuador.
- Velasquez, P., Messmer, M., Raible, C.C., 2020. A new bias-correction method for precipitation over complex terrain suitable for different climate states: a case study using WRF (version 3.8.1). *Geosci. Model Dev.* 13, 5007–5027. <https://doi.org/10.5194/gmd-13-5007-2020>

- Wang, C., Qian, Y., Duan, Q., Huang, M., Berg, L.K., Shin, H.H., Feng, Z., Yang, B., Quan, J., Hong, S., Yan, J., 2020. Assessing the sensitivity of land-atmosphere coupling strength to boundary and surface layer parameters in the WRF model over Amazon. *Atmos. Res.* 234, 104738. <https://doi.org/10.1016/j.atmosres.2019.104738>
- Wang, C., Qian, Y., Duan, Q., Huang, M., Yang, Z., Berg, L.K., Gustafson, W.I., Feng, Z., Liu, J., Quan, J., 2021. Quantifying physical parameterization uncertainties associated with land-atmosphere interactions in the WRF model over Amazon. *Atmos. Res.* 262, 105761. <https://doi.org/10.1016/j.atmosres.2021.105761>
- Wang, X., Tolksdorf, V., Otto, M., Scherer, D., 2021. WRF-based dynamical downscaling of ERA5 reanalysis data for High Mountain Asia: Towards a new version of the High Asia Refined analysis. *Int. J. Climatol.* 41, 743–762. <https://doi.org/10.1002/joc.6686>
- Wijayarathne, D.B., Coulibaly, P., 2020. Identification of hydrological models for operational flood forecasting in St. John's, Newfoundland, Canada. *J. Hydrol. Reg. Stud.* 27, 100646. <https://doi.org/10.1016/j.ejrh.2019.100646>
- Winsemius, H.C., Aerts, J.C.J.H., van Beek, L.P.H., Bierkens, M.F.P., Bouwman, A., Jongman, B., Kwadijk, J.C.J., Ligtoet, W., Lucas, P.L., van Vuuren, D.P., Ward, P.J., 2016. Global drivers of future river flood risk. *Nat. Clim. Chang.* 6, 381–385. <https://doi.org/10.1038/nclimate2893>
- Wood, A.W., Hopson, T., Newman, A., Brekke, L., Arnold, J., Clark, M., 2016. Quantifying Streamflow Forecast Skill Elasticity to Initial Condition and Climate Prediction Skill. *J. Hydrometeorol.* 17, 651–668. <https://doi.org/10.1175/JHM-D-14-0213.1>
- Yang, Q., Dai, Q., Han, D., Chen, Y., Zhang, S., 2019. Sensitivity analysis of raindrop size distribution parameterizations in WRF rainfall simulation. *Atmos. Res.* 228, 1–13. <https://doi.org/10.1016/j.atmosres.2019.05.019>
- Yang, Q., Yu, Z., Wei, J., Yang, C., Gu, H., Xiao, M., Shang, S., Dong, N., Gao, L., Arnault, J., Laux, P., Kunstmann, H., 2021. Performance of the WRF model in simulating intense precipitation events over the Hanjiang River Basin, China – A multi-physics ensemble approach. *Atmos. Res.* 248, 105206. <https://doi.org/10.1016/j.atmosres.2020.105206>
- Zheng, Y., Alapaty, K., Herwehe, J.A., Del Genio, A.D., Niyogi, D., 2016. Improving High-Resolution Weather Forecasts Using the Weather Research and Forecasting (WRF) Model with an Updated Kain–Fritsch Scheme. *Mon. Weather Rev.* 144, 833–860. <https://doi.org/10.1175/MWR-D-15-0005.1>
- Zhong, X., Ruiz-Arias, J.A., Kleissl, J., 2016. Dissecting surface clear sky irradiance bias in numerical weather prediction: Application and corrections to the New Goddard Shortwave Scheme. *Sol. Energy* 132, 103–113. <https://doi.org/10.1016/j.solener.2016.03.009>